博士論文

Studies on translational buffering upon splicing inhibition

（スプライシング阻害時に働く翻訳緩衝機構に関する研究）

ジャガット　クリシュナ　チピ　シュレスタ

Jagat Krishna Chhipi Shrestha

博士論文

Studies on translational buffering upon splicing inhibition

（スプライシング阻害時に働く翻訳緩衝機構に関する研究）

Jagat Krishna Chhipi Shrestha

ジャガット　クリシュナ　チピ　シュレスタ

A dissertation submitted to the

Department of Biotechnology, Graduate School of Agricultural and Life Sciences,

The University of Tokyo

in partial fulfillment of the requirements for the degree of

DOCTOR OF PHILOSOPHY

指導教員　　吉田　稔

March 2019

Jagat Krishna Chhipi Shrestha Supervisor: Professor Minoru Yoshida

Studies on translational buffering upon splicing inhibition

Abstract

Proper gene expression is maintained and monitored by several layers of cellular control mechanisms. Under most circumstances errors in splicing, such as intron retention are suppressed via the nonsense mediated decay (NMD) pathway. However, chemical splicing inhibition by spliceostatin A (SSA) lead to a number of transcripts evading NMD and reaching the translation stage despite containing intronic sequences. This evasion of quality control results in truncated proteins. So far it has remained unclear how cells cope with these aberrant peptides. Here we present evidence that translation of improperly spliced transcripts leads to proteotoxic stress response via JNK phosphorylation and subsequent downregulation of global protein synthesis via inhibition of translation initiation through the mTOR pathway. Genome-wide ribosome profiling upon splicing inhibition reveals the translation of intron until in-frame stop codon. The results of this study suggest a novel layer of quality control mechanisms to buffer the production of aberrantly truncated proteins and to maintain protein homeostasis upon the splicing modulation. Besides the mTOR pathway, many genes known to be highly expressed in tumors appeared sensitive to SSA treatment, underlining the potential of splicing inhibitors in the development of novel therapeutic strategies.

Acknowledgements

I am greatly privileged to articulate my special, deepest and sincere gratitude to my reverent supervisors Prof. Minoru Yoshida, Dr. Shintaro Iwasaki and Dr. Tilman Schneider-Poetsch for their meticulous and exemplary guidance, incessant inspiration, valuable comments and kind constructive supervision conferred throughout the research work. It would never have been successfully completed without their valuable time, consistent encouragement and prolific advice. Thank you very much for the continuous support.

My heartily thanks go to Dr. Yuichi Shichino, Ms. Mari mito, Ms. Rie Yokoyama, Mr. Tomoya Fujita, Mr. Yusuke Kimura and all the members of Iwasaki RNA Systems Biochemistry Laboratory RIKEN for technical helps, faithful discussions and maintaining the efficient and productive lab environment ever.

I gratefully acknowledge Dr. Hiroki Kobayashi, Dr. Ken Matsumoto, Dr. Kazuki Sasaki, Dr. Hilbert Magpantay, Dr. Elliot Bradshaw, Dr. Tariq Mohammad, Dr. Asad Ali Shah, and all the members of Yoshida chemical genomics research group, Drug discovery seed compound exploratory unit, Molecular ligand target research team and Laboratory of microbiology (University of Tokyo) for their faithful advice, consistent support and enthusiastic suggestions.

I am thankful to my senior Dr. Reina Fukushima for assisting me during the initial days in Japan. I owe a special gratitude and sincere thanks to Ms. Kazuko Uchida, Ms. Junko Noda, Ms. Mari Aoki and Ms. Megumi Takase from Yoshida lab, RIKEN for all kinds of help and support throughout my stay during this period.

Thank you very much Japanese government for the MEXT (Monbukagakusho) scholarship grant. Thanks to all the Nepalese community members at Wako, Saitama for making the stay more beautiful, memorable and inspiring. I am very much grateful to my family members for their incessant support, encouragement and affection. I am immensely thankful to my wife Ms. Sapana Shrestha who always stood beside me during all ups and down, encouraging and supporting to try my best aiming high.

Abbreviations

4EBP1	eukaryotic translation initiation factor 4E (eIF4E) binding protein 1
5' TOP	5' terminal oligopyrimidine
5' UTR	5' untranslated region
Ac-SSA	Acetylated-SSA
AS	Alternative splicing
BPS	Branch point sequence
CBB	Coomassie Brilliant Blue
CDKN1B	Cyclin Dependent Kinase Inhibitor 1B
CDS	Coding sequence
CST	Cell signaling technology
DMEM	Dulbecco's modified eagle medium
DTT	Dithiothreitol
eIF	eukaryotic initiation factor
FLuc	Firefly Luciferase
GLM	Generalized linear model
GO	Gene ontology
HCV-IRES	Hepatitis C virus internal ribosome entry site
HEPES	4-(2-hydroxyethyl)-1-piperazineethanesulfonic acid
IC50	half maximal inhibitory concentration
IGV	Integrative genomics viewer
IR	Infrared
IVT	*In vitro* transcription
LAR II	Luciferase Assay Reagent II
LC-MS/MS	Liquid chromatography-tandem mass spectrometry
MA plot	M (log ratio) and A (mean average) scales plot
MISO	Mixture of isoforms
mRNA	messenger RNA
mTOR	mammalian target of rapamycin
mTORC	mTOR complex
NGS	Next generation sequencing
NMD	Nonsense mediated decay
OP-puro	O-Propargyl-puromycin
ORF	Open reading frame
PAGE	Polyacrylamide gel electrophoresis
plaB	Pladienolide B
PNK	Polynucleotide kinase
PPT	Polypyrimidine tract

pre-mRNA	Precursor mRNA
PTC	Pre-termination codon
QC	Quality control
RAB32	RAS oncogene family gene
RLuc	*Renilla* Luciferase
RNA	Ribonucleic acid
RNAi	RNA interference
RNA-seq	RNA sequencing
RP	Ribosomal protein
RPM	reads per million
rRNA	ribosomal RNA
RT-PCR	Reverse transcription - PCR
S6K1	p70S6 kinase 1
SF3b	Splicing factor 3b complex
siRNA	Small interfering RNA
SSA	Spliceostatin A
TE	Translation Efficiency
TR-FRET	Time-resolved fluorescence resonance energy transfer
tRNA	transfer RNA
UCSC	University of California, Santa Cruz
UPS	Ubiquitin-proteasome system

Table of Contents

List of Figures

List of Appendices

List of Tables

Chapter 1 Introduction

1.1 Splicing in the central dogma of molecular biology

The cellular and organismal phenotype is determined by the flow of information from DNA to RNA to protein. This principle is the most fundamental concept of molecular biology and known as the central dogma. The information lies encoded in the form of the DNA sequence using four different nucleotides A, G, C and T that are transcribed into RNA sequences and subsequently translated into proteins which act as structural and functional units of the cell (Crick, 1970). To date, comprehensive studies have uncovered numerous mechanisms of regulation and control of this dogma during diverse physiological conditions. Basically, transcription and translation have thus far been mainly studies in isolation while the interplay between the two is gathering much interest because of its potential to discriminate accurate gene expression control (Raj and van Oudenaarden, 2008).

Compared to prokaryotic gene expression, the regulation of transcription and translation proceeds at many more levels in eukaryotes. While bacteria produce multicistronic transcripts, which are translated cotranscriptionally, eukaryotes generate transcripts for one gene product at a time. In addition, eukaryotic transcripts require extensive post-transcriptional processing before they are suitable for translation. Besides capping, poly-adenylation and nuclear export, many eukaryotic transcripts need to undergo splicing, the removal of intervening polynucleotide stretches called introns from the coding sequence, exons. Eukaryotic pre-mRNAs co-transcriptionally undergo sequential processing events in the nucleus to become mature mRNAs. DNA inside the nucleus is transcribed into pre-messenger RNA (pre-mRNA) which are subjected to capping, splicing and polyadenylation to convert to mature mRNAs (Crick, 1979) (Darnell, 2013). Mature mRNAs are exported out to the cytosol where translation machinery, ribosomes translate this message into the functional protein (Figure 1.1). Hence, regulation of gene expression can occur at multiple stages and is more complex in eukaryotes. Based on the evidence of more than three decades of work, alternative splicing

in eukaryotes plays a key role in the flow of genetic information from transcription to translation (Kornblihtt *et al.*, 2013).

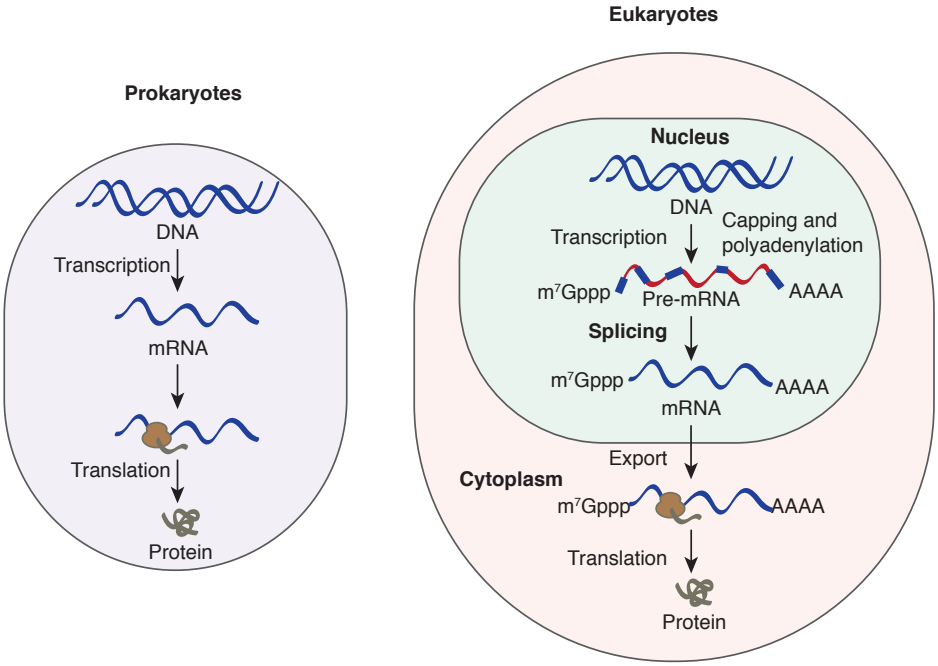

Figure 1.1 Schematic of central dogma in molecular biology.

Splicing out introns and ligating exons from pre-mRNAs occur co-transcriptionally with very high precision and fidelity inside the nucleus (Smith *et al.*, 1989). The process is catalyzed by a multimeric ribonucleoprotein called the spliceosome (Will and Lührmann, 2011). Five small nuclear ribonucleoprotein particles (snRNPs)- U1, U2, U4, U5 and U6 each containing a small nuclear RNA (snRNA) and associated proteins bind to their target sites on pre-mRNAs in a stepwise and specific manner. The intron is defined between the 5' splice site (5' ss) and the 3' splice site (3' ss). Upstream of the 3' ss lies the branch point sequence (BPS), containing the adenosine residue which will carry out the nucleophilic attack on the 5' ss, followed by the polypyrimidine tract (PPT). First, U1 snRNP binds to the 5' ss followed by binding of accessory factors, U2AF to the BPS and PPT forming the E complex assembly. Then recruitment of the U2 snRNP occurs at the BPS via base pairing with the snRNP's RNA complement, which is termed A complex. The U4/U5/U6 tri-snRNP complex then binds, forming B complex after which U1 and U4 dissociated, leaving the catalytically active spliceosome called C-complex (Figure 1.2).

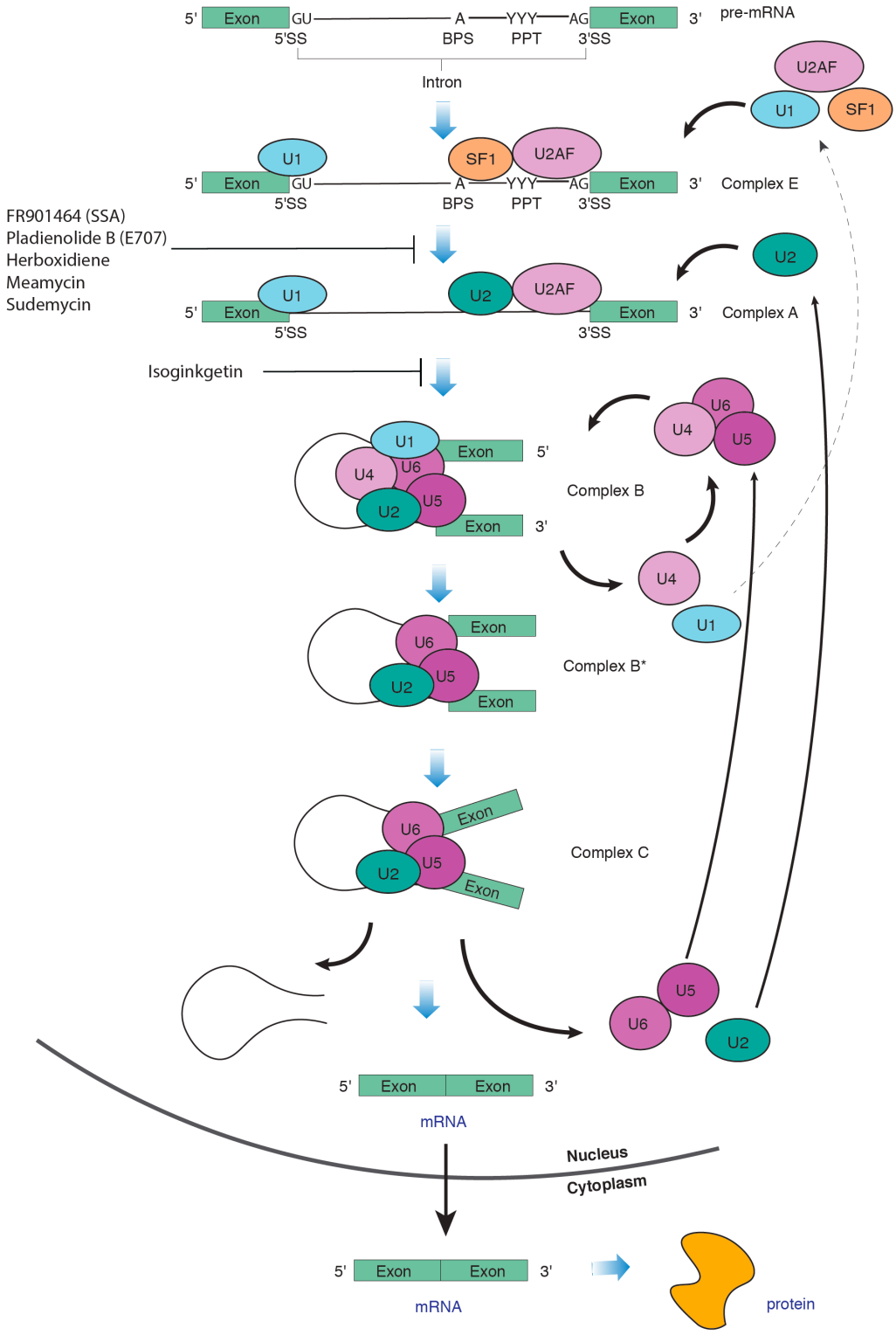

Figure 1.2 Schematic representation of spliceosome assembly, catalysis and small molecules inhibiting particular steps.

(modified from (Schneider-Poetsch *et al.*, 2010))

Two sequential transesterification reactions occur, thereby forming a phosphodiester bond between the 5' and 3' exons excising out the intron. The 2'-hydroxyl group of the BPS adenosine nucleotide attacks the 5' ss during the splicing initiation process which frees the 3'-hydroxyl group at the end of the 5' exon, which then carries out a nucleophilic attack on the 3' ss, excising the intron and linking 5' and 3' exons together (Figure 1.3) (Wahl *et al.*, 2009) (Schneider-Poetsch *et al.*, 2010).

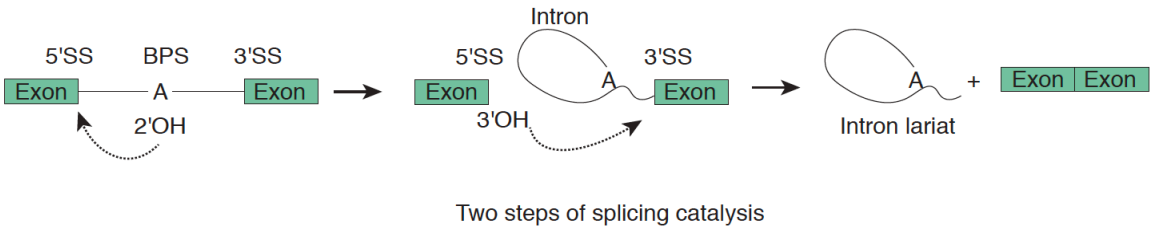

Figure 1.3 Schematic representation of intron removal.

(modified from (Vigevani, 2016))

Alternative splicing of pre-mRNAs allows expression of multiple proteins isoforms with different functions from the same gene/primary transcript (Smith *et al.*, 1989) (Schneider-Poetsch *et al.*, 2010). Generally, alternative splicing is marked by exon skipping, intron retention, alternative 5' or 3' splice site usage and mutually exclusion of exons (Figure 1.4). During evolution of the eukaryotes, alternative splicing played a key role to maintain the extended proteome from similar number of genes. More than 95% of human genes have potential to undergo alternative splicing (Wang *et al.*, 2008) (Kornblihtt *et al.*, 2013). Furthermore, changes in patterns of splicing by alternative splicing are closely linked to the disease development such as cancer. As for example, vascular endothelial growth factor (VEGF) consist of two possible splice sites in exon 8. The selection of proximal splice site produces angiogenic isoform of VEGF whereas distal splice site selection yields an isoform having anti-angiogenic properties (Kaida *et al.*, 2012). Therefore, pre-mRNA splicing is essential step in the central dogma.

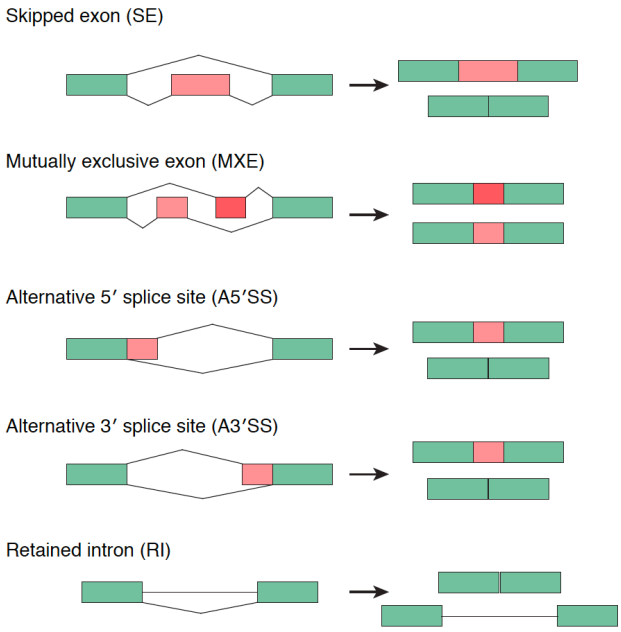

Figure 1.4 Schematic of major alternative splicing events.

1.2 Translational control of gene expression

Translation is a crucial step in the regulation of gene expression. In prokaryotes, translation is coupled with transcription whereas eukaryotic translation proceeds in the cytoplasm after transcription, processing and export of the mRNA from the nucleus. Alteration in translation occurs rapidly in response to various internal and external factors such as cell starved or stressed condition and diseased condition (Sonenberg and Hinnebusch, 2009). The decoding of messenger RNA (mRNA) into protein involves sequential steps of translation initiation, elongation, termination and recycling of ribosome (Figure 1.5). Each of the three steps plays an essential role in defining the cellular proteome, sustaining homeostasis and regulating cell proliferation and growth. The fidelity of translation is governed by the proper interaction between the translation factors, mRNA, transfer RNAs (tRNAs), the ribosome and additional interacting proteins. Hence, a number of diseases including different types of cancer results from aberrant regulation of protein synthesis (Sonenberg and Hinnebusch, 2009) (Groppo and Richter, 2009) (Hershey *et al.*, 2012). Figure 1.5 presents the fundamental outline of the eukaryotic translation process.

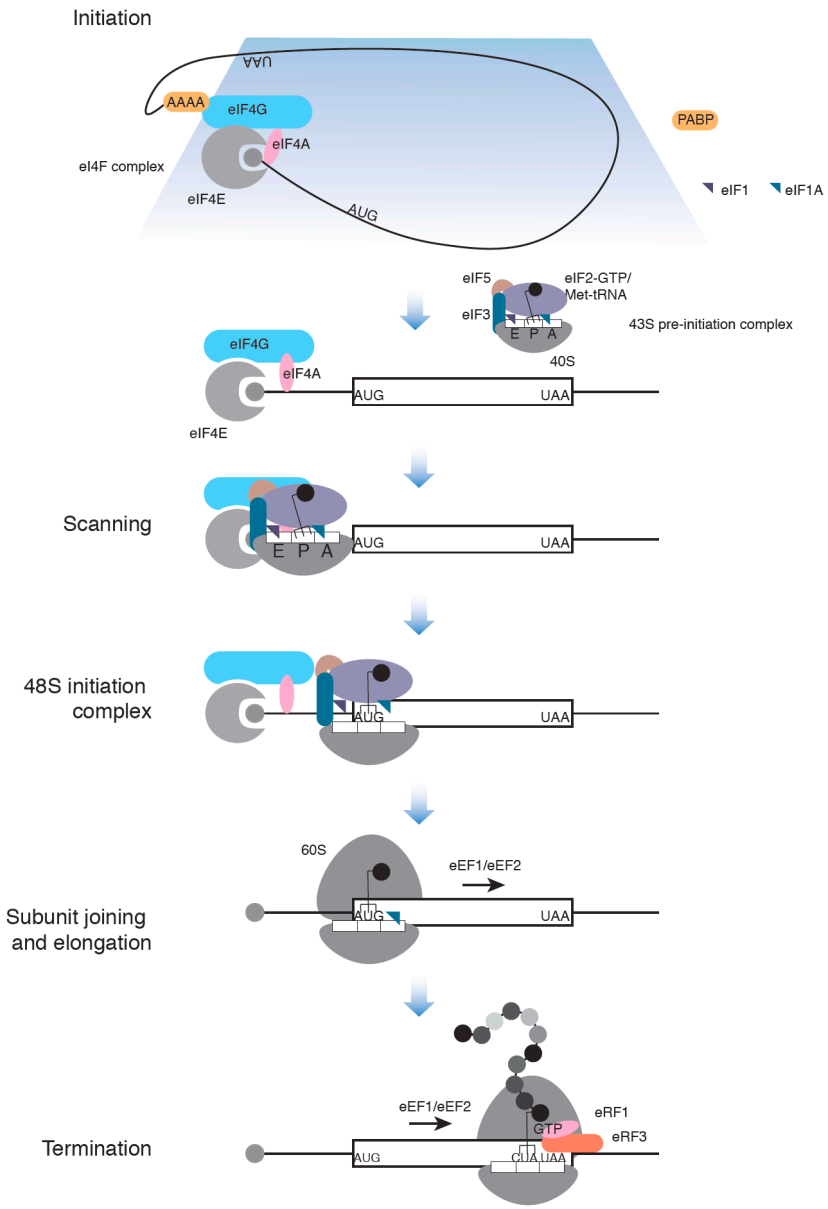

Figure 1.5 Schematic of fundamental outline of the eukaryotic translation process.

(modified from (Groppo and Richter, 2009))

Translation initiation

Translation initiation is the most highly regulated step during protein synthesis (Aitken and Lorsch, 2012). It begins with the formation of the 43S pre-initiation complex (PIC) by the assembly of eukaryotic

initiation factors (eIFs) 1, 1A, 3 and 5 along with the 40S ribosomal subunit and a ternary complex (TC) comprising eIF2, GTP and Met-tRNA$_i$. The eIF4F complex, consisting of the cap-binding protein eIF4E, the helicase eIF4A and the scaffold protein eIF4G binds the mRNA message together with the poly-A binding protein with the help of eIF4B. Facilitated by eIF3, the PIC binds the prepared mRNA (Hershey *et al.*, 2012) (Aitken and Lorsch, 2012) (Groppo and Richter, 2009) (Hinnebusch and Lorsch, 2012). Bound at the 5' end of the mRNA, the PIC scans the 5' untranslated region (5' UTR) until an AUG initiation codon is recognized (Figure 1.5). Upon start codon recognition, eIF1 is expelled prompting conversion of eIF2 to its GDP-bound state, assisted by the GTPase-activating protein eIF5. eIF1A along with a second GTPase, eIF5B facilitate assembly of the 60S subunit forming the 80S initiation complex (Aitken and Lorsch, 2012) (Groppo and Richter, 2009) (Nürenberg and Tampé, 2013).

Translation elongation

The translating ribosomes are 80S ribosomes comprising an acceptor site (A-site), a peptidyl site (P-site), and an exit site (E-site). The Met-tRNA$_i$ occupies the P site of the ribosome during recognition of start codon and translation elongation begins by the recruitment of the aminoacyl-tRNA (aa-tRNA) to the ribosomal A site by elongation factor-ternary complex, eEF1A-TC (eEF1A, GTP and aa-tRNA). In similar manner, the next amino acid to be incorporated into the growing peptide is delivered by aa-tRNA by base pairing the tRNA anticodon with the mRNA codon (Villa N., 2014). Every new amino acid is added by the peptide bond formation, catalyzed by the peptidyl transferase center of ribosome. eEF2-GTP then promotes the translocation of the A-site tRNA to the P-site, and P-site tRNA to the E-site creating A-site vacant for next incoming aa-tRNA (Figure 1.5). The elongation process continues until it encounters stop codon in mRNA (Groppo and Richter, 2009).

Translation termination

When a stop codon is encountered during elongation by ribosomal A-site, release factors (eRF1/eRF3) recognize the stop codon and subsequent hydrolysis of GTP promotes peptide hydrolysis from

the P-site tRNA and further dissociates ribosomal subunits that can proceeds for the new translation process (Figure 1.5) (Villa N., 2014).

1.3 Quality control mechanisms for pre-mRNA splicing

Multiple layers of quality control preserve the fidelity of this biochemical process. If unspliced pre-mRNAs were to be translated, aberrant polypeptides would result that may affect protein homeostasis and lead to pathological outcomes. Two important layers of quality control ensure production of correctly spliced products are: spliceosome mediated kinetic proofreading and recognition of aberrantly spliced products for subsequent degradation by non-sense mediated decay (NMD) (Hilleren and Parker, 2003a) (Egecioglu and Chanfreau, 2011).

Spliceosome mediated kinetic proofreading and recognition

The spliceosome specifically binds to splicing substrates (the GU dinucleotide at the 5' splice site, the AG dinucleotide at 3' splice site and the branchpoint Adenosine) for catalysis (Figure 1.2 and 1.3) (Wahl *et al.*, 2009). Proofreading of the consensus splice sites and branchpoint sequence are carried out by the DExD/H box ATPases prp16, prp22 and prp5 respectively during the two-step splicing process (Smith *et al.*, 2008) (Koodathingal *et al.*, 2010). Recently, prp43 along with prp16 were identified to have a role in proofreading the 5' splice-site and enhancing the removal of suboptimal exons and lariat intermediates by spliceosomal dissociation from these intermediates (Mayas *et al.*, 2010). Many other spliceosomal proteins likely function to minimize splicing errors are yet to be unraveled, which ensures the fidelity of pre-mRNA splicing.

Nuclear retention and degradation of aberrant transcripts

On the other hand, beyond the proofreading by the spliceosome itself, the cell possesses further quality assurance mechanisms to maintain expression of properly spliced mRNA (Hilleren and Parker, 2003a) (Egecioglu and Chanfreau, 2011). In the nucleus, improperly spliced pre-mRNA substrates can be

degraded by the nuclear exosome. With its exo- and endonuclease activity including the 5'-3' exonuclease Rat1P/Xrn2 (Johnson, 1997) (Moore *et al.*, 2006) (Egecioglu and Chanfreau, 2011) (Figure 1.6), the exosome can co-transcriptionally degrade aberrant transcripts. The molecular mechanism of how degradation is induced upon the recognition of unspliced products has remained obscure. In *Saccharomyces cerevisiae*, Mlp1p/Mlp2p have been suggested to be nuclear retention factors, preventing pre-mRNAs from being exported to the cytoplasm and translated (Galy *et al.*, 2004). Also, the pre-mRNA retention and splicing complex (RES) has been implicated in retention of pre-mRNAs in nucleus studied by using the β-galactosidase reporter system consisting either the pre-mRNA or mRNA in-frame (Dziembowski *et al.*, 2004). However, the effect on endogenous transcripts have not been studied yet.

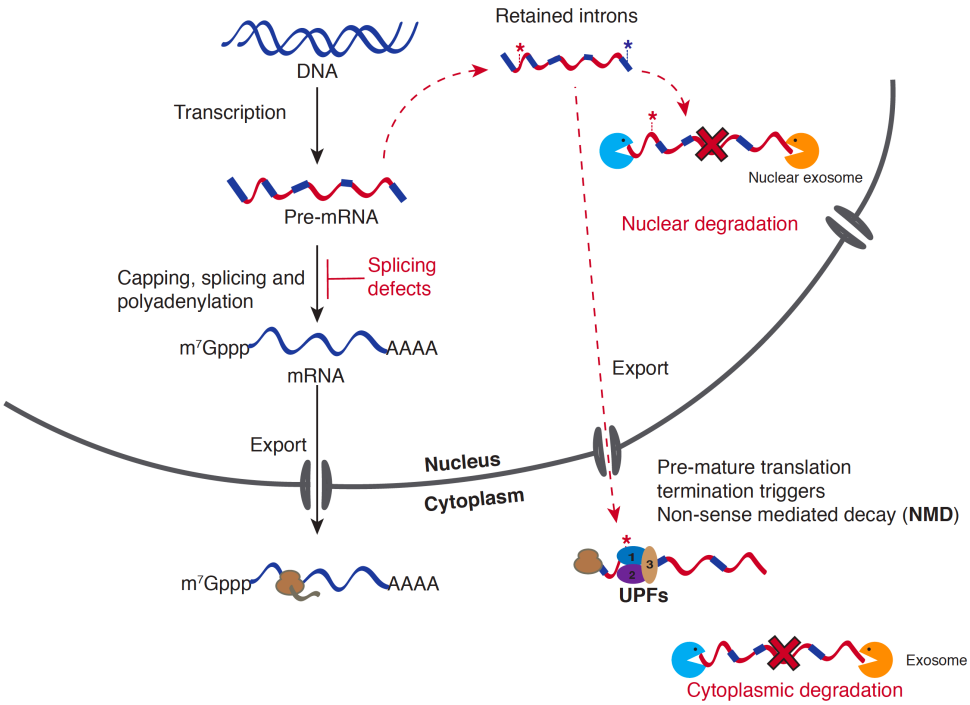

Figure 1.6 Schematic representation of quality control surveillance mechanisms for pre-mRNAs upon splice inhibition (modified from (Doma and Parker, 2007))

Non-sense mediated decay (NMD)

Several studies have reported the escape of the endogenous and exogenous unspliced pre-mRNAs from the nuclear surveillance mechanism to the cytoplasm (Hilleren and Parker, 2003b) (Kaida *et al.*, 2007) (Mayas *et al.*, 2010) (Yoshimoto *et al.*, 2017) (Carvalho *et al.*, 2017). This phenomenon likely results in the translation of escaped pre-mRNAs into the aberrant proteins (Figure 1.6). Introns are enriched with the translation termination signals which halt translation to produce truncated proteins. In the cytoplasm, these unspliced pre-mRNAs are primarily degraded by nonsense-mediated decay (NMD), a translation dependent RNA degradation mechanism targeting pre-termination codons (PTCs) containing RNA molecules. The cytoplasmic exosome and exonuclease Xrn1 plays an active role in NMD of unspliced pre-mRNAs (Isken and Maquat, 2008) (Kervestin and Jacobson, 2012). Exon junction complex (EJC) is deposited on the mRNA concomitant to splicing process near each of the exon-exon junctions. Although, according to the EJC dependent NMD model, PTCs are accepted to be distinguished from normal stop codon by its presence at least 50-55 bases upstream of the last EJC, the precise mechanism of NMD is still obscure (Popp and Maquat, 2013) (Brogna *et al.*, 2016). Cytoplasmic turnover provides a large fraction of the RNA surveillance activity to eliminate unspliced pre-mRNAs evidenced by extensive accumulation of unspliced pre-mRNAs upon NMD inactivation (Egecioglu and Chanfreau, 2011) (Carvalho *et al.*, 2017).

1.4 Splicing modulators as novel drugs and bioprobes

As pointed out above, the U2 snRNP is a fundamental subunit of the spliceosome that binds to the BPS during spliceosome assembly. U2 snRNP consists of U2 snRNA and seven Sm proteins, two protein subcomplexes; splicing factor 3a (SF3a) and splicing factor 3b (SF3b). They assist in the binding of U2 snRNP to pre-mRNA (Will and Lührmann, 2001). SF3b consists of SF3B1 (SAP155), SF3B2 (SAP145), SF3B3 (SAP130), SF3B4 (SAP49), SF3B5, SF3B14 and PHF5A.

Several small molecule compounds have been discovered as natural products or their derivatives that can modulate splicing efficiency in specific or general manner such as FR901464, meayamycin,

pladienolides, herboxidiene and other splicing modulators (Figure 1.7) (Kaida *et al.*, 2007) (Kotake *et al.*, 2007) (Mizui *et al.*, 2004) (Sakai *et al.*, 2002a, 2002b) (Albert *et al.*, 2007, 2009; Gao *et al.*, 2013) (Effenberger *et al.*, 2017). Many of splicing modulators have been observed to target the SF3b subunit of the spliceosome thereby modulating the splicing efficiency. One of them is FR901464 which was discovered as enhancer of SV40 promoter transcription during the quest of transcriptional regulators acting as a novel antitumor agent. Nakajima *et al.* isolated three compounds from *Pseudomonas* sp. i.e. FR901463, FR901464 and FR901465 which exhibited elevated transcriptional activity along with potent anti-tumor activities. FR901464 showed the strongest effect on the murine solid tumors as well as tumor cell lines *in vivo* at low nanomolar half-maximal inhibitory concentrations (IC_{50}). Cell cycle arrest was reported to be observed at G1 and G2/M phases (Nakajima *et al.*, 1996b) (Nakajima *et al.*, 1996a). Cell cycle regulatory protein cyclin-dependent protein kinase 2 (CDK2) along with cyclin E or A activates the G1 to S phase transition. p27, member of cell cycle regulator blocks the G1 to S phase transition by binding and inhibiting CDK2 complex. FR901464 induced the expression of c-terminally truncated form of p27 (represented as p27*) which plays a role to inhibit G1 to S phase transition at least partly. P27* is actually the translated product of first exon and first intron until the first in-frame stop codon of *CDKN1B* (Kaida *et al.*, 2007) (Satoh and Kaida, 2016). A more stable methyl ketal derivative of FR901464 showed similar activity to the parent compound and was shown to bind the SF3b complex and inhibit splicing. Hence it was dubbed spliceostatin A (SSA). SSA leads to weaker binding of U2 snRNP to the BPS, making weaker splice sites particularly sensitive to the compound (Corrionero *et al.*, 2011). Splicing process is inhibited by FR901464 and SSA prior to cleavage of both 5' and 3' phosphodiester bonds (Kaida *et al.*, 2007). In presence of SSA a subset of pre-mRNAs is exported to the cytosol (Kaida *et al.*, 2007) (Yoshimoto *et al.*, 2017).

A concurrent study on the *Streptomyces* natural product pladienolide B (PlaB) showed that this structurally unrelated molecule displayed activity, virtually indistinguishable from SSA's effect on the SF3b complex. Following discovery and mechanistic analysis of SSA and PlaB, several more molecules were identified or synthesized with similar effect. (Kotake *et al.*, 2007) (Albert *et al.*, 2009) (Hasegawa *et al.*,

2011). Therefore, it became possible for the first time to chemically inhibit mRNA splicing, allowing detailed studies not only into splice mechanisms but also into the physiological effect of splicing inhibition on RNA metabolism and gene regulation. More recently, cryoelectron microscopy (cryo-EM) of recombinant SF3B complex with SF3b inhibitors pladienolide B and E7107 has been revealed separately. The structure suggests a binding model in which SF3b inhibitor compound sits in the pocket locking the SF3B1 protein in an open and inactive conformation and hence prevent the binding of branch point adenosine (BPA) of pre-mRNA (Finci *et al.*, 2018) (Cretu *et al.*, 2018). However, extending similar studies with other splicing modulators and *in vivo* study seems essential to provide potential insights in therapeutics targeting splicing machinery.

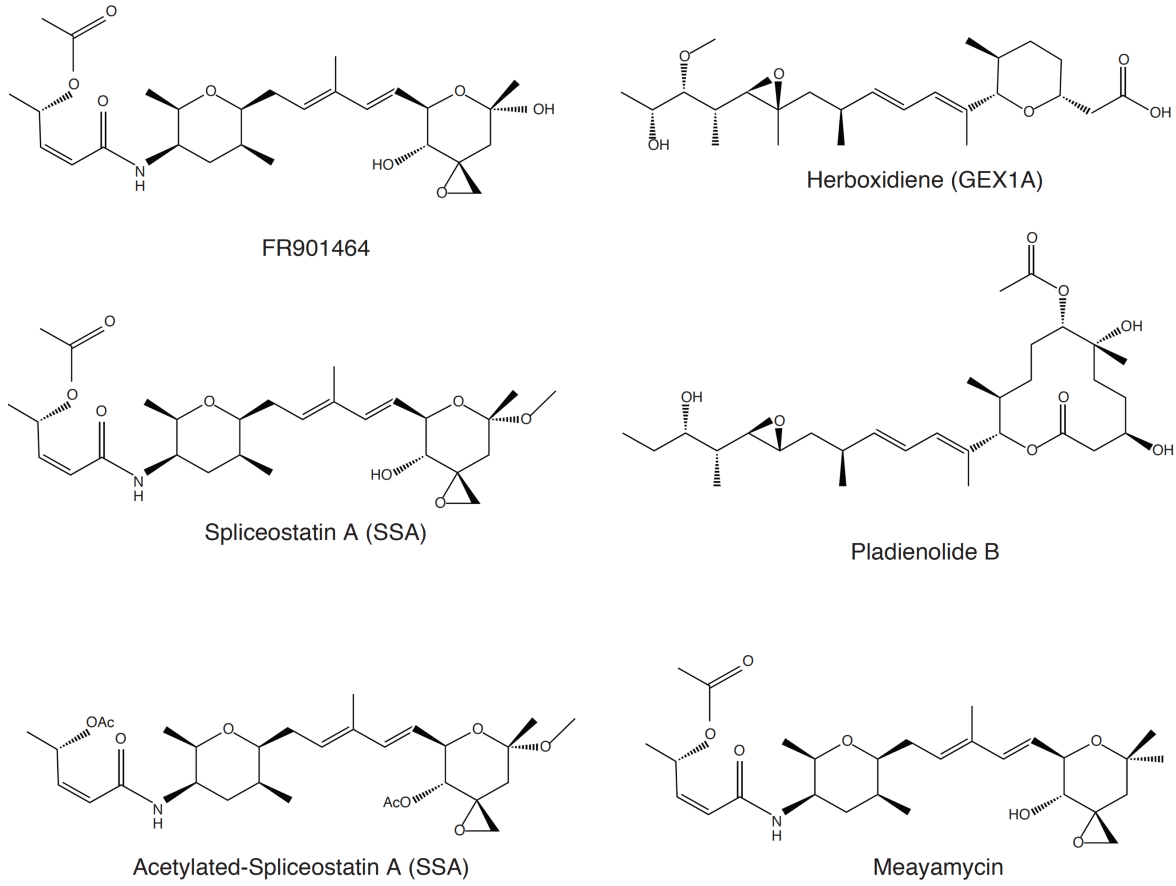

Figure 1.7 Structure of splicing modulators and their derivatives

1.5 Objectives of the study

Maintenance of integrity of proper gene expression is fundamental for cellular physiology, with mRNA splicing taking a particular prominent role (Hilleren and Parker, 2003a) (Shoemaker and Green, 2012). Studying the molecular mechanism and regulation of splicing and the fates of improperly spliced transcripts presents a means to understand a fundamental cellular process and its relation to disease.

With the observation of p27* it became clear that at least a subset of pre-mRNAs was exported to the cytoplasm and translated even though the transcripts should have been degraded via the non-sense mediated decay (NMD) pathway (Cheng and Maquat, 1993) (Lejeune *et al.*, 2003) (Kaida *et al.*, 2007) (You *et al.*, 2007) (Trcek *et al.*, 2013). Our study aimed at understanding which kind of mRNA would manage to circumvent quality control and how cells sense this aberrant translation. Additionally, we expect to understand which proteins beyond p27* might account for SSA's cellular activity and its specific toxicity to tumor cells.

Here I used SSA as a tool compound to monitor mRNA fate and protein productions.

Chapter 2 Translation of transcripts with retained introns

2.1 Background

Genome wide quantitative analysis of gene expression provides a comprehensive insight into the fundamental cellular response upon the alteration in the exogenous and endogenous factors. Various technologies based on hybridization and sequencing have been developed to study quantitatively the transcriptome. With the limitation of relying on existing information using the customized hybridization based approaches like micro-array analysis, RNA sequencing (RNA-seq) is the most recent approach for the genome wide transcriptome profiling using the deep sequencing technologies. It offers less background noise and extended range of detection. Importantly, it directly reveals the sequences offering classification of all the transcript species, including mRNAs, small RNAs and non-coding RNAs. Moreover, the technique is crucial to identify the novel transcript isoforms and analyze unknown genes (Wang *et al.*, 2009) (Hrdlickova *et al.*, 2017). Many of the genome-wide analyses of gene expression are measured by RNA-seq. However, transcript abundance often shows poor correlation with protein levels and translation regulation can greatly affect and alter the further expression of transcripts into the protein (Maier *et al.*, 2009) (de Sousa Abreu *et al.*, 2009) (Schwanhäusser *et al.*, 2011). Hence, advances in global proteomic profiling like mass spectrometry and more recently ribosome profiling provides the instant and comprehensive information on the total protein abundance and rate of cellular translation. This approach provides the best overview of proteome dynamics to date, encompassing gene-specific translation regulation rather than only monitoring transcript expression (Ingolia *et al.*, 2009) (Liu *et al.*, 2017).

Previous studies on transcription, splicing, translation or RNA quality control were limited by studying each process in isolation. With the advent of high-throughput sequencing-base methods, it has become possible to observe how perturbation in one system affects gene regulation on the whole. To monitor global changes in transcription and translation upon splicing inhibition by SSA, I set out to perform ribosome

profiling and RNA sequencing of HeLa S3 cell lysate after SSA treatment. While mRNA sequencing has become an established method for measuring gene expression, it actually only provides information on transcript sequence and transcript concentration. mRNA abundance by itself, however, is not a good indicator of gene expression as high transcript levels do not necessarily result in high protein output (Schwanhäusser *et al.*, 2011). Therefore, I combined my analysis with ribosome profiling to ascertain which messages actually reached the translation machinery. Additionally, inferences to the insights on how they are regulated upon splicing inhibition explain the functional cellular response in comprehensive manner. Individual reporter assay has been reported earlier that SSA induced expression of a C-terminally truncated version of the p27 cyclin-dependent kinase (CDK) inhibitor. The shortened protein, dubbed p27* is stable and biologically active in inhibiting CDK 2 (Kaida *et al.*, 2007). However, p27* production alone cannot account for all cellular effects observed upon splicing inhibition. This suggests that further many factors play a role in SSA's biological effect. Discovering those factors in global and comprehensive manner *in vivo* upon SSA is technically challenging. But, the application of recent technology, ribosome profiling is invaluable to address this limitation. Ribosome profiling is the relatively latest technique for the *in vivo* genome wide translatome study which employs deep sequencing of ribosome-protected mRNA fragments providing snapshot of all the active ribosomal positions under translation of particular transcripts in a cell at a specific time point. This technique is more powerful in the sense that it reveals what is being translated, when and how this translation is regulated, and where specifically it occurs (Ingolia *et al.*, 2014) (Brar and Weissman, 2015) (Ingolia, 2016). Genome-wide quantitative analysis of translation can be achieved with nucleotide resolution. It is an invaluable tool for measuring ribosome occupancy, elongation speed, translation efficiency, defining alternative translation initiation sites, and depiction of ORFs. Detail explanation of the technical procedure is explained in the material and method section (Figure 2.1 and 2.6).

Global transcriptome analysis upon different chemical inhibition of SF3B1 has been reported recently to understand the genome wide changes in transcript isoforms (Tseng *et al.*, 2015) (Yoshimoto *et al.*, 2017) (Wu *et al.*, 2018). Moreover, I have applied ribosome profiling technique as well as RNA

sequencing to retrieve even more comprehensive and clear picture of gene expression control in the genome-wide transcriptome as well as translation level upon the splicing inhibition by SSA. Moreover, normalizing ribosome footprints change to the change in mRNA reads, we can achieve the translation efficiency (TE) of each of the transcripts under the perturbed condition (detail explanation in next chapter) which can delineate the expression regulation of each of the transcripts hence providing concrete analysis and inferences. This chapter provides a novel insight to the fates of improperly spliced sub-group of transcripts upon chemical inhibition of SF3B1.

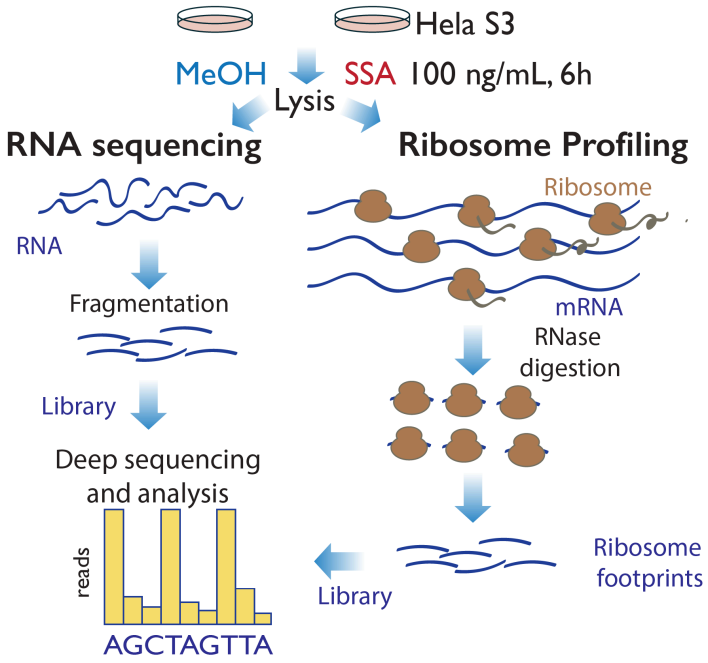

Figure 2.1 Schematic experimental design upon SSA challenge.

HeLa S3 cells were subjected to vehicle (MeOH) and SSA (100 ng/ml) for 6 hr before lysis. Library preparation for the total RNA extracted and simultaneously for the ribosome protected mRNAs were performed (as described in methods) and quantitative data were analyzed (as described in methods) after deep sequencing by HiSeq4000 (Illumina).

2.2 Results and discussion

2.2.1 Reproducibility and validity of RNA sequencing reads and ribosomal footprints

To monitor global changes in transcription and translation upon splicing inhibition by SSA, I set out to perform simultaneous ribosome profiling and RNA sequencing of HeLa S3 cell lysate after SSA treatment (Figure 2.1). I monitored transcript levels via RNA transcriptome sequencing, combined with ribosome profiling to ascertain which messages actually reached the translation machinery. RNA sequencing generated more than 100 million mapped reads (Table 2) and ribosome profiling generated 6-8 million mapped reads for each sample (Table 1). Two biological replicates of the methanol (MeOH) control compound showed high reproducibility of the RNA-Seq and ribosome profiling experiments (Pearson's r = 0.99 for both experiments) (Figure 2.2A). I observed the distinct hallmarks of ribosome profiling; the expected size of ribosome footprints with the major fraction of footprint length of 28 nt (Figure 2.2B) and the distinct three-nucleotide periodicity along the coding sequence (CDS) (Figure 2.2C and 2.2D) for the control and compound treated samples.

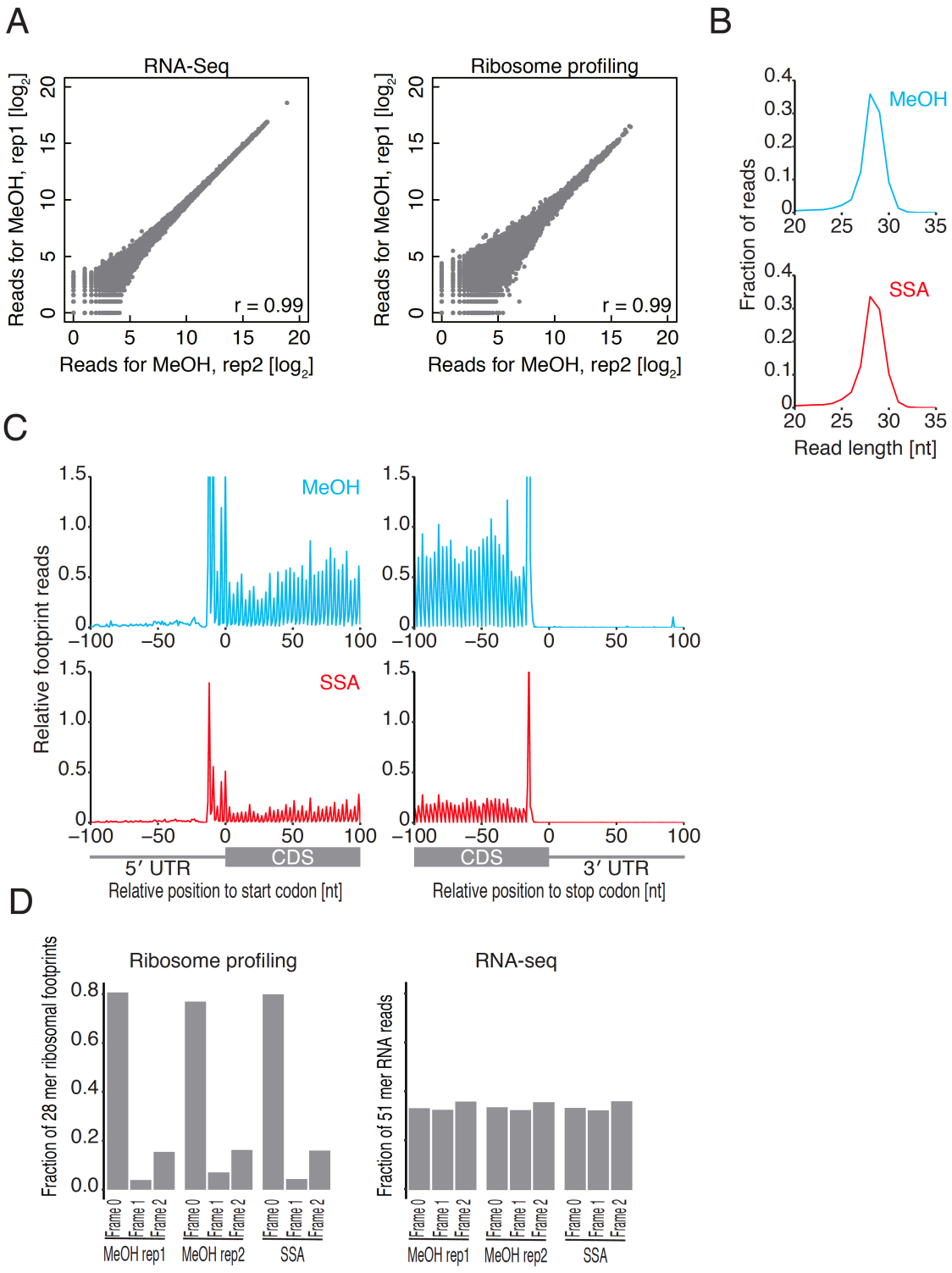

Figure 2.2 Reproducibility and validity of the RNA-seq and ribosome profiling experiment.

(A) High reproducibility of the RNA-seq and ribosome profiling experiment as shown by the Pearson correlation coefficient (r) between two independent experiments under vehicle treatment. (B) Fraction of ribosome footprint reads for the different length

of footprints. Maximum fraction of footprint reads was of 28 nucleotides. (C) Meta-gene analysis combining distribution of ribosome footprint density for all the coding sequences upon MeOH control and SSA around the CDS start (left panel) and stop codon (right panel). Reads are normalized to the sum of mitochondrial footprint reads. (D) Read distribution for the three different frames of open reading frame in ribosome profiling (left panel) and RNA-seq data (right panel) for MeOH and SSA. Example of 28 nucleotide long footprints reflect homogenous codon periodicity in ribosome profiling.

2.2.2 SSA induces global intron retention

Global intron retention was observed upon the splicing modulation by SSA. The assessment of alternative splicing modulation upon SSA in the RNA-seq data showed the differential effect on alternative splicing events where exon skipping and intron retention were the mostly affected events (Figure 2.3A), substantiating the result of previous studies on SF3b inhibitors (Kotake *et al.*, 2007) (Larrayoz *et al.*, 2016) (Yoshimoto *et al.*, 2017) (Vigevani *et al.*, 2017) (Wu *et al.*, 2018). Differential expression analysis by counting reads from introns (see Materials and Methods for details) confirmed that intron retentions was induced in a large variety of transcripts (Figure 2.3B). Meta-gene analysis combining the reads for sub-group of significantly upregulated introns also distinctly revealed the higher intron retention upon SSA (Figure 2.3C). Validating the intron retention by SSA for representative transcript *DNAJB1* by RT-PCR clearly showed the accumulation of unspliced products (Figure 2.3D). I am much interested to investigate how much fraction of these pre-mRNAs can actually reach the translation machinery globally after splicing inhibition. Hence, the ribosome profiling will be providing insights into it.

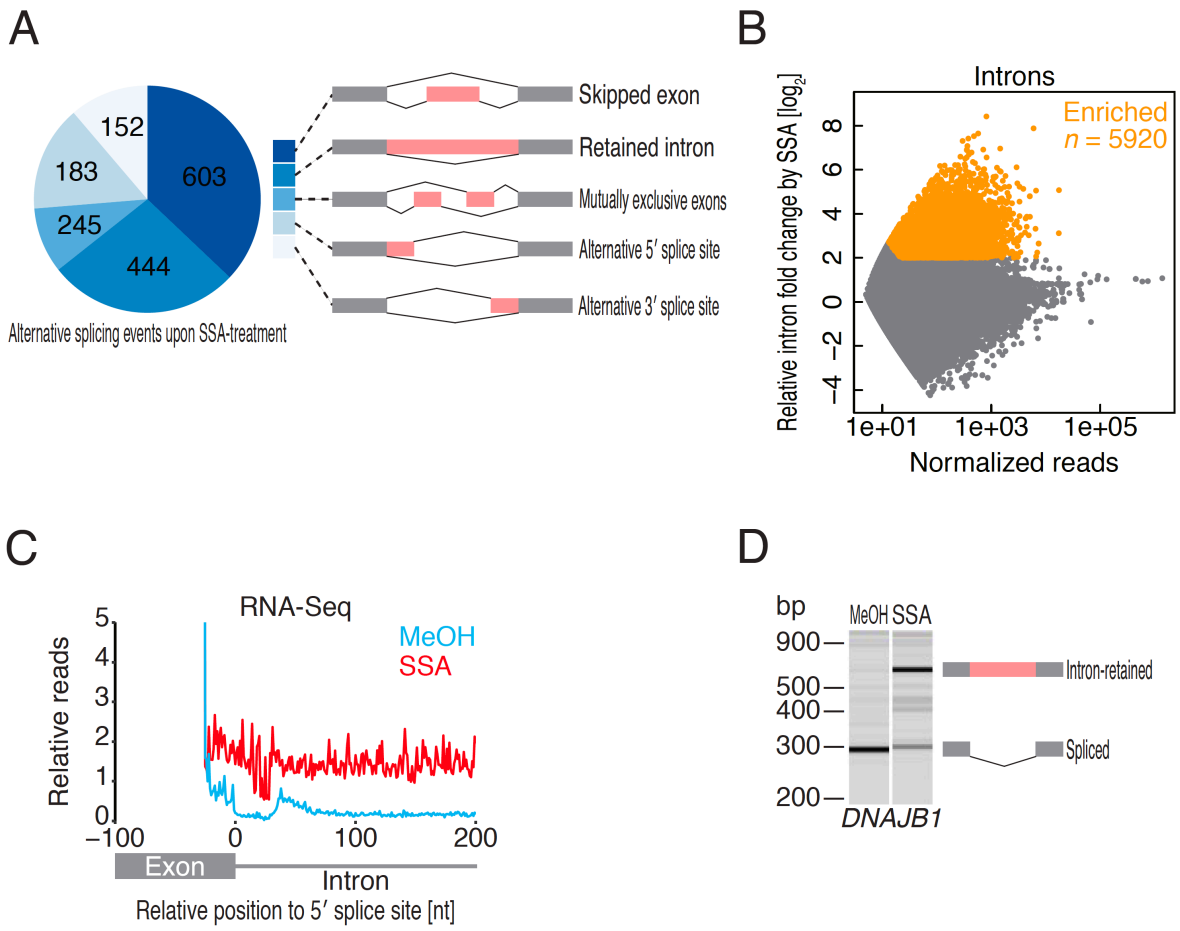

Figure 2.3 SSA induces global intron retention.

(A) Schematic representation of the major Alternative Splicing (AS) events and SSA-induced splicing modulation observed by transcriptome-wide analysis (see Materials and Methods for the detail). (B) Relative retained intron fold change by SSA in RNA-seq data. The significantly retained introns (adjusted p-value, FDR <0.01, fold change >2) were highlighted in orange colour. (C) Meta-gene analysis combining reads for intron retained subgroup of transcripts from RNA-seq were significantly higher following SSA treatment. The number of reads are normalized relative to the sum of exonic reads for 100 nucleotides upstream to the splice site. (D) RT-PCR analysis to detect spliced and unspliced forms of the gene, *DNAJB1*, a representative transcript using primers spanning for exon 2 and 3.

2.2.3 Subset of retained introns were translated under SSA treatment

Splicing modulation by SSA allows the translation of subset of retained introns. Among the 5920 significantly enriched introns upon SSA (Figure 2.3B), a subset of higher number of retained introns (>

1100) were subjected to translation (Figure 2.4A). This provides an evidence to the export of unspliced products and further translation. Our result supports many reports indicating the export of unspliced products along with the mature mRNAs to cytoplasm (Mayas *et al.*, 2010) (Yoshimoto *et al.*, 2017) (Carvalho *et al.*, 2017). The fates of these pre-mRNAs should primarily be NMD mediated degradation due to the presence of introns which are mostly enriched with pre-termination codons (PTCs) (Isken and Maquat, 2008) whereas the translation into truncated peptides is also inevitable (You *et al.*, 2007) (Trcek *et al.*, 2013). Moreover, from the meta-gene analysis combining distribution of footprint reads as well as investigating individual transcripts in the ribosome profiling data, we found that the translation ends at the first in-frame PTC of retained intron (Figure 2.4B and Figure 2.4C). Indeed, CDKN1B gene encoding the p27 tumor suppressor was translated along the first intron until the PTC which validates the previous observation for CDKN1B gene by reporter assay and generated truncated protein product (denoted as p27*) (Figure 2.4C, upper left panel, and Figure 2.4D) (Kaida *et al.*, 2007). These data demonstrated that mRNAs with retained introns could be exported into the cytoplasm and undergo translation until the premature termination codons generating truncated peptides.

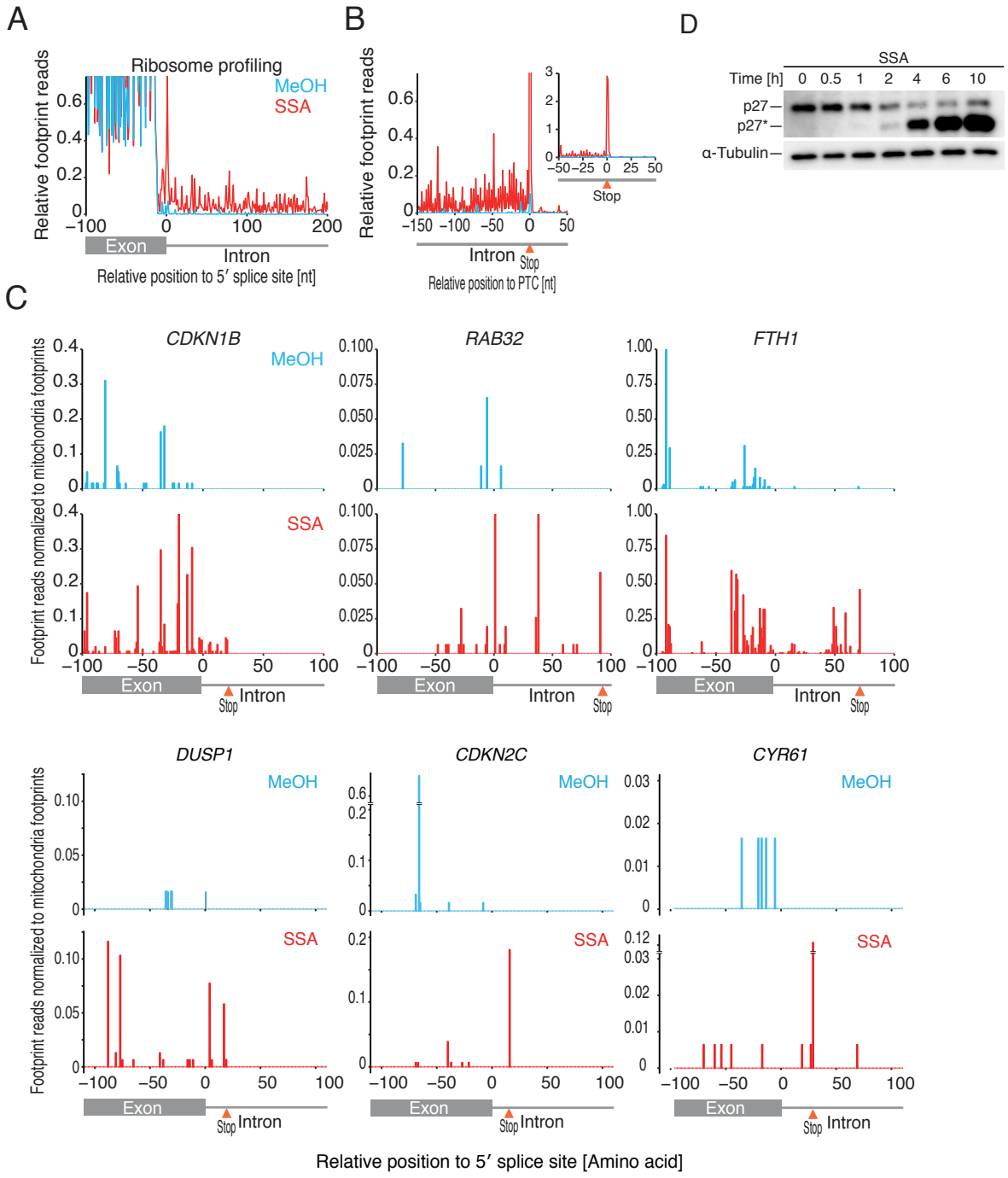

Figure 2.4 Subset of retained introns are translated until first in-frame PTC under SSA treatment.

(A) Meta-gene analysis combining ribosome footprint density relative to the 5' splice site for the 1106 introns, subset translated among the significantly enriched introns (Figure 2.3B). The reads are normalized relative to the sum of exonic reads for 100 nucleotides upstream to the splice site. (B) Meta-gene analysis of ribosome footprint density relative to the first in-frame pre-termination codon (PTC) of the translated introns. The reads are normalized relative to the sum of exonic reads for 100

nucleotides upstream to the splice site. (C) Individual examples of introns of transcripts under translation after splicing inhibition by SSA. Reads are normalized to the sum of mitochondrial footprint reads. (D) Immunoblotting of stable truncated protein p27* in HeLa S3 cell lines treated with 100 ng/mL SSA for different time periods (0, 0.5, 1, 2, 4, 6, 10 hr).

Furthermore, in agreement to exon skipping as another major effect on AS by SSA in transcriptome analysis (Figure 2.3A), we observed the clear decrease in ribosome footprints onto skipped exons during metagene analysis of those transcripts (Figure 2.5).

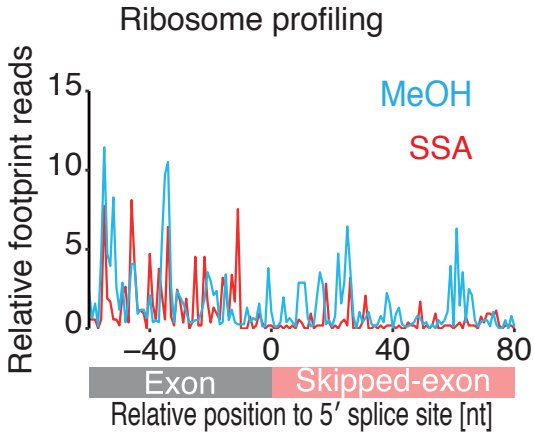

Figure 2.5 SSA also induce exon skipping.

Meta-gene analysis combining the ribosome footprints density relative to the exon-exon junction between 5' exon and skipped exon for the transcripts observed as SSA-induced skipped exon isoforms. The reads were normalized to the sequencing depth as reads per million (RPM).

2.3 Conclusion

The current data implies the RNA-seq and ribosome profiling as the highly efficient tool for global and comprehensive analyses of transcriptome and translatome respectively. I observed global retention of intron upon splicing inhibition by SSA and the subset among them were evidenced to be exported to cytoplasm since translation until the first in-frame PTC were observed for higher number of pre-mRNAs. Hence, the aberrant translation products are expected upon splicing inhibition mediating SSA-dependent toxicity.

2.4 Materials and methods

2.4.1 Compounds and cell culture

Compound SSA was solubilized in methanol. HeLa S3 cells was maintained in Dulbecco`s modified eagle medium (DMEM) supplemented with 10% heat inactivated Fetal Bovine Serum (FBS) in a humidified incubator at 5% CO_2 and 37˚C.

2.4.2 Ribosome profiling library preparation

HeLa S3 cells were treated either with SSA (100 ng/mL) or its solvent MeOH (control, replicates) for 6 hr before lysis. From cell lysis until the library preparation for the ribosome profiling and data analysis after sequencing by HiSeq4000 (Illumina) was performed as protocol optimized in Iwasaki lab modified from (Ingolia *et al.*, 2013) (McGlincy and Ingolia, 2017) (Iwasaki *et al.*, 2016) (Iwasaki, 2018). Schematic experimental approach is shown in (Figure 2.1). Stepwise method of preparing ribosome profiling library is described below (Figure 2.6).

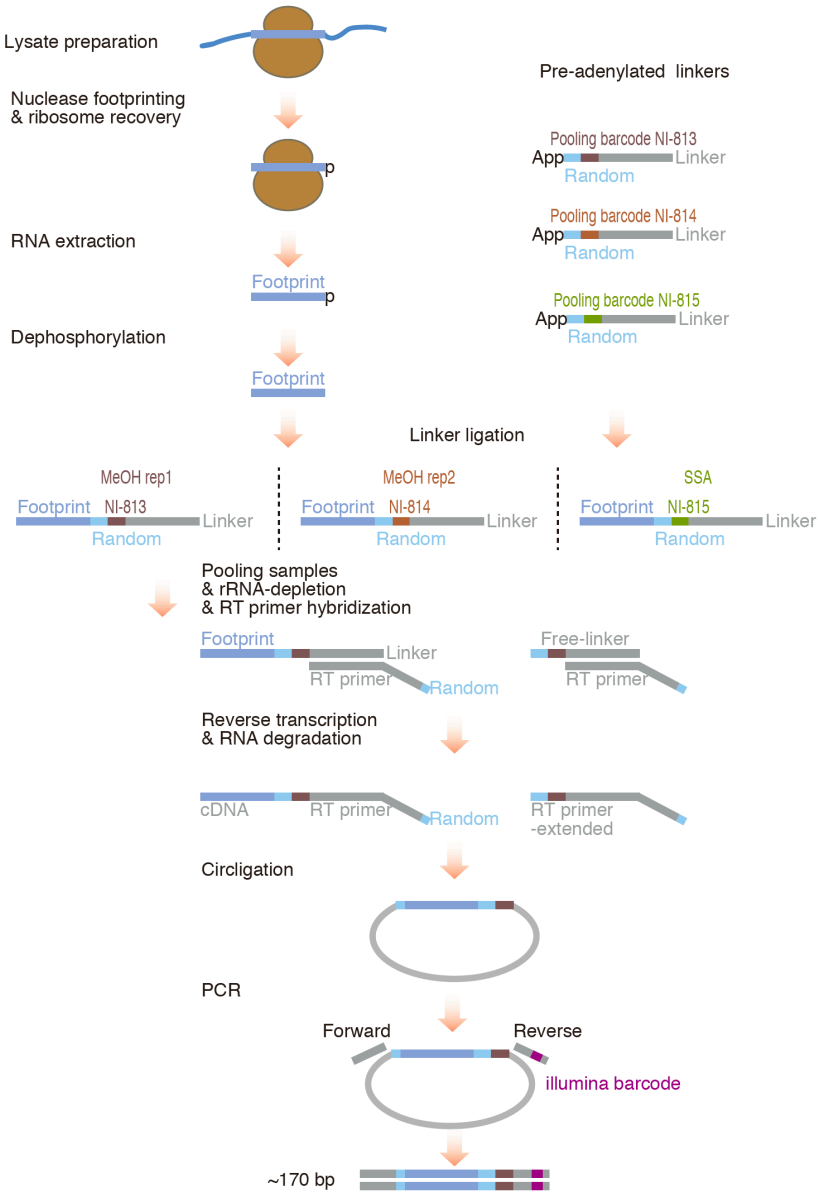

Figure 2.6 Schematic detail diagram of the ribosome footprinting protocol.

In general, cell lysate is nuclease digested and ribosome protected mRNA fragments are purified, adaptor ligated and reverse transcribed to generate the cDNA library which is subjected to deep sequencing and computational analysis (modified from (Ingolia *et al.*, 2013) (McGlincy and Ingolia, 2017) (Iwasaki, 2018)).

Preparation of cell lysate

Cell lysis was performed in-dish on ice after gentle wash by ice-cold PBS. Four hundred µL ice-cold lysis buffer (recipe as follows) was applied per 10 cm dish ensuring coverage of entire surface and cells were scraped down and transferred into microfuge tube. Two hundred µL of ice-cold lysis buffer was again added to the dish to rinse thoroughly and pool into the respective tubes. Individually, 7.5 µL of Turbo DNase I was added and incubated on ice for 10 min. Lysate was clarified by centrifugation at 20,000 x g for 10 min at 4˚C.

Lysis buffer

Component	Amount per run (µL)	Final in 5 ml
1 M Tris-HCl pH 7.5	100	20 mM
5 M NaCl	150	150 mM
1M $MgCl_2$	25	5 mM
0.1M DTT	50	1 mM
100 mg/ml cycloheximide	5	100 µg/ml
10% Triton X-100	500	1%
RNase-free water	4170	NA

Nuclease footprinting and ribosome recovery

Three hundred µL of lysate with 20 µg RNA was digested with 1 U/µg RNase I (Epicenter) at 25˚C for 45 min. Ten µL SUPERase-In (Invitrogen) was added to stop the nuclease digestion. Digestion was transferred to an ultracentrifuge tube before underlaying 0.90 mL of 1M sucrose cushion prepared immediately prior to use as follows. A visible interface between the layers were formed upon floating of lysate on top of sucrose. Ribosomes were pelleted by centrifugation in a TLA110 rotor at 100,000 rpm for 1 hr at 4˚C. The pellets were dissolved by 300 µL of TRIzol reagent (ThermoFisher Scientific) and purified using Direct-zol (Micro-prep, zymo-research).

Sucrose cushion (~8 samples)

Component	Amount per run (µL)	Final in 5 ml
1 M Tris-HCl pH 7.5	200	20 mM
5 M NaCl	300	150 mM
1M $MgCl_2$	50	5 mM
0.1M DTT	100	1 mM
100 mg/ml cycloheximide	10	100 µg/ml
sucrose	3.4 g	1M
20 U/ µl SUPERase.In	10	20 U/mL
RNase-free water	7130	NA

Footprint Fragment Purification

The purified RNA fragments were subjected to denaturing polyacrylamide gel electrophoresis (PAGE) using 15% TBE-Urea gel along with the RNA size marker lane with mixed 26 and 34 nucleotides markers NI801 and NI800 respectively (Figure 2.7). Gels were visualized staining with 1x SYBR Gold using transilluminator and RNA samples from size 26 to 34 nucleotides were excised from the gel and purified using isopropanol precipitation method. Three µl Glycoblue was used as co-precipitant, and 500 µl of isopropanol was used followed by chilling for 1 hr at -20ºC. RNA was precipitated at 20,000 g for 30 min at 4ºC. Further 150 µl of 70% ethanol wash was performed prior dissolving RNA and perform next reaction.

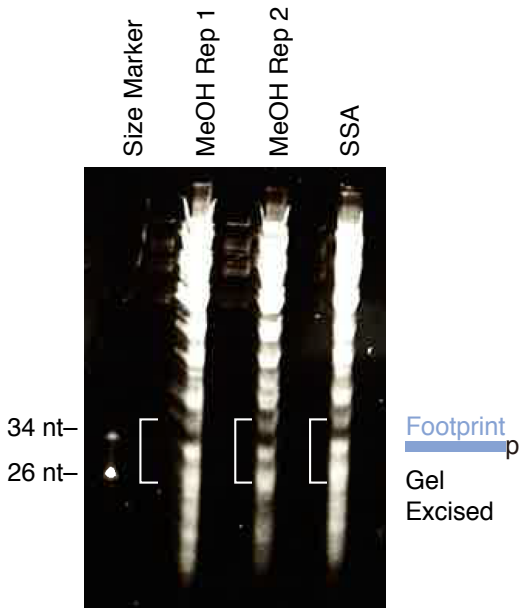

Figure 2.7 Ribosomal footprints from nuclease digested pellet in Hela S3 cell lysate.

Two biological replicates for the MeOH control and SSA treated cell lysates were separated using denaturing urea-PAGE. To prevent contamination, samples were loaded into the adjacent wells. NI-800 (34 nt) and NI-801 (26 nt) were used as RNA size marker ladders.

Dephosphorylation and Linker ligation

Next, the size-selected RNA samples were dephosphorylated applying T4 Polynucleotide kinase (PNK, New England Biolabs) to prepare RNA for ligation of the linker sequences with specific barcodes. Dephosphorylation reaction was performed at 37˚C for 1hr mixing following components.

Component	Amount per run (µL)	Final
RNA sample	7	NA
T4 PNK Buffer (10x)	1	1x
T4 PNK (10 U/ µL)	1	10 U
SUPERaseIN (20 U/ µL)	1	20 U

Linker ligation was performed in same tube upon completion of dephosphorylation reaction. Mixture components were as described below and incubated at 22˚C for 3hr.

Component	Amount per run (µL)	Final
50% (w/v) PEG-8000	7	17.5%
10x T4 RNA ligase buffer	1	1x
Preadenylated linker (20 µM)	1	1 µM
T4 Rnl2(tr) K227Q (200 U/µl)	1	100 U

Different linkers with specific barcode were used for each sample for further pooling.

Sample	Primer	Barcode	Oligonucleotide Sequence
MeOH rep1	NI-813	CTAGA	5´-/5Phos/NNNNNCTAGAAGATCGGAAGAGCACACGTCTGAA/3ddC/
MeOH rep2	NI-814	GATCA	5´-/5Phos/NNNNNGATCAAGATCGGAAGAGCACACGTCTGAA/3ddC/
SSA	NI-815	GCATA	5´-/5Phos/NNNNNGCATAAGATCGGAAGAGCACACGTCTGAA/3ddC/

"N" stands for any of the nucleotide.

The unreacted linker was separated from the ligated products by resolving ligated reaction samples after pooling onto denaturing PAGE (Figure 2.8). Ligated products are heavier in molecular weight which are excised from gel and purified using isopropanol purification method.

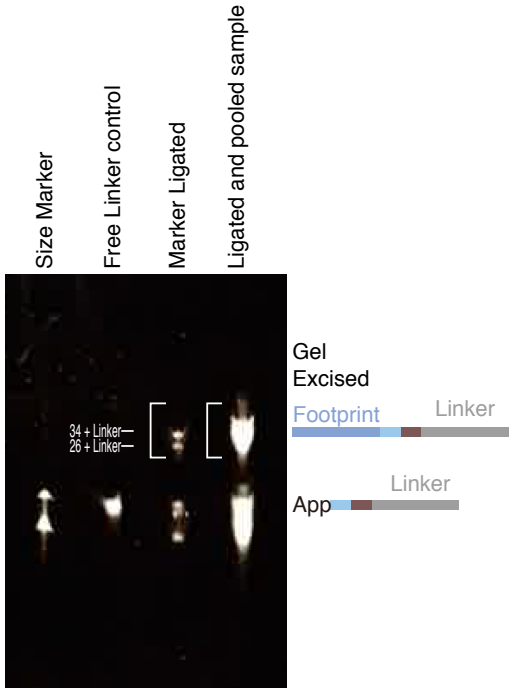

Figure 2.8 Linker ligation of ribosomal footprints

Ribosomal RNA depletion

Linker-ligated products were gel purified and ribosomal RNA (rRNA) depletion was carried out using Ribo-zero Gold rRNA removal kit (Illumina) following the manufacturer`s protocol with few modification. Firstly, 225 µL/reaction magnetic beads were washed and prepared. Then rRNA reduction reaction was performed combining as follows,

Component	Amount per run (µL)
RNA	26
Ribo-Zero reaction buffer	4
Ribo-zero rRNA removal solution	10

It was incubated at 68°C for 10 min and then leaved at RT for 5 min. Reaction was added to 65 µl beads and immediately mix and vortexed and incubated at RT for next 5 min. Reaction was put into magnetic stand and upon 1 min stand, supernatant was collected to a new tube on ice. RNA was then purified using Oligo Clean and Concentrator kit (Zymo research) according to the manufacturer`s instruction. Elution of RNA was done using RNase free water (10 µL) in the final step.

Reverse transcription

The rRNA depleted pooled footprint fragments were then reverse transcribed by preparing following reaction mixture and incubating at 50˚C for 30 min. After the reverse transcription reaction, RNAs were hydrolyzed by adding 2.2 µL 1M NaOH and incubating at 70˚C for 20 min. The cDNA was purified using oligo clean and concentrator kit and separated from unextended RT primer using denaturing PAGE (Figure 2.9).

Component	Amount per run (µL)	Final
RNA sample & NI-802 primer	12	NA
Protoscript II buffer (5x)	4	1x
dNTPs (10 mM each)	1	0.5 mM each
DTT	1	5 mM
SUPERase.In (20 U/µl)	1	20 U
Protoscript II (200 U/µl)	1	20 U

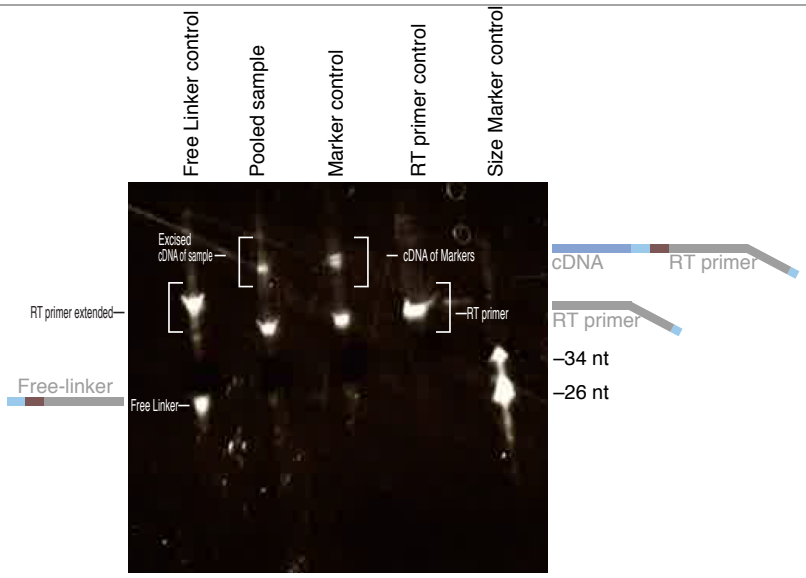

Figure 2.9 Reverse transcription of adaptor ligated ribosomal footprints

Circularization of cDNA

Circularization of cDNA was performed by making reaction mix as follows and incubating at 60˚C for 1hr. Heat inactivation of circligase was done successively at 80˚C for 10 min in a thermal cycler.

Component	Amount per run (µL)	Final
First strand cDNA	12	NA
CircLigase II buffer (10×)	2	1×
Betaine (5 M)	4	1 M
$MnCl_2$ (50 mM)	1	2.5 mM
CircLigase II (100 U/µl)	1	100 U

PCR Amplification

PCR amplification of ribosome profiling library was performed with the circularized cDNA template for varying number of cycles as 6, 8, 10, 12 and 14 cycles using following PCR reaction and cycling conditions. Cycle 10, 12 and 14 showed the prominent library size band upon gel electrophoresis on a 15% polyacrylamide non-denaturing gel which was excised and recovered from gel for further quality check (Figure 2.10).

Component	Amount per run (µL)	Final
Phusion HF buffer (5×)	20	1×
dNTPs (10 mM each)	2	0.2 mM each
Forward Primer NI798 (100 µM)	0.5	500 nM
Reverse Primer NI799 (100 µM)	0.5	500 nM
Circularized cDNA template	5	NA
Nuclease free water	71	NA
Phusion polymerase (2 U/µl)	1	2U

Temperature	Time	Cycle
98˚C	30 s	1×
98˚C	10 s	6,8,10,12,14×
65˚C	10 s	
72˚C	5 s	
4 ˚C	-	1×

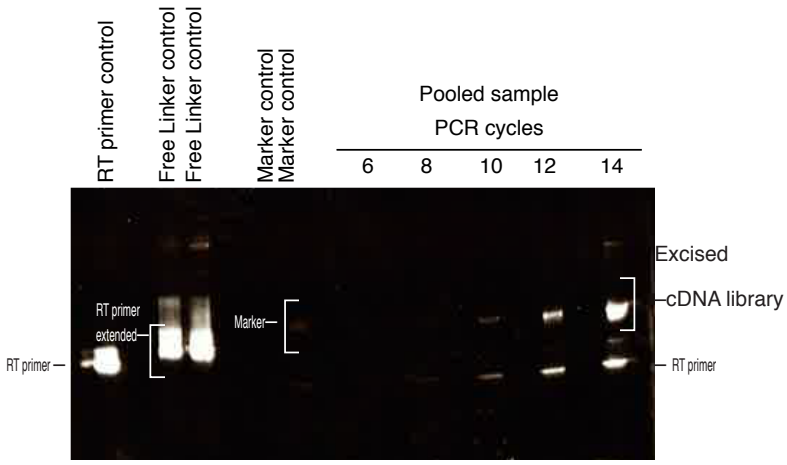

Figure 2.10 PCR product of pooled cDNA library

Library Quality check

Before library was used for next generation sequencing, the quality of purified ribosome footprint fragment library from 14 cycle of PCR product was checked using Multi-NA microchip electrophoresis system (Bioanalyzer, Shimadzu). The perfect library size of 171 bp was observed (Figure 2.11).

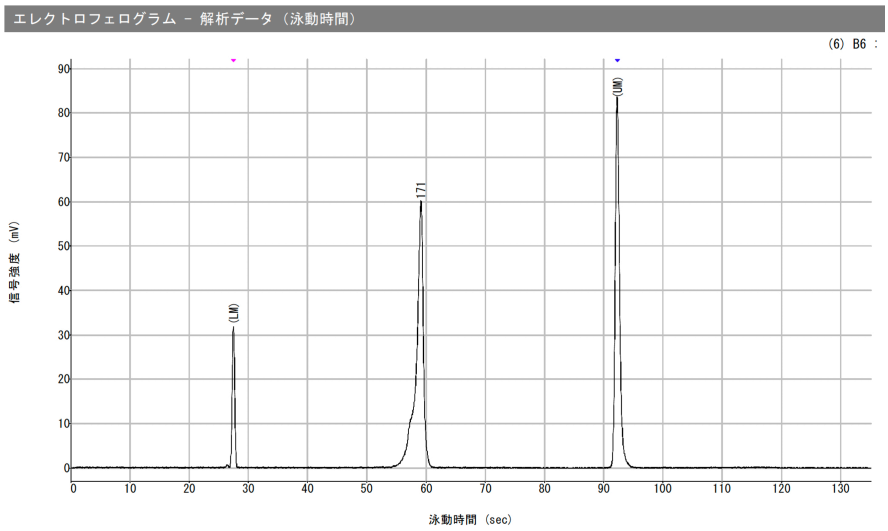

Figure 2.11 Multi-NA microchip electrophoresis system (Shimadzu) showing the chromatogram of pooled ribosome footprint fragment cDNA libraries.

The average length of the fragments is 171 bp (concentration = 8.61 ng/μL). LM and UM corresponds to the lower and upper molecular weight markers, respectively.

Primer List for ribosome profiling

Primers	Sequence
NI798	5'-AATGATACGGCGACCACCGAGATCTACACTCTTTCCCTACACGACGCTC
NI799	5'-CAAGCAGAAGACGGCATACGAGATCGTGATGTGACTGGAGTTCAGACGTGTG
NI800	5'-AUGUACACUAGGGAUAACAGGGUAAUCAACGCGA-(Phos)
NI801	5'-AUGUUAGGGAUAACAGGGUAAUGCGA-(Phos)
NI802	5´(Phos)NNAGATCGGAAGAGCGTCGTGTAGGGAAAGAG(iSp18)GTGACTGGAGTT CAGACGTGTGCTC (Phos) indicates 5'-phosphorylation, (iSp18) indicates a hexa-ethyleneglycol spacer and Ns represent random nucleotides

Next generation sequencing and bioinformatics analysis

The footprint libraries were sent for sequencing on an Illumina Hiseq4000 at sequencing facility in the University of California, Berkeley. The workflow followed for the data analysis is as showed in (Fig 2.12) (Dr. Shintaro Iwasaki).

Figure 2.12 Overview of the bioinformatics workflow/pipeline for ribosome profiling sequence analysis.

To the raw Fastq sequence after Illumina sequencing, the trimming of a common 3′- adaptor sequence (AGATCGGAAGAGCACACGTCTGAA) that was linked to specific multiplexed index oligos containing ribosome footprints was firstly done using fastx_clipper and then demultiplexed sample-wise accordingly along with the ligated barcodes. We then used Bowtie 2 (Langmead and Salzberg, 2012) to map the clipped reads to a human rRNA, tRNA, snoRNAs and microRNA reference database and captured un-aligned reads only. They were aligned and mapped to the human genome (hg19; known reference genes from University of California, Santa Cruz (UCSC)) using Tophat (Trapnell *et al.*, 2009). The PCR duplicated reads were suppressed based on random barcodes in reads. Empirical estimation of nucleotides on ribosomal A-site were done on the basis of footprint length. The A-site offsets were 15 for 27-28 nt and 16 for 29-31nt ribosomal footprints. I obtained 6-8 M mapped footprint reads per sample (Table 2.1). I used fp-count (*https://github.com/ingolia-lab/RiboSeq/blob/master/riboseq.cabal*) to compute read counts that mapped

uniquely to the reference sequence and calculated relative gene enrichment using DESeq upon SSA perturbed condition (Anders and Huber, 2010). Re-normalization of the calculated –fold change to the total mitochondrial footprints as the internal standard was done (Iwasaki *et al.*, 2016) (McGlincy and Ingolia, 2017).

Table 2.1 Statistics of sequence analysis of ribosome profiling library pool

Sample	Filterized raw reads	Ribosomal footprint reads	percentile	rRNA depleted reads	percentile	mapped to genome	percentile	Final reads after duplication removal	percentile
MeOH rep 1	359845289	47150981	13.10	17455860	37.02	15607861	89.41	7954957	50.97
MeOH rep 2		51690383	14.36	15764855	30.50	13980599	88.68	6867761	49.12
SSA		58639913	16.30	13910024	23.72	11814724	84.94	6177425	52.29

2.4.3 RNA sequencing library preparation and analyses

The same lysate that was used for ribosome profiling library preparation was simultaneously used for preparing RNA sequencing library. Total RNA was extracted using Trizol LS (3 volumes) and purified by Direct-zol RNA Kits (Micro-prep, zymo-research). The library was prepared by some modification in TruSeq Stranded mRNA Library Prep kit (Illumina) as follows.

Ribosomal RNA depletion

Ribosomal RNA was removed using Ribo-zero kit (Illumina, steps followed were as described above in ribosome profiling library preparation). rRNA reduction reaction was performed combining as follows,

Component	Amount per run (µL)
RNA	1µg
Ribo-Zero reaction buffer	4
Ribo-zero rRNA removal solution	8
RNase-free water	µl
	40 µl

RNA purification

RNAclean XP beads was used for purification of rRNA depleted RNA. Fragment prime Finish Mix was thawed on ice. The required amount of mixing is as follows,

Component	Amount per run (µL)
Sample after rRNA depletion	90
1.8 × RNAclean XP beads	160
	250 µl

Tubes with the mixture was incubated at RT for 5 min and put onto magnetic stand at RT for another 5 min. Supernatant was cleared away after then. Beads were washed slowly taking care of dislodgement placing on the magnetic stand by 80% ethanol (200 µl). Supernatant was discarded. This washing process by 80% ethanol was performed three times. Finally, ethanol was completely discarded. 19.5 µl of Fragment Prime Finish Mix was used to elute purified RNA, beads were mixed well by either vortex or pipetting and incubating at RT for 2 min. Tubes were placed onto magnet stand for next 5 minutes. 17 µl of the elutes were transferred to the new PCR tubes to prepare for subsequent reaction.

Fragmentation and First Strand cDNA synthesis

First Strand Synthesis ActD Mix was thawed on ice. 17 µl of each of purified RNA was denatured at 94 ˚C for 8 min and subsequently incubated at 4 ˚C for 5 min. Immediately following synthesis mixture was prepared and individually 8 µl was dispensed on to the denatured purified RNA.

Component	Amount per run (µL) × 1
First Strand Mix	7.2
Protoscript II	0.8
	8 µl

All the sample mixtures were well mixed and subjected to the following first strand cDNA synthesis reaction condition.

25 ˚C	10 min
42 ˚C	50 min
70 ˚C	15 min
4 ˚C	∞

Second Strand cDNA synthesis

Second Strand Mix was thawed on ice and following reaction mixture and condition were used for the second strand cDNA synthesis.

Component	Amount per run (µL) × 1
First Strand cDNA	25
Second Strand Mix	25
	50 µl

16 ˚C	**60 min**
25 ˚C	∞

AMPure beads was used to purify the second strand cDNA. Following mixture was prepared and kept at RT for 15 min.

Component	Amount per run (µL) × 1
Second Strand cDNA	50
AMPure beads	90
	140 µl

Mixture tubes were placed onto magnet stand and the supernatant was discarded. While in the magnet stand, beads were washed by 200 µL 80% ethanol taking care not to break or dislodge them. After each 30s incubation, ethanol was discarded and washing was repeated thrice in total. Finally, elution was performed by 52.5 µL resuspension buffer at RT for 5 min. 50 µL of elute was used for End repair reaction to be done next.

End Repair

End Repair Mix was thawed on ice and following reaction condition was used for the end repair of the cDNA synthesized.

Component	Amount per run (µL) × 1
Purified Second Strand cDNA	50
Resuspension Buffer	10
End Repair Mix	40
	100 µl

The mixture was incubated at 30 ˚C for 30 min followed by AMPure bead purification as mentioned above. Final elution was done by 17.5 µL of resuspension buffer.

Adenylate 3′ End

A-tailing Mix was thawed on ice and A-tailing reaction was prepared and performed as follows.

Component	Amount per run (µL) × 1
End Repair cDNA	15
Resuspension Buffer	2.5
A-tailing Mix	12.5
	30 µl

37 ˚C	30 min
70 ˚C	5 min
4 ˚C	∞

Immediately next, adaptor ligation was performed.

Adaptor ligation

Stop Ligation buffer and Adapter index were thawed on ice. Ligation reaction was carried out as follows.

Component	Amount per run (µL) × 1
Adenylated 3′ End cDNA	30
Resuspension Buffer	2.5
Ligation Mix	2.5
Adapter Index	2.5
	37.5 µl

Samples	Adapter Index used
MeOH Rep 1	Index 2 (CGATGT)
MeOH Rep 2	Index 5 (ACAGTG)
SSA	Index 4 (TGACCA)

Different adapter indices were used for different samples as listed above. The mixture was incubated at 30 ˚C for 10 min followed by stopping of ligation reaction by 5 µl of Stop Ligation Buffer. Adaptor ligated and 3′ end adenylated cDNA library was finally purified with the AMPure beads for two times and ~20 µl of eluted library was tested by Multi-NA microchip electrophoresis system to show the valid chromatogram of RNA-seq library of ~ 255 bp (Fig 2.13). Raw data analysis was performed as for ribosome profiling (Fig 2.12). Splitting by barcode was not required since samples were not pooled during RNA-sequencing.

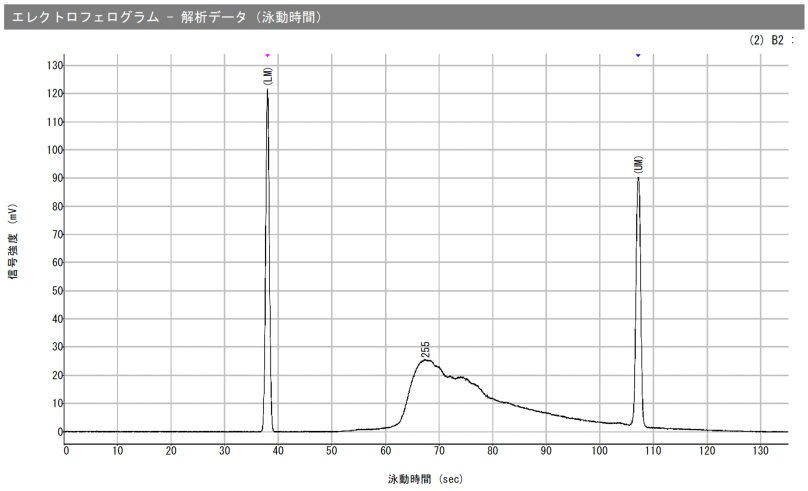

Figure 2.13 Multi-NA microchip electrophoresis system (Shimadzu) showing the chromatogram of RNA-seq library for control treated cell lysate cDNA library.

The average length of the fragments is 255 bp (concentration = 14.88 ng/μL). LM and UM corresponds to the lower and upper molecular weight markers, respectively. Similar chromatogram was observed for replicates and compound treated RNA-seq libraries too.

RNA sequencing generated more than 100 million mapped reads for the control and compound treated samples (Table 2).

Table 2 Statistics of sequence analysis of RNA-seq library pool

sample	Total reads	Filterized/Clipping adaptor	percentile	rtRNA depleted	percentile	mapped to genome	percentile
MeOH rep1	137442826	128194953	93.27	127899489	99.770	121652672	95.12
MeOH rep2	114425767	106686442	93.24	106310358	99.647	100956252	94.96
SSA1	133995415	124429245	92.86	123843128	99.529	116177056	93.81

MISO (Mixture-of-Isoforms), a probabilistic framework was used to assess differential major alternative splicing events upon splice inhibition using the human (hg19) alternative event annotations of splice events in GFF3 format downloaded from MISO annotation page (Katz *et al.*, 2010). To identify SSA regulated events using MISO framework, I used the following filtering criteria: (i) Both inclusion and exclusion reads is ≥ 1 such that (ii) the sum of inclusion and exclusion reads ≥ 10 and (iii) the absolute value of the difference for percent spliced in (ΔPSI) between vehicle and SSA is ≥ 0.2 (iv) the bayes factor is ≥ 10. Particularly for the differential intron expression analysis, I have used DESeq (Anders and Huber, 2010) using the UCSC bed file for introns based on the mapping of reads onto them. Following criteria was setup for the assessments: (i) reads ≥ 5 (ii) introns within the ORF were considered (iii) 5' splice sites with MAXENT (splice site) score > 2.5 were used to minimize the background and (iv) transcripts were finally normalized to the library size and the sum of total intronic and CDS reads.

2.4.4 Antibodies and immunoblotting

Antibodies against α-tubulin (B-5-1-2) was purchased from Sigma. Mouse monoclonal antibodies against p27 (KIP1) was bought from BD Transduction Laboratories. The equal volume of lysate was dissolved in 2× SDS-PAGE sample buffer and denatured at 100˚C for 10 min. Equal amounts of protein lysates were resolved using SDS-PAGE. Semi-dry transfer of protein onto polyvinylidene difluoride

membrane (PVDF, Millipore) membranes was done by electroblotting. Membranes were incubated to the primary and secondary antibodies consecutively with Tween-TBS (TBST) wash in between. So, formed immune complexes were detected using the Immobilon Western Chemiluminescent HRP substrate (Millipore) and luminescence was analyzed using a LAS-4000 image analyzer (GE Healthcare).

2.4.5 RT-PCR analysis

HeLaS3 cells were treated with 100 ng/mL SSA, 100 ng/mL pladienolide B or their vehicle for 6 hr and 10 hr separately. Cell lysis was performed using ribosome profiling lysis buffer with 1% Triton-X (without cycloheximide). Then, total RNA was extracted using Trizol LS (ThermoFisher Scientific, 10296010) and purified by Direct-zol RNA Kits (Micro-prep, zymo-research, R2062) as mentioned before. Six hundred and thirty nano gram total RNA was annealed to random 9 mer primer (TAKARA, 3802) at 65˚C for 5 min and reverse-transcribed using protoscript reverse transcriptase (protoscript II) (New England Biolabs, M0368L), same as a step of reverse transcription during ribosome profiling library preparation. PCR was performed on equal volume of the acquired cDNA from RT reaction in 25 µL of reaction mixture applying PCR PrimeSTAR Max Premix (2 ×) (TAKARA, R045) and 0.8 µM of each primer of the appropriate pair. All the primers were purchased from Eurofins as follows.

Gene	**Location**	**Primer sequences** (Kotake *et al*., 2007)
DNAJB1	Exon 2	GAACCAAAATCACTTTCCCCAAGGAAGG (fwd)
	Exon 3	AATGAGGTCCCCACGTTTCTCGGGTGT (rev)

PCR conditions were 98˚C for 3 min; 35 cycles of 98˚C for 10 s, 52˚C for 15 s and 72˚C for 60 s; followed by 72˚C for 3 min. PCR products were visualized by Bioanalyzer MultiNA system using DNA-1000 separation buffer and SYBR gold.

Chapter 3 Differential expression analysis upon SSA reveals inhibition of translation

3.1 Background

Research related to life science and disease has been revolutionized by novel techniques utilizing the Next Generation Sequencing (NGS) bringing up the huge information which were not possible before. The data observed from combination of these techniques have distinct ability to distinguish the gene regulation mechanism either in the transcriptional or translational level. Ribosome profiling better correlates with the protein abundance rather than with mRNA levels. Ribosomal density on a transcript reflects the amount of encoded proteins made since each footprint designates a single ribosome translating the message to protein (Ingolia, 2016) (Liu *et al.*, 2017). However, inferring as translational changes by only quantitating ribosome footprint density may produce an artifact since the changes may have been arising from transcript isoform differences rather than translational changes. Hence, simultaneous analysis of transcriptional and translational changes must be taken into account to delineate the regulation effects and to minimize the possible artifacts from the transcriptional changes (Figure 3.1) (Weinberg *et al.*, 2016) (Ingolia, 2016).

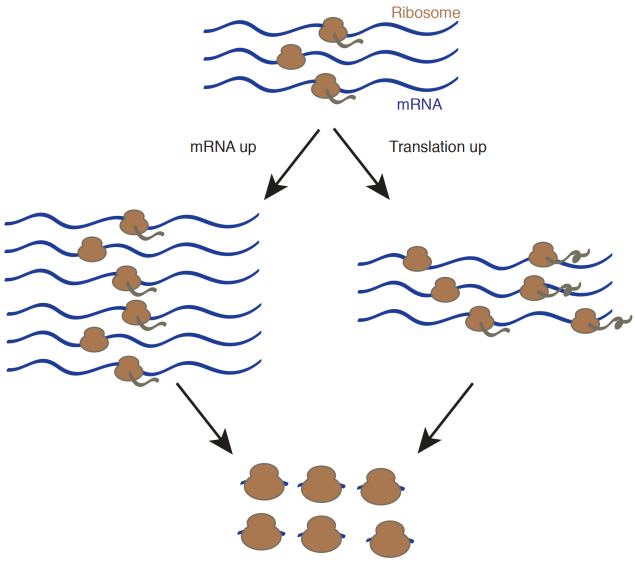

Figure 3.1 Schematic representation of alteration in ribosome footprint density under higher mRNA abundance or increased translation condition.

The translational efficiency (TE) of each of the individual transcripts offers the effect of the ribosomal footprint density change from ribosome profiling against the transcript abundance from RNA-seq as a baseline. So, the observed change is restricted to the translational control. The effect of individual factor such as drug treatment here in this case can be fit into the generalized linear model (GLM) framework to analyze the transcriptional and translational changes inferences (Ingolia, 2016). These models provide statistical inferences to the effects of individual factors such as drug treatment in multi-factor experimental design along with potential interaction between these factors (McCarthy *et al.*, 2012). In our analysis, factor is library type, hence the GLM depicts the translational efficiency of a transcript as the effect of the "ribosome profiling" library type against the "RNA-seq" baseline, and translational control is indicated by significant interactions with experimental variables (Ingolia, 2016) (Calviello and Ohler, 2017).

Many downstream metabolic events are affected upon splicing modulation. Splicing is essential for the efficient transport of mRNAs (Reed, 2003). Splicing modulation by SSA has been reported to affect the subcellular distribution of mRNAs. The fraction of unspliced mRNAs gets accumulated and retained inside the nucleus upon SSA treatment although subset of them make their way to cytoplasm (Kaida *et al.*, 2007) (Yoshimoto *et al.*, 2017) (Carvalho *et al.*, 2017). Subsequently, the effects on the localization of pre-mRNA, export of mRNAs to the cytoplasm, turnover of transcripts etc. upon splicing inhibition are expected to influence the translation process. It would be interesting to understand if translational control is being regulated along with these changes upon splicing modulation. In this chapter, translational efficiency change for the individual transcripts and per genome wide case will be explored along with their functional aspects.

3.2 Results and discussion

3.2.1 SSA strongly affects global translation

To understand the impact of the splicing inhibition on transcriptome and translatome, further analysis of RNA-seq and ribosome profiling data was carried out. Read counts from the deep sequencing require proper normalization before drawing the inferences since greater sequencing depth for any of the

sample yields more counts for each of the genes. Typically, the library size factor is used relying on the assumption of similar expression of the most genes between different samples (Bullard *et al.*, 2010). More recently, it has been shown that during the broad expression change the normalization to the library size actually does not sound relevant and normalization utilizing spike-in RNA standard makes more sense (Lovén *et al.*, 2012). The signal from the same amount of synthetic RNA included early during library preparation is used to normalize the read counts between samples (McGlincy and Ingolia, 2017). Moreover, mitochondrial ribosomal footprints can be used as internal spike-ins for the ribosome profiling if mitoribosomes are not affected by the perturbation to be studied (Iwasaki *et al.*, 2016) (McGlincy and Ingolia, 2017). Here I also used mitochondrial ribosomal footprints as internal spike-ins to normalize the overall translation change since SSA has not been reported to affect mitochondrial translation. It provides relatively robust control over the normalization by sequencing depth only leading to more accurate quantitation of expression fold change for each of the transcripts (McGlincy and Ingolia, 2017) (Ingolia, 2016) (Iwasaki *et al.*, 2016). Translation was observed to be much more strongly inhibited by SSA than one would have anticipated by the changing levels of mRNA abundance alone (Figure 3.2A, Figure 2.2C). Nascent peptide labeling using O-Propargyl-puromycin (OP-puro) and following fluorophore conjugation by CLICK reaction (see methods for detail) (Liu *et al.*, 2012) (Iwasaki and Ingolia, 2017) further supported the strong effect of SSA on global translation (Figure 3.2B and 3.2C).

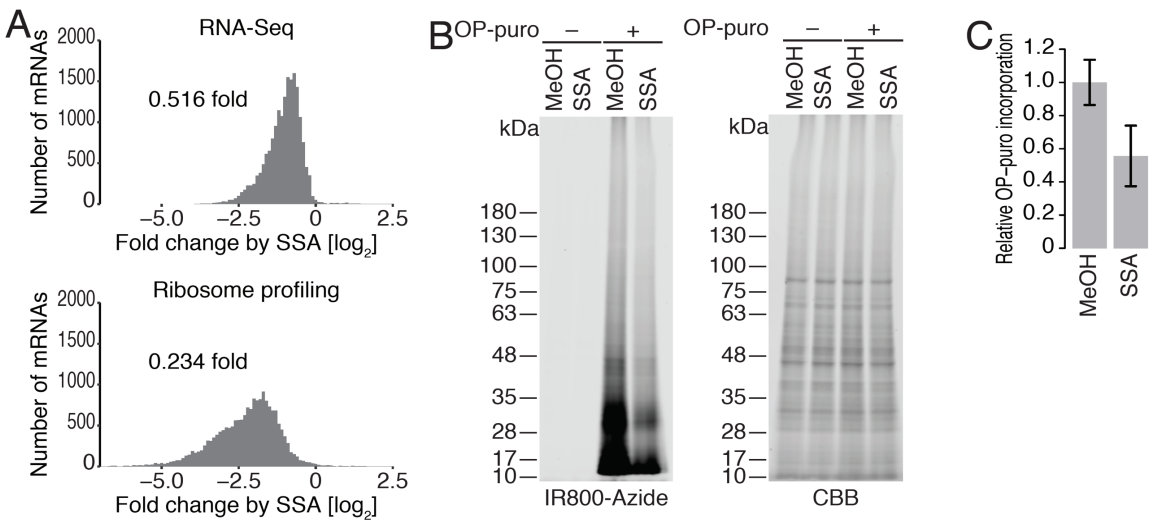

Figure 3.2 Global translation was strongly affected upon SSA.

(A) Histogram of transcription-fold change by RNA sequencing (upper panel) and histogram of ribosome footprint fold change by ribosome profiling (lower panel) when cells were treated with 100 ng/mL SSA for 6 hr compared to MeOH (vehicle), normalized to the number of reads for mitochondrial transcripts. Median-fold change is shown. Bin width is 0.1. (B) Change in translation activity upon SSA treatment in HeLa S3 cells monitored by nascent peptide labeling with OP-puro. Nascent peptides with incorporated OP-puro were visualized by click reaction with azide conjugated IR-800 dye (LI-COR) (representative lanes) (n=3) and (C) quantification of the IR signal intensity was performed by Image studio ver 5.2 (LI-COR Biosciences). Data represent mean and s.d. (n=3).

3.2.2 Differential gene expression analysis upon SSA reveals sensitivity of ribosomal protein translation independent of splicing

Global translation decreases upon splicing inhibition led me to explore individual mRNAs differentially affected by SSA in translation and their functional implications associated with. Translational efficiencies (TEs) for each of the transcripts were calculated by taking the ratio of ribosome footprints counts over the RNA-seq read counts. Indeed, differential TE change across transcripts reflected higher number of significantly downregulated mRNAs (n=124) as compared to the significantly upregulated ones (n=57) (Figure 3.3A). Implication of functional pathways on the basis of TE change would uncover the effect on the major functional pathways upon change in translation after splicing inhibition. Therefore, investigation

of the pathway enrichments in Kyoto encyclopedia of genes and genomes (KEGG) revealed ribosome, tight junctions, the mTOR pathway, and the cell cycle as sensitive transcripts (Figure 3.3B, Appendix 1 and 2). Similar terms were confirmed in gene ontology (GO) analysis (Figure 3.3C). Also, significant decrease in cumulative fraction of TE change by SSA for the cytosolic ribosome transcripts validate the pathway enrichment analysis (Figure 3.3D). These analyses infer that the reduction of ribosomal protein synthesis is one of the reason for the global translation repression (Figure 3.2).

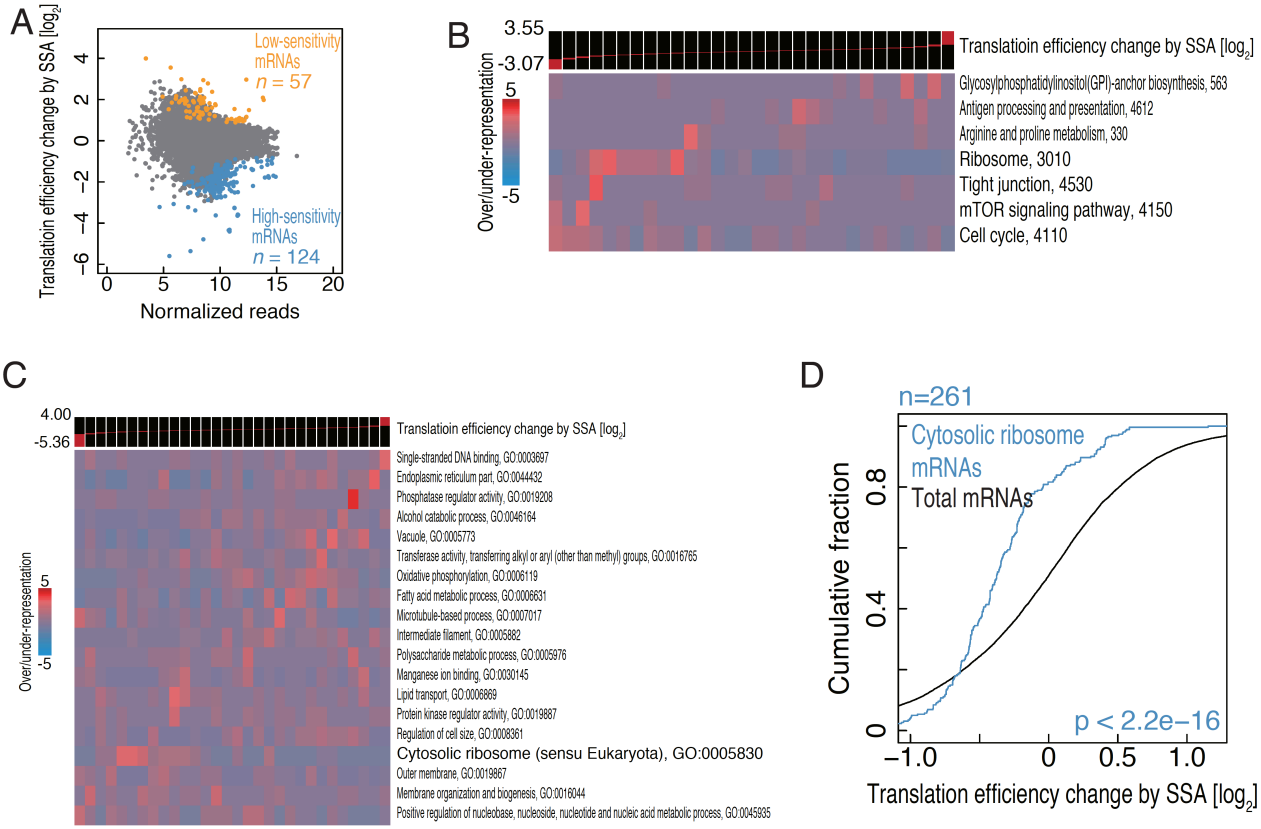

Figure 3.3 Differential translational change upon SSA reveals sensitive functional pathways.

(A) MA plot, M (log ratio) and A (mean average) scales plot, of mRNA reads between 100 ng/mL SSA treatment and MeOH (vehicle) normalized to the library sizes versus translation efficiency -fold change by 100 ng/mL SSA treatment highlighting low sensitive and high sensitive genes at adjusted p-value, FDR <0.05. (B) KEGG pathway analysis along differential TE fold change between SSA treated and untreated conditions with iPAGE as previously described (Goodarzi *et al.*, 2009). (C) GO pathway analysis along differential TE fold change between SSA treated and untreated condition with iPAGE. (D) Cumulative

distribution of TE fold change by SSA corresponding to cytosolic ribosome genes. Significance is calculated by Wilcoxon`s test.

Although translation of cytosolic ribosome mRNAs was significantly downregulated upon SSA (Figure 3.3D), many of the ribosomal protein transcripts were independent of splicing inhibition without significant intron retention as evidenced in the RNA seq data (Figure 3.4A) and RT-PCR experiment (Figure 3.4B) using primers to amplify consecutive exons with/out intron in between. This agrees presence of translational level control upon splicing modulation by SSA.

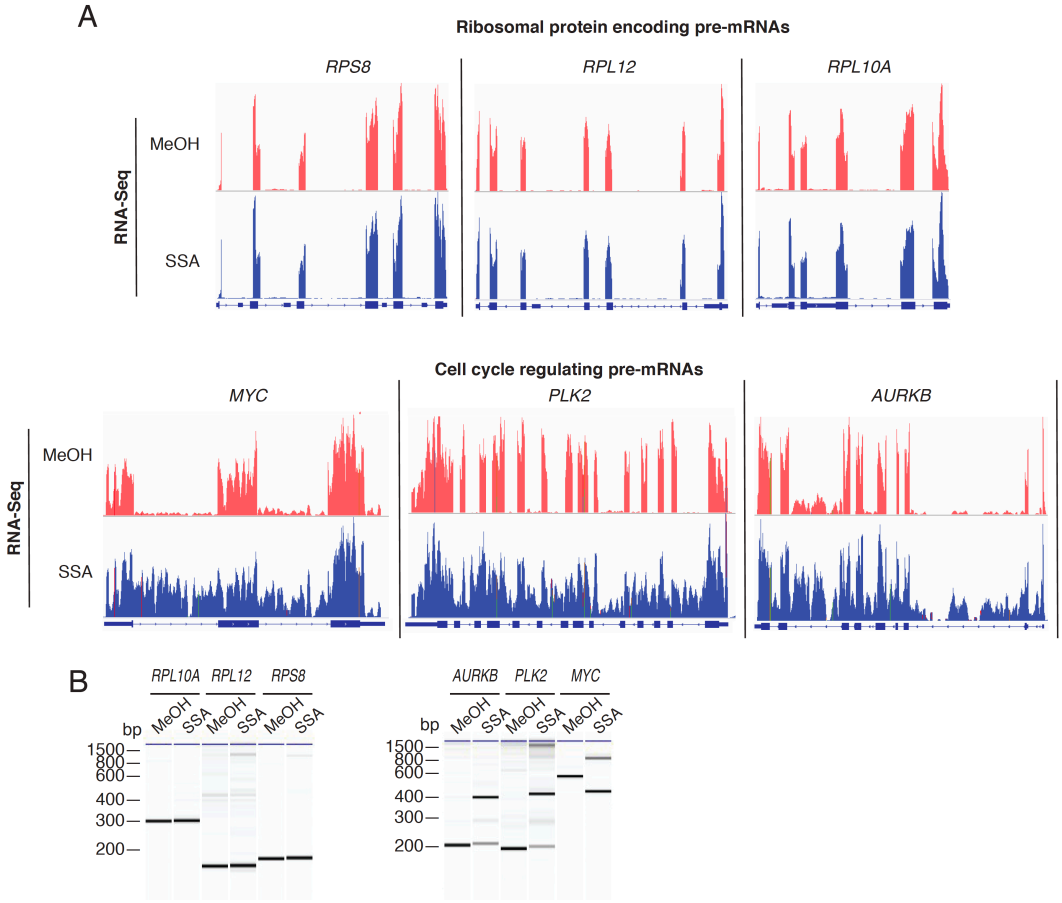

Figure 3.4 Ribosomal protein transcripts are independent of splicing inhibition.

(A) IGV (Integrative Genomics Viewer) plots showing effect of SSA on individual ribosomal protein pre-mRNAs and cell cycle regulating pre-mRNAs from RNA-seq data. (B) RT-PCR analysis to detect spliced and unspliced forms of the genes upon SSA treatment using primers spanning for consecutive exons: *RPS8* (exon 3- exon 4), *RPL12* (exon 5-exon 6), *RPL10A* (exon 5-exon 6), *MYC* (exon 1 – exon 2), *PLK2* (exon 4 – exon 5), and *AURKB* (exon 4 – exon 5).

Investigating the effect individually in RNA-seq and ribosome profiling data upon splicing inhibition separately inferred the functional pathways, pathways in cancer, cell cycle, systemic lupus erythematosus, and chromatin assembly were significantly downregulated using Gene Ontology (GO) and KEGG (Appendix 5 and 6). Many genes including oncogenes were also affected in RNA level such as *TM2D3, BCL10, SLC38A2, RAE1, KIF2C, PUS1* and others (Appendix 1A, 2).

3.3 Conclusion

Taken together, genome wide translation is more strongly repressed than could be explained by the decrease in transcription. Simultaneous analysis of transcriptional and translational changes clearly delineated the regulation effects and minimized the possible artifacts from the transcriptional changes. Splicing modulation by SSA inferred global repression of translation where specifically translation change showed enrichment of transcripts from functional pathways ribosome, the mTOR pathway, and the cell cycle as the most sensitive ones. Furthermore, many ribosomal protein transcripts were independent of splicing inhibition confirming the presence of translational control upon splicing inhibition. The next chapter will enlighten the observed translational regulation upon splicing inhibition.

3.4 Materials and Methods:

3.4.1 Bioinformatics analysis

Investigation of ribosome footprints was performed using fp-count on each of the individual transcripts. Similarly, both the differential ribosome footprint reads estimation and RNA expression analyses were performed using DESeq (Anders and Huber, 2010) based on the mapping of reads onto the CDS. Calculation of the translation efficiency for each of the transcripts was done by dividing the ribosome footprint density by the RNA read density (reads exclusively mapping to the exons for each gene normalized to the library size and mitochondrial footprint density).

Pathway enrichment analysis was performed by iPAGE as previously described (Goodarzi *et al.*, 2009). IGV ver 2.4.10 (Integrative Genomics Viewer) was used to make the RNA-seq read coverage plots.

3.4.2 Op-puro assay

Protein synthesis change can be measured by the metabolic labeling of nascent protein. Conventionally, newly synthesized protein has been monitored by ^{35}S methionine labeling, but radio-isotope handling is hassle. Alternatively, OP-puro is a puromycin derivative with terminal alkyne that mimics as aminoacyl -tRNA and added to C-terminal end of nascent peptide under active translation which can be click reaction to add fluorophore (IR800) and detected by SDS-PAGE (Figure 3.5) (Iwasaki and Ingolia, 2017).

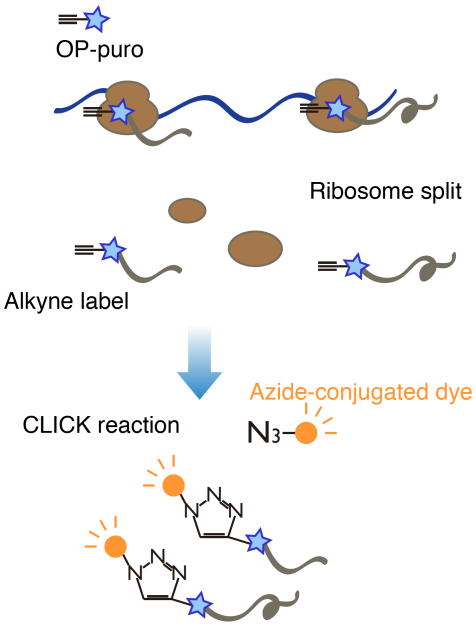

Figure 3.5 Schematic representation of OP-puro assay
modified from (Iwasaki and Ingolia, 2017)

Nascent peptides were labelled by 20 μM OP-puro (Jena Bioscience, NU-931-05) in 24-well dishes for 30 min after SSA or MeOH challenge for 5.5 hr. Cells were washed with ice-cold PBS and lysed with 60 μl buffer (20 mM Tris-HCl, pH 7.5, 150 mM NaCl, 5 mM $MgCl_2$, and 1% Triton X-100), and centrifuged at 20,000 g at 4°C for 10 min. Supernatants were used for nascent peptide labeling with 50 μM azide conjugated IR-800 dye (LI-COR Biosciences, 929-60000) by a Click-iT Cell Reaction Buffer Kit

(Thermofisher Scientific, C10269) according to the manufacturer's instructions and run on SDS-PAGE. Images were acquired by Odyssey CLx Infrared Imaging System (LI-COR, 9140) for detection of nascent peptides with IR 800 nm signal and total proteins stained with CBB (Wako, 178-00551) with IR 700 nm signal. Quantification of the images were performed using LI-COR Odyssey imaging software, Image studio ver 5.2.

3.4.3 RT-PCR analysis

HeLa S3 cells were treated with 100 ng/mL SSA, and their vehicle for 6 hr. Cell lysis was performed by using ribosome profiling lysis buffer with 1% Triton-X. Then, total RNA was extracted using Trizol and purified by Direct-zol RNA Kits as mentioned before. Annealing of 800 ng total RNA to random 9 mer primer was done at 65˚C for 5 min and reverse-transcribed using protoscript reverse transcriptase (protoscript II). PCR was performed on equal volume of the acquired cDNA from RT reaction in 25 μL of reaction mixture applying PCR PrimeSTAR Max Premix (2 ×) (TAKARA) and 0.8 μM of each primer of the appropriate pair. All the primers were purchased from Eurofins as follows.

Gene	**Location**	**Primer sequence**
RPS8	Exon 3	GTGTGCGGGGAGGTAACAAGAAATA (fwd)
	Exon 4	TGTGCTGTCGATGAGCACGATGCAA (rev)
RPL12	Exon 5	TCAACATTGCTCGACAGATGCGGCA (fwd)
	Exon 6	GGCATTCCACAGCACCACTGTTGAT (rev)
RPL10A	Exon 5	CGTTTTTGGCCTCAGAGTCTCTGAT (fwd)
	Exon 6	GGCTTGCCCATGGTGCTCTTGATAT (rev)
MYC	Exon 1	TCTCAGAGGCTTGGCGGGAAAAAGA (fwd)
	Exon 2	AGAAATACGGCTGCACCGAGTCGTA (rev)
PLK2	Exon 4	CAAGAAAGGTGTTGACAGAGCCAGA (fwd)
	Exon 5	CTCCTTCTGTGTTCCAAGGGTTCTA (rev)
AURKB	Exon 4	AGAATAGCAGTGGGACACCCGACAT (fwd)
	Exon 5	ATTTCGATCTCTCTGCGCAGCTGAT (rev)

PCR conditions were 98˚C for 3 min; 35 cycles of 98˚C for 10 s, 52˚C for 15 s and 72˚C for 60 s; followed by 72˚C for 3 min. PCR products were visualized by Bioanalyzer MultiNA system using DNA-1000 separation buffer and SYBR gold.

Chapter 4 Splicing inhibition induces mTORC1 mediated translation repression

4.1 Background

Following up on our gene ontology analysis, we detected significant inhibition of the mTOR pathway. As mTOR signaling affects translation initiation and ribosome biogenesis, its inhibition could also account for both the decrease in protein output as well as the TE decrease in genes associated with ribosome production. Among the gene categories affected by SSA, high translation sensitivity to mRNA coding ribosomes (Figure 3.3D) reminded us the mTORC1 inactivation. It is likely to hypothesize that mTORC1 inhibition is playing an important role in SSA-induced global translation repression (Chapter 3).

The mTOR pathway (mammalian target of rapamycin) is a central regulator of the translation machinery and consequently cell proliferation. mTOR is a serine/threonine protein kinase pathway containing two distinct complexes: mTORC1 and mTORC2 (Figure 4.1A). mTORC1 is a master regulator of translation. mTORC1 modulates translation mostly through direct phosphorylation of eukaryotic translation initiation factor 4E (eIF4E) binding protein 1 (4EBP1). The cap-binding protein eIF4E, together with the helicase eIF4A and the scaffold protein eIF4G, forms an essential part of the eIF4F complex, required for cap-dependent translation. 4EBP phosphorylation prevents 4EBP from binding to eIF4E, allowing eIF4E to form part of eIF4F. mTORC1 phosphorylates human 4EBP1 at multiple sites, Thr 37, Thr46, Ser65, and Thr70 that subsequently release 4EBP1 from eIF4E (Gingras *et al.*, 1999) (Proud, 2018). Hence inhibition of mTORC1 leads to decreased 4EBP1 phosphorylation and therefore increased inhibition of eIF4E function through binding of 4EBP to its target. Furthermore, other factors such as ribosomal protein S6 kinase regulated by mTORC1 via phosphorylation of p70S6 kinase 1 (S6K1) which plays a critical role in translation activation and ribosome biogenesis. S6K phosophorylates multiple substrates involved in translation initiation such as regulatory subunit (eIF4B) of RNA helicase eIF4A resulting into the 43S scanning towards the start codon (Figure 4.1B) (Ma and Blenis, 2009).

Control of mRNA translation plays a critical role in gene expression, and subsequently cell growth and proliferation. Since translation consumes a substantial fraction of cellular metabolic energy, it is tightly regulated at different levels and especially during initiation phase which is rate limiting. Thus, many initiation controls have been known. Most of eukaryotic mRNAs have a 5' m^7Gppp cap and are translated in a cap-dependent manner by the binding of eIF4F initiation complex. The cap-binding protein (eIF4E), scaffold protein (eIF4G) and the RNA helicase eIF4A constitute the eIF4F complex (see chapter 1, Introduction) (Mamane *et al.*, 2006) (Proud, 2018). Depending on various extracellular and intracellular environmental cues of cell, complex regulation of translation has been reported (Figure 4.1A) (Laplante and Sabatini, 2012) (Thoreen *et al.*, 2012).

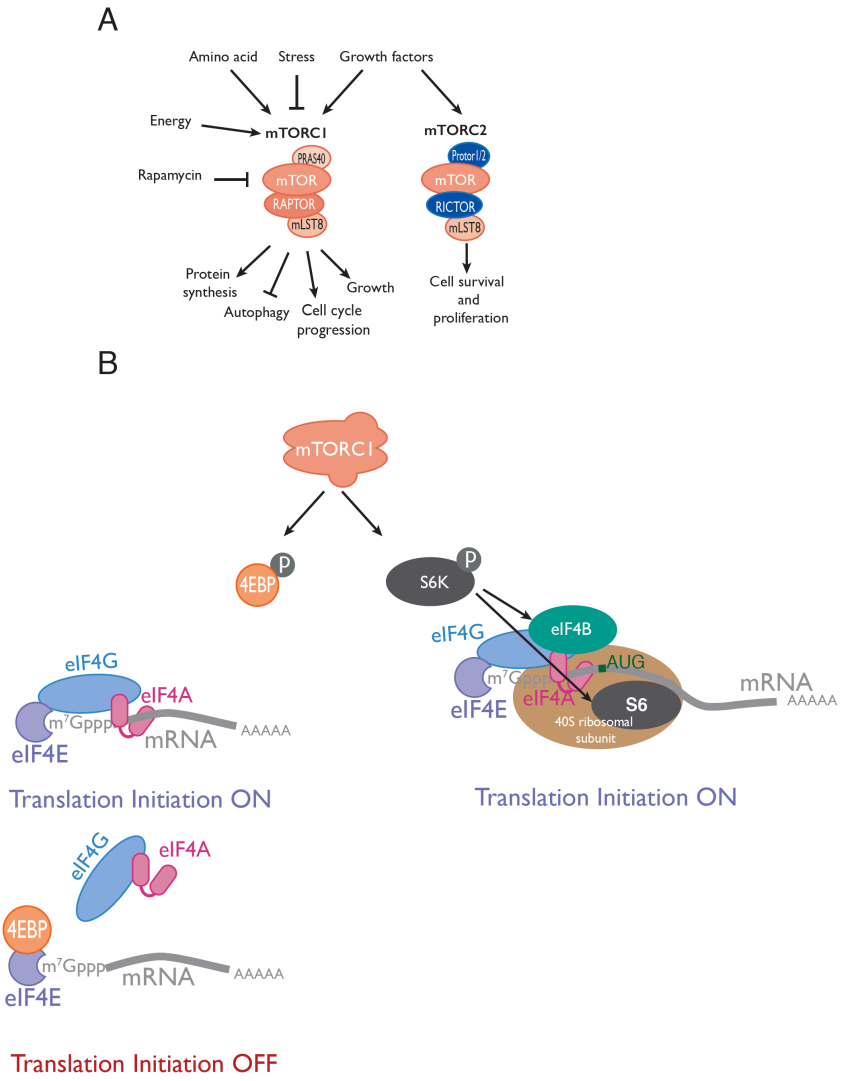

Figure 4.1 mTOR controls translation.

(A) Schematic of mTOR complexes and signaling. (B) Translation initiation regulation by mTORC1 via phosphorylation of repressor protein 4EBP1 and S6K.

Under the mTORC1 inhibited condition, non-phosphorylated 4EBP1 binds to eIF4E inhibiting eIF4F complex formation and repress the initiation of translation (Figure 4.1B). The name mTOR stems from the macrolide compound rapamycin which specifically targets and inhibits this protein kinase. Rapamycin does not bind to the active site of mTOR, specifically acts as an allosteric inhibitor of mammalian TOR (mTOR, also called as mechanistic TOR) complex1 (mTORC1) (Li *et al.*, 2014) whereas mTORC2 is characteristically insensitive to rapamycin (Saxton and Sabatini, 2017). Compared to rapamycin, mTOR kinase inhibitors like pp242 and Torin 1 strongly inhibit mTORC signaling. Studies upon mTOR/mTORC1 inhibition by rapamycin and pp242 employing ribosome profiling showed the predominant decrease in the ribosome footprints on 5' terminal oligopyrimidine (TOP) mRNAs (Thoreen *et al.*, 2012) (Hsieh *et al.*, 2012). These mRNAs have cytidine immediately after the 5' cap, followed by 4-14 consecutive pyrimidines consecutively (Jefferies *et al.*, 1994). To test the hypothesis of whether repression of translation observed in chapter 3 is consequences of effect on mTORC1, I considered to investigate the mTORC1 activity upon splicing inhibition by SSA in this chapter.

4.2 Result and discussion

4.2.1 mTORC1 activity is sensitive to splicing inhibition by SSA

Pathway analysis identified the mTOR pathway as a potential downstream SSA target (Figure 3.3B and 4.1A). Hence, to test whether mTORC1 signaling is inhibited by SSA, the phosphorylation statuses of key mTORC1 substrates 4EBP1 (T37/46, S65) and S6K1 (T389) were examined. As a negative control experiment, acetyl-SSA (Ac-SSA; Figure 1.7, bottom left), an inactivated derivative of SSA was used, which does not appear to bind SF3b (Kaida *et al.*, 2007). As a result, SSA, but not Ac-SSA showed dephosphorylation of these proteins in a time-dependent manner suggesting mTORC1 inactivity upon splicing inhibition (Figure 4.2A, 4.2B and Appendix 3).

mTOR inhibition affects the translation of target mRNAs. In the ribosome profiling data, I then sought for translational changes of principle mTOR sensitive mRNAs, 5' TOP mRNAs upon SSA treatment. Firstly, the categorization of the 5' TOP motif containing mRNAs was curated from a nanoCAGE experiment (Gandin *et al.*, 2016), which defines 5' end of mRNAs. CAGE refers to the Cap Analysis of Gene Expression that identifies the transcription start site (5' end of transcripts). Technically, as little as 10 ng of total RNA is sufficient for the preparation of nanoCAGE libraries. From the RNA, the first strand cDNA synthesis reaction is performed with the reverse transcription (RT) primer along with the template switching (TS) oligonucleotide. Next generation sequencing of the library and sequence analysis further relative to the TS oligonucleotide provides the information of 5' end (Salimullah *et al.*, 2011) (Gandin *et al.*, 2016). SSA treatment showed a significant decrease of translation for these mRNAs (Figure 4.2C). Furthermore, the observed changes in translation correlated highly between mTORC1 inhibition and SSA treatment. The transcripts that were strongly repressed in translation by mTOR kinase inhibitor pp242 as observed by the ribosome profiling with pp242 (Iwasaki *et al.*, 2016) were significantly sensitive to SSA (Figure 4.2D). The correspondence between translationally SSA-sensitive mRNAs and mTORC1 inhibition-sensitive mRNAs implies that, by SSA treatment, mTORC1 inhibition may be induced and could explain the biased translation repression.

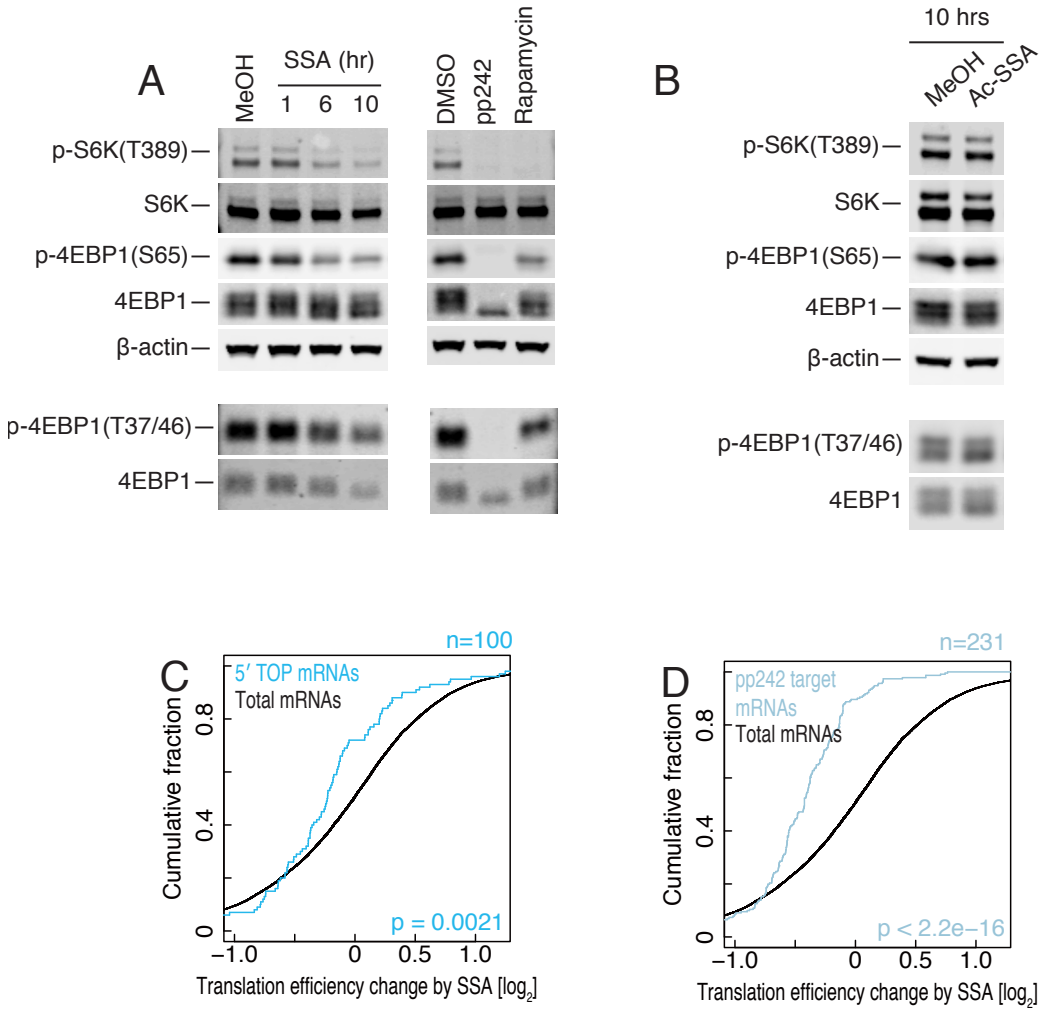

Figure 4.2 Splicing inhibition by SSA induces mTORC1 mediated translation repression.

(A) Representative western blot (n=3) for HeLa S3 cell lysate probing for phosphorylated and total S6 Kinase (S6K) and eIF4E-binding protein (4-EBP1), mTORC1 substrates. (B) Representative western blot for HeLa S3 cell lysate prepared by treating with acetylated-SSA (Ac-SSA) probing for phosphorylated and total S6 Kinase (S6K) and eIF4E-binding protein (4-EBP1), mTORC1 substrates. (C) Cumulative distribution of TE fold change by SSA corresponding to 5' Terminal Oligo Pyrimidine motif (TOP) containing mRNAs. Top motif containing mRNAs were curated from 5' UTR list (Gandin *et al.*, 2016) after scrutinization for the motifs. Significance is calculated by Wilcoxon`s test. (D) Cumulative distribution of TE fold change by SSA largely overlap with genes sensitive to an pp242, ATP site mTOR inhibitor (2.5 μM) (Iwasaki et al., 2016). Significance is calculated by Wilcoxon`s test.

Given that dephosphorylated 4EBP1 bind to the cap-binding protein eIF4E inhibiting eIF4F initiation complex formation during the translation initiation of 5' m^7Gppp capped mRNAs (Sonenberg and

Hinnebusch, 2009), I hypothesized that the SSA mediated translation sensitivity of different mRNAs might be determined by 5' m^7Gppp cap and 5' UTR. I confirmed that a capped and 5' TOP motif containing UTR was sensitive to SSA in a *Renilla* luciferase reporter assay, whereas 5' cap and eIF4F complex independent HCV-IRES (Hellen and Sarnow, 2001) was totally resistant (Figure 4.3).

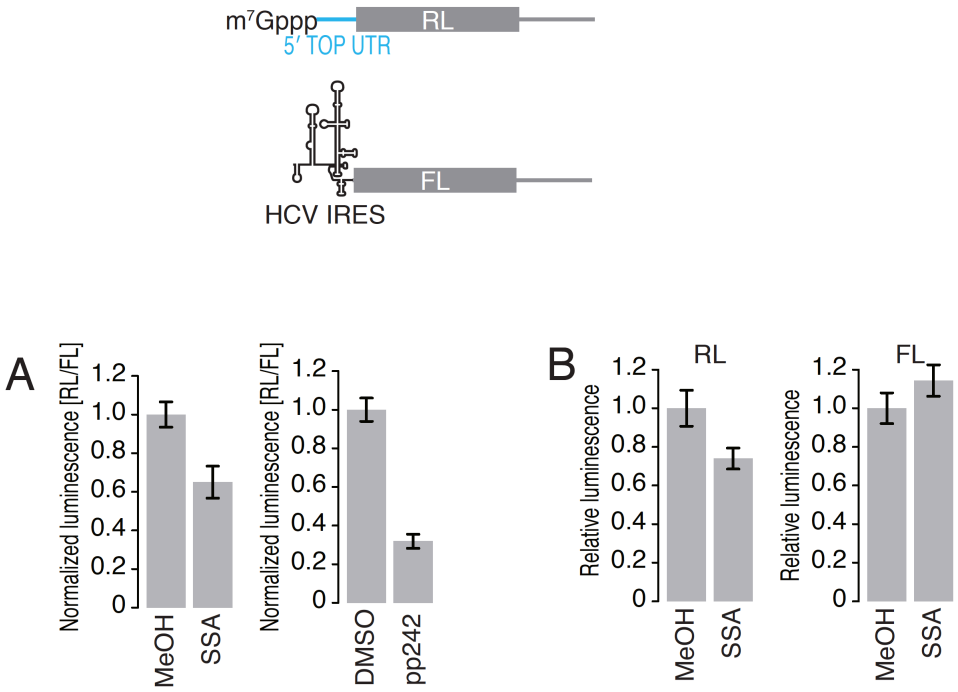

Figure 4.3 5' TOP mRNAs are significantly sensitive to SSA.

The 5' UTR of TOP motif containing gene *EIF2S3* was fused to the *Renilla* luciferase and Firefly luciferase fused with upstream HCV-IRES was used as a negative control for non-capped and non-TOP motif containing mRNA. These reporter mRNAs were transfected for 4 hr after 2 hr treatment of SSA and luciferase reporter assay was performed to quantitate the luciferase reporter protein. Data represent mean and s.d. (n = 3). (A) Normalized to the HCV-IRES firefly luciferase. (B) Expression of 5' TOP *Renilla* luciferase and 5' HCV-IRES firefly luciferase.

Moreover, the dephosphorylation of 4EBP1 upon SSA treatment was further supported by m^7Gppp cap on beads pull down assay which showed more 4EBP1 attached (Figure 4.4, Dr. Iwasaki). As SSA-induced dephosphorylated 4EBP1 potentially binds to cap binding protein eIF4E resulting in translation initiation repression hence more 4EBP1 was appeared upon m^7GTP cap pull down via eIF4E. (Figure 4.1B).

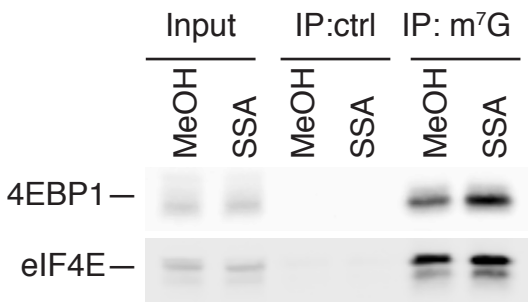

Figure 4.4 5' m^7G cap pulldown assay was congruent to SSA dephosphorylating 4EBP1.

HelaS3 cells were either treated with methanol control or SSA for 10 hr. Cell lysis was performed using hypotonic lysis buffer. m^7G cap beads were used for the pull-down assay. Representative western blot probing for 4EBP1 and eIF4E was shown (n=2).

4.2.2 mTORC1 activity is sensitive to alternative splicing inhibition

These observations led me to hypothesize that mTORC1 inhibition is not specific to SSA only but more generally observed when splicing is inhibited. Hence, we repeated the above assays by SF3B1 inhibition via a Pladienolide B (PlaB) (Figure 1.7, middle right), an alternative inhibitor of SF3B1, and knock-down of SF3B1, which also induces intron retentions (Figure 4.5A, and B). Both recapitulated a similar dephosphorylation pattern in 4EBP1 and S6K as observed for SSA treatment (Figure 4.5C, D, and 4.2A).

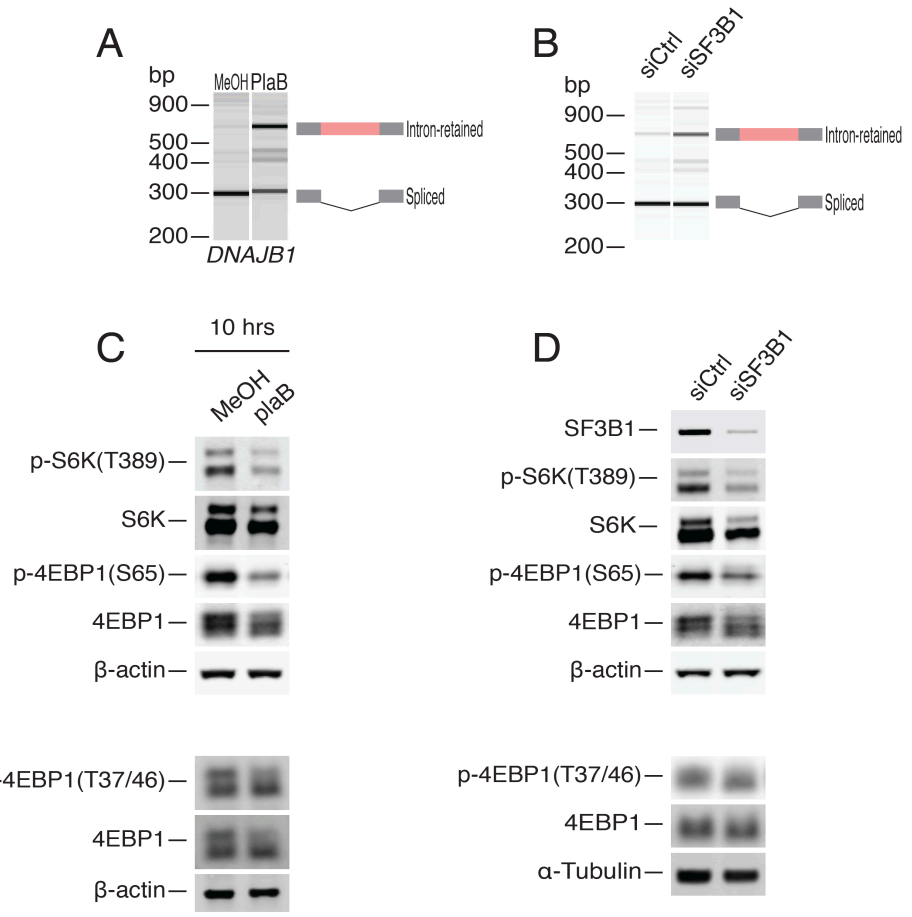

Figure 4.5 Alternative splicing inhibition recapitulate the effect of SSA.

Hela S3 cells were either treated with MeOH control or 1 μg/mL PlaB for 10 hr. Alternatively, RNAi mediated SF3B1 knock-down was performed in HeLa S3 cell lines parallel with negative control siRNA knock-down. RT-PCR analysis to detect spliced and unspliced forms of the gene, *DNAJB1*, representative transcript, using primers spanning for exon 2 and exon 3 upon PlaB treatment (A) and upon knockdown of SF3B1 (B). (C) Representative western blot (n=3) for HeLa S3 cell lysate probing for phosphorylated and total S6 Kinase (S6K) and eIF4E-binding protein (4EBP1), mTORC1 substrates.

4.2.3 SSA indirectly inhibits mTORC1

While it did seem unlikely that an inhibitor of mRNA splicing would also directly target mTOR, we had to control for the contingency and ensure that SSA did not inhibit mTOR function *in vitro*. Examining kinase activity of recombinant mTOR *in vitro* in the presence of both SSA and PlaB did not show inhibition of kinase activity (Figure 4.6), indicating the effect on mTORC1 was not evoked by direct targeting.

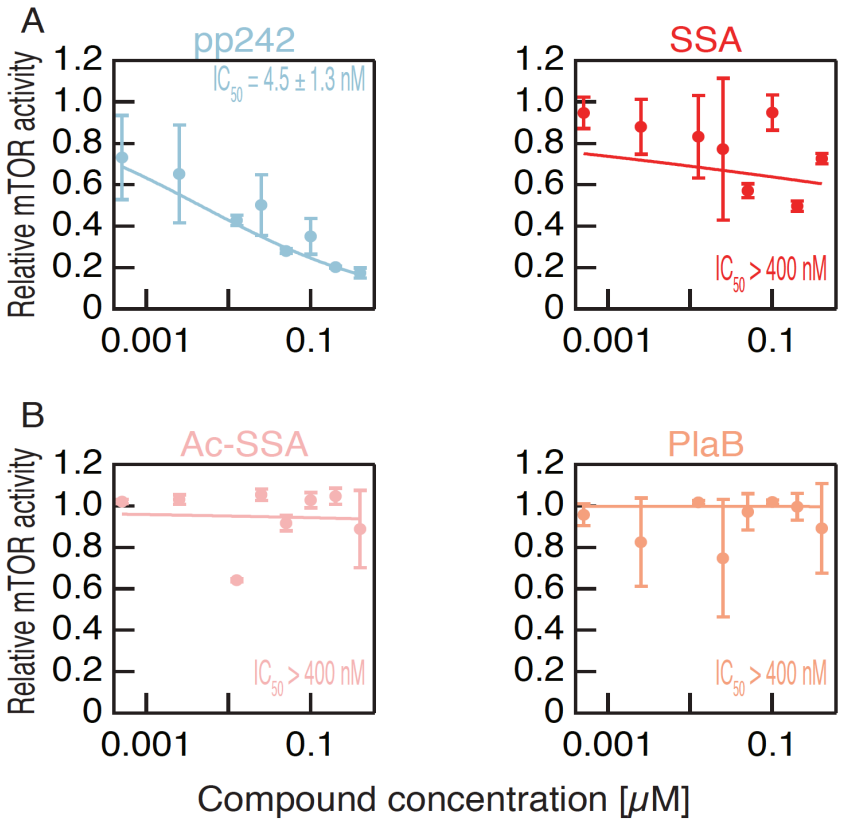

Figure 4.6 SSA indirectly inhibits mTOR kinase.

(A) *In vitro* mTOR kinase activity shown by pp242 (left panel) and SSA (right panel) with their respective IC50 value. (B) *In vitro* mTOR kinase activity shown by Ac-SSA (left panel) and PlaB (right panel) with their respective IC50 value.

4.3 Conclusion

mTORC1 signaling impacts many key cellular functions and directly controls translation initiation. These data confirmed that splicing perturbation induces mTORC1 inhibition and thereby represses translation of a subset of mRNAs which are under the control of mTORC1. It will be interesting to investigate the reasons why cell induces mTOR mediated translational control upon splicing inhibition. In the next chapter, I will provide the further insights on the investigation to this reason.

4.4 Materials and methods

4.4.1 Compounds and cell culture .

Compounds SSA, acetylated SSA and pladienolide B were solubilized in methanol. Rapamycin (Wako chemicals, 188-02811) and pp242(Sigma, P0037) were dissolved in DMSO. HeLa S3 cells were maintained in DMEM supplemented with 10% heat inactivated Fetal Bovine Serum in a humidified incubator at 5% CO_2 and 37˚C.

4.4.2 Western blotting

Cells were lysed using the same lysis buffer as used for the ribosome profiling experiment with 1× protease inhibitor cocktail (Roche, 04693132001), skipping cycloheximide. Equal volumes of protein lysates were resolved using SDS-PAGE gels (Bolt Bis-Tris Plus Gels, Life Technologies, NW04127). Proteins were transferred to nitrocellulose membranes (BIO-RAD, 1620145) and the membrane was blocked by Odyssey blocking buffer (TBS) (LI-COR Biosciences, 927-50000). Blocking and antibody incubations were performed at room temperature for 1 hr and membranes were rinsed with TBS containing 0.1% Tween-20 after each antibody incubation. Anti-4EBP1 [Cell Signaling Technology (CST), 9452, 1:1000], anti-phospho-4EBP1 (Thr37/46) (CST, 2855, 1:1000), anti-phospho-4EBP1 (Ser65) (CST, 9456, 1:1000), anti-p70 S6 kinase (49D7) (CST, 2708, 1:1000), anti-eIF4E (CST, 9742, 1:1000), anti-phospho-p70 S6 kinase (Thr389) (108D2) (CST, 9234, 1:1000), anti-β-actin (MBL, M177-3, 1:1000), anti-β-actin (LI-COR Biosciences,926-42212, 1:1000), and anti-α-tubulin (Sigma, B-5-1-2, 1:1000) were used as primary antibodies. IR-dye (680 or 800 nm) conjugated secondary antibodies (LI-COR Biosciences, 925-68070/71 and 926-32210/11, 1: 10,000) were used for the detection. Images were collected by Odyssey CLx Infrared Imaging System (LI-COR Biosciences, 987-15227). LI-COR Odyssey imaging software, Image studio ver 5.2 was used for the quantification of the images.

4.4.3 Plasmids and DNA constructs

psiCHECK2 plasmid (Promega) was kindly provided by Dr. Iwasaki with DNA fragment containing 5' UTR sequence of TOP mRNA, EIF2S3 inserted between T7 promoter and ORF of *Renilla* luciferase (hRluc) in vector (Promega).

EIF2S3 (uc004dbc.3): TTTCCTTCCTCTTTTGGCAAC.

PCR amplification of required region was done by using T7 and RLuc R primer to use for *in vitro* transcription template. The primers used were,

T7: TAATACGACTCACTATAGG (fwd)

RLuc R: CTGTGTGTTGGTTTTTTGTGTG (rev)

In vitro transcription, capping and polyadenylation of reporter RNA was done using a T7-Scribe Standard RNA IVT Kit (C-AS3107), ScriptCap m^7G Capping System (C-SCCE0625) and a ScriptCap 2'-O-Methyltransferase Kit (C-SCMT0625), and A-Plus Poly(A) Polymerase Tailing Kit (C-PAP5104H) according to the manufacturer`s protocol (CELLSCRIPT). *In vitro* transcribed RNA containing 5' HCV-IRES between T7 promoter and ORF of Firefly Luciferase (FLuc) without m^7G cap, A-cap (Adenosine as 5' cap) instead was used as negative control since translation can occur cap-independently. The reagent was kindly supplied by Dr. Shichino (Iwasaki lab).

HCV IRES:

GCCAGCCCCCTGATGGGGGCGACACTCCACCATGAATCACTCCCCTGTGAGGAACTACTGTCT
TCACGCAGAAAGCGTCTAGCCATGGCGTTAGTATGAGTGTCGTGCAGCCTCCAGGACCCCCC
CTCCCGGGAGAGCCATAGTGGTCTGCGGAACCGGTGAGTACACCGGAATTGCCAGGACGACC
GGGTCCTTTCTTGGAGTTACCCGCTCAATGCCTGGAGATTTGGGCGTGCCCCCGCAAGACTGC
TAGCCGAGTAGTGTTGGGTCGCGAAAGGCCTTGTGGTACTGCCTGATAGGGTGCTTGCGAGT
GCCCCGGGAGGTCTCGTAGACCGTGCACCATGAGCACGAATCCTAAACCTCAAAGAAAAACC
AAACGTAAC.

4.4.4 Luciferase Reporter assay

HeLa S3 cells (1×10^5) were seeded onto the 24 well plates in triplicates. Equal concentration (0.02 µg) of *in vitro* transcribed, capped and poly(A) tailed mRNAs were transfected onto 24-well dishes using a TransIT-mRNA Transfection Kit (Mirus, MIR 2250) according to the manufacturer`s instruction. Two hr after 100 ng/mL SSA treatment, mRNAs were transfected, and 4-hr post-transfection, cells were washed

with PBS and lysed with 1 x passive lysis buffer (Promega). The luciferase assay was performed with Dual-luciferase reporter assay system (Promega, E1910) according to the manufacturer`s instructions. Accordingly, *firefly* luciferase (FLuc) was detected by Luciferase Assay Reagent II (LAR II) and *Renilla* luciferase (RLuc) was detected by STOP and GLO (*Renilla*-GLO). Luminescence was detected with a GLOMAX (Promega, 9100-102).

4.4.5 7-methyl-guanosine (m^7G) pulldown assays

Following 10 hr of 100 ng/mL SSA treatment, Hela S3 cells were washed with ice-cold PBS and lysis was performed using 1200 µl hypotonic lysis buffer [10 mM HEPES-NaOH (pH 7.5), 10 mM KCl, 1.5 mM $MgCl_2$, 1mM DTT, 1× Protease Inhibitor Cocktail for use with mammalian cell and tissue extracts [Nacalai]. After centrifugation at 20,000 × g (4˚C) for 10 min, lysate was used for the pulldown experiment. Equal amounts of protein extract lysate were pre-cleared with 150 µl of Pierce Control Agarose Resin (Thermo Fisher Scientific) equilibrated with hypotonic lysis buffer, at 4 °C for 1 hr. The pre-cleared lysate was incubated with 40 µl of Pierce Control Agarose Resin or γ-aminophenyl-m^7GTP (C10-spacer)-Agarose (Jena Bioscience) equilibrated with hypotonic wash buffer [10 mM HEPES-NaOH pH 7.5, 10 mM KCl, 1.5 mM $MgCl_2$, 1 mM DTT, 0.02% Triton-X 100, and 50 µg/ml tRNA from baker's yeast (Sigma-Aldrich)], at 4 °C for 1 hr, and then washed with hypotonic wash buffer 3 times. Agarose beads were resuspended by 20 µl of hypotonic lysis buffer and 20 µl of 2x loading buffer and boiled at 100°C for 4 min. The pulled down proteins were examined by western blotting.

4.4.6 RNA interference and transfection

ON-TARGETplus non-targeting siRNA #1 (D-001810-01-05) and ON-TARGETplus Human SF3B1 siRNA SMARTpool against human SF3B1 (L-020061-01-0005) were obtained from Dharmacon. For the knockdown experiment, 2×10^5 HeLa S3 cells per well were seeded in six-well plates. On the next day, 30 pmol of siRNA was transfected into cells using Lipofectamine RNAiMAX transfection reagent

(Thermo Fisher Scientific, 13778150) according to the manufacturer's manual. After 36 hr post transfections, cells were lysed as mentioned above for the western immunoblotting.

4.4.7 *In vitro* mTOR kinase assay

The mTOR kinase activity was performed by LANCE Ultra time-resolved fluorescence resonance energy transfer (TR-FRET) assay (PerkinELmer, U-TRF #26), following the manufacturer's instructions. mTOR enzyme (10 nM), ATP (90 μM), and ULight-p70S6K (Thr389) peptide (25 nM) were incubated in kinase buffer (50 mM HEPES pH 7.5, 1 mM EGTA, 3 mM $MnCl_2$, 10 mM $MgCl_2$, 2 mM DTT, and 0.01% Tween 20) at room temperature for 1 hr in white 384-well opti-plates. The reaction was stopped by adding EDTA to 10 mM. A europium-labeled anti-phospho p70S6K (Thr389) antibody was then used to a final concentration of 2 nM for the detection of phosphorylated peptide. Signal intensity of the emitted light was measured with an EnVision Multilabel reader (Perkin Elmer, 21040010) in TR-FRET mode (excitation at 320 nm and emission at 665 nm).

Chapter 5 Truncated protein induced by SSA causes proteotoxic stress and feeds back to repress translation via mTORC1

5.1 Background

mTORC1 immediately sense the proteotoxic stress via the activation of stress activated protein kinase JNK (C-JUN N-terminal kinase). Protein homeostasis or proteostasis is a fundamental function for normal cell physiology. Cellular protein synthesis is dynamically regulated to maintain proteostasis. Control over protein synthesis can minimize aberrant protein synthesis and avoid the accumulation of flawed proteins. Synthesis of truncated proteins are likely to be improperly folded or become non-functional (Wolff *et al.*, 2014). The most prominent central regulator of protein synthesis is the mTOR complex, which directly senses a variety of endogenous and exogenous cues to control translation process accordingly. Along with amino acids and growth factors, mTORC1 also senses and responds quickly to a large variety of stresses. Cellular stress induces reduction in mTORC1 activity reflecting an adaptation strategy of cells to their environment (described in chapter 4: Background) (Figure 4.1, Figure 5.1) (Su and Dai, 2017) (Su *et al.*, 2016). Attenuation of protein translation particularly occurs under proteotoxic stress (Lindquist, 1981). In cells, expression of heat shock proteins (HSPs) is a known hallmark of the proteotoxic stress response (PSR). In addition, recent reports showed that JNK signaling is the most significant responsive pathway during proteotoxic stress, indicated by elevated T183/Y185 phosphorylation after JNK activation (Johnson and Nakamura, 2007) (Su *et al.*, 2016). Furthermore, proteotoxic stress has been suggested to be immediately sensed by mTORC1 by disintegration of its component proteins to suppress translation via phosphorylation of JNK for the adaptive response (Su *et al.*, 2016) (Figure 5.1).

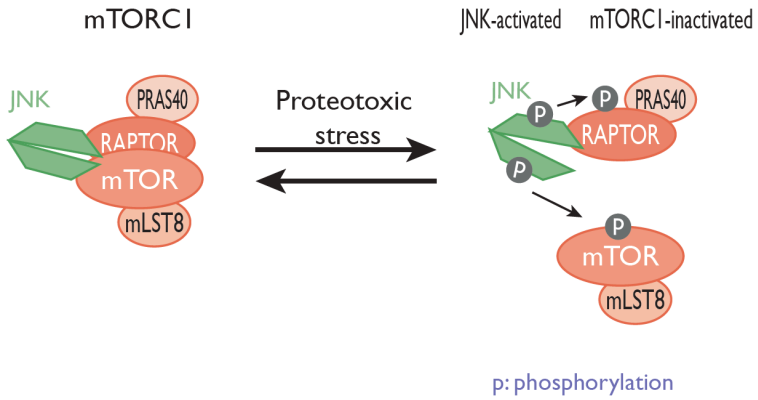

Figure 5.1 Schematic representation of proposed model JNK-mTORC1 interactions

(modified from (Su *et al.*, 2016))

Indeed, the results I have documented in the previous chapters lack the mechanisms to explain how splicing inhibition induces mTOR mediated translational control. To understand the mechanism of mTOR inhibition upon splicing inhibition, based on recent report (Su *et al.*, 2016), I hypothesized that synthesis of number of truncated proteins upon splicing inhibition (chapter 2, Figure 2.4) may cause the cell proteotoxic activating JNK signaling and subsequently inactivate mTORC1 suppressing further aberrant translation (chapter 3 and 4).

Aberrant translation products are inevitable upon splicing inhibition. Cell protein quality control after the synthesis of these truncated proteins would be sequestration of the misfolded proteins, aggregation into specific subcellular compartments, refolding attempt and/or degradation of the group of aberrant proteins by the ubiquitin-proteasome system (UPS) or through autophagy-lysosome system to minimize the detrimental effect to the cells (Vilchez *et al.*, 2014) (Wolff *et al.*, 2014). Efficiency and specificity of each of these systems are still the subjects for further study.

In this chapter, I tried to elucidate the mechanistic link between splicing inhibition and mTOR downregulation.

5.2 Results and discussion

5.2.1 SSA causes proteotoxic stress and affects mTORC1 activity

Based on the recent report showing that proteotoxic stress caused by heat shock and stressor compounds such as proteasome inhibitor, MG132 is immediately sensed by c-Jun N-terminal kinase (JNK), thereby leading to the inhibition of mTORC1, I am motivated to assess whether truncated protein translation upon splicing inhibition by SSA also results into the proteotoxic stress (Su *et al.*, 2016). So, to monitor the cell proteotoxic stress, I investigated the T183/Y185 phosphorylation status of stress activated protein kinase (p-JNK) upon splicing inhibition. Consistently, activation of JNK signaling was shown by its increased phosphorylation upon SSA treatment (Figure 5.2A). The activation of JNK has also been reported by a former lab member indicating stress upon SSA treatment to the cells (Khan, 2014). The biologically inactive form of SSA, Ac-SSA could not recapitulate the SSA`s phenotype as expected (Figure 5.2B) whereas the alternative SF3B1 inhibitor pladienolide B also induced JNK phosphorylation (Figure 5.2C). Elevated JNK phosphorylation indicated cellular proteotoxic stress upon splicing inhibition. Taking into account recent publications as shown in Figure 5.1(Su *et al.*, 2016), it is plausible that this activated JNK stress could be the reason for the inactivation of mTORC1 by splicing inhibition.

To monitor the link between activated JNK signaling and mTORC1 mediated translation repression, I turned to examine the phenotype of phosphorylated JNK. Under proteotoxic stress, phosphorylated JNK disintegrates the mTORC1 complex resulting into phosphorylation of mTORC1 components, RAPTOR on S863 and mTOR on S567 (Su *et al.*, 2016) (Figure 5.1). Under SSA treatment, RAPTOR was phosphorylated on S863, which indicates JNK-mediated inactivation of the mTORC1 complex (Figure 5.2D). Indeed, knockdown of the most common gene variants of JNK (JNK1 and JNK2) could rescue of SSA`s phenotype, observed by higher phosphorylation of 4EBP1 upon SSA (Figure 5.2E). Additionally, SSA induced a decrease in translation of 5′ TOP motif containing mRNA (Figure 4.3) was rescued upon knockdown of JNK1 and JNK2 (Figure 5.2F). This result suggests that stress activation upon splicing inhibition is affecting

mTORC1 at least in a part. Furthermore, it is plausible that expression of truncated proteins upon splicing inhibition induces a JNK-mediated stress response affecting suppression of mTOR mediated translation repression to buffer the further translation of aberrant proteins.

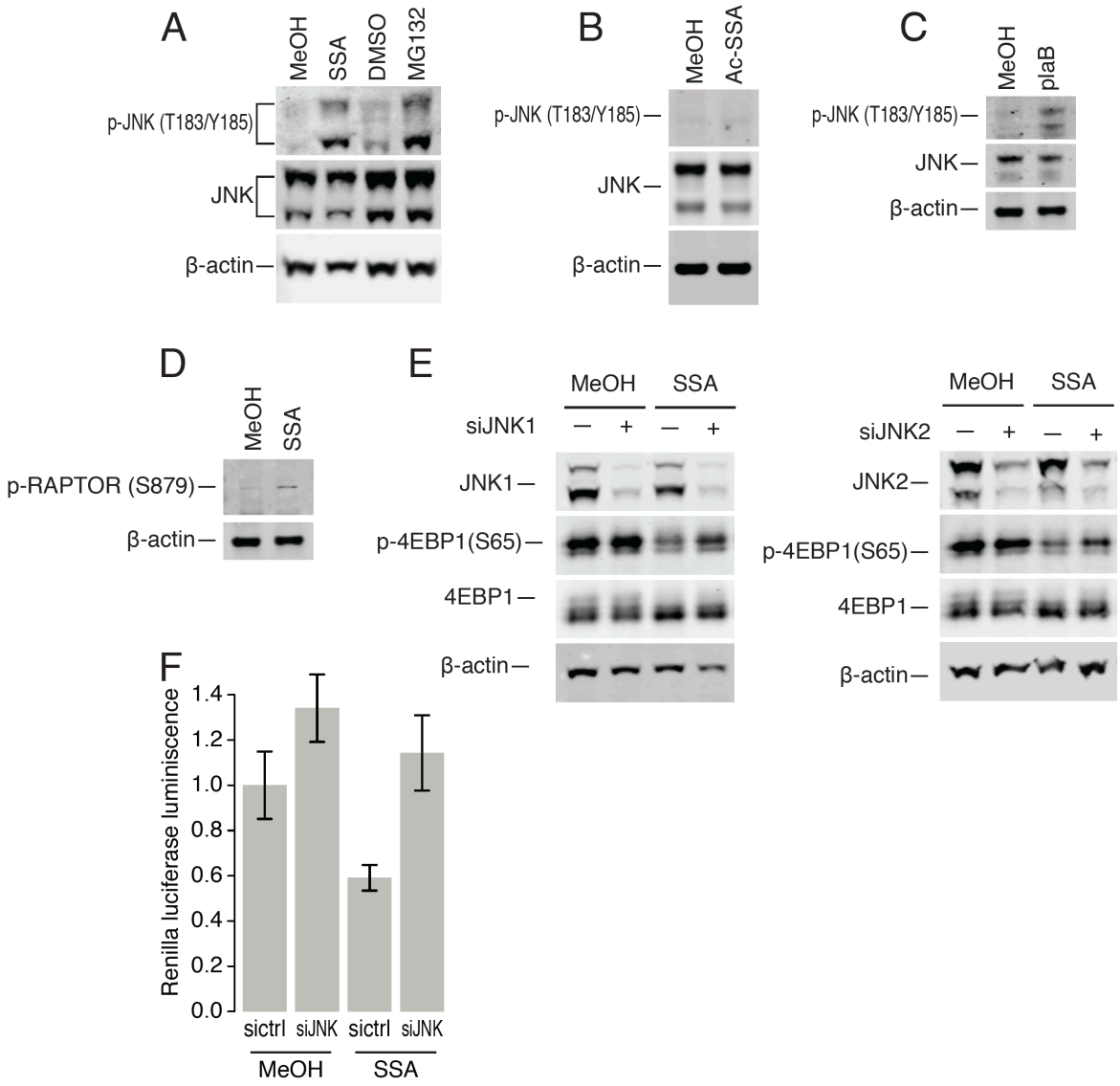

Figure 5.2 SSA induce proteotoxic stress and leads to translation repression via mTORC1 inhibition.

(A) HeLa S3 cells were either treated with vehicles, 100 ng/mL SSA or 0.5 μM MG132 for 10 hr and the cell lysates were immunoblotted with the indicated antibodies. (B) HeLa S3 cells were either treated with MeOH or 100 ng/mL Ac-SSA for 10 hr and the cell lysates were immunoblotted with the indicated antibodies. (C) HeLa S3 cells were either treated with MeOH or 1 μg/mL pladienolide B for 10 hr and the cell lysates were immunoblotted with the indicated antibodies. (D) HeLa S3 cells were either treated with vehicle or 100 ng/mL SSA for 10 hr and the cell lysates were immunoblotted with the indicated

antibodies. (E) JNK1 knock-down (Left panel) and JNK2 knock-down (right panel) were performed in HeLa S3 cell lines parallel with negative control siRNA knock-down for 48 hr and SSA or MeOH were treated for 10 hr post-transfection of siRNAs. The cell lysates were immunoblotted with the indicated antibodies. (F) JNK1/2 knock-down was performed in HeLa S3 cell lines parallel with negative control siRNA knock-down for 48 hr and SSA or MeOH were treated for 6 hr post-transfection. The 5' UTR of TOP motif containing gene *EIF2S3* was fused to the *Renilla* luciferase (from figure 4.3). These reporter mRNAs were transfected for 4 hr after 2 hr treatment of SSA and luciferase reporter assay was performed to quantitate the luciferase reporter protein. Data represent mean and s.d. (n = 3).

5.2.2 Truncated proteins induced proteotoxic stress and feeds back to repress translation via mTORC1

In order to investigate if the expression of truncated proteins mimics the phenotypes of splicing inhibition by SSA, I selected RAB32 (Ras-related protein) as a representative transcript, which has shown ribosome footprints from the intron until the first in-frame stop codon upon SSA treatment (Figure 2.4C, upper middle panel). Expression of its truncated form (represented as RAB32*), but not the full length CDS region exhibited phosphorylation of JNK and simultaneous dephosphorylation of mTORC1 substrates, 4EBP1 and S6K1 (Figure 5.3A and 5.3B). However, FLAG tagged RAB32* was not observed during western immunoblotting in supernatant of lysate though it was observed aggregated in the pellet during cell lysis (Figure 5.3B and 5.3C). After synthesis of truncated proteins, to minimize the damaging effect to the cell, either the protein will be aggregated in cellular compartment or will be subjected to the degradation mediated by proteasome or lysosome (Vilchez *et al.*, 2014) (Wolff *et al.*, 2014). Here, in case of RAB32*, these expressed truncated proteins were clearly observed to be aggregated. In contrast p27*, truncated protein product from CDKN1B* (Figure 5.3A) was soluble and did not affect stress mediated mTORC1 activity (Appendix 7). P27* has been reported to be biologically active as a full-length protein (Kaida *et al.*, 2007). Taken together, SSA-induced aggregated truncated proteins collectively are possibly feeding back to repress translation via mTORC1.

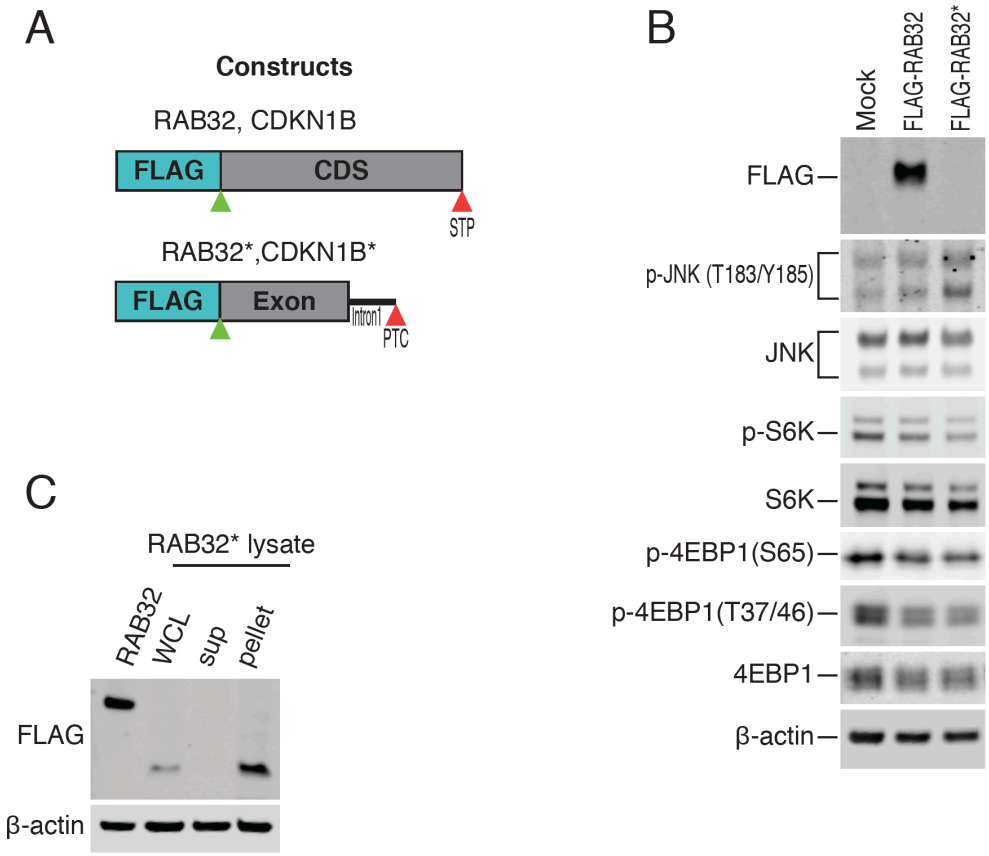

Figure 5.3 SSA induce proteotoxic stress leading to translation repression via mTORC1 inhibition.

(A) Schematic representation of reporter constructs for the gene RAB32, CDKN1B is shown. DNA constructs with either full length CDS (upper) or ORF until the first in-frame stop codon (lower) on the first intron with a N-terminal FLAG tag were made and inserted individually in the expression plasmid CDNA5/FRT/TO by Gibson assembly (New England Biolabs). Green colour is translation start site and red colour is stop codon. (B) HeLa S3 cell lines were transfected with equal amounts (1 µg) of the individual FLAG tagged plasmid constructs using FuGENE HD (promega) as the DNA transfection reagent. Cells were harvested 48 hr post transfection. Total and phosphorylated form of stress activated protein kinase JNK, key mTORC1 substrates S6K and 4EBP1 have been analyzed by western blotting using the indicated antibodies. Transfection reagent without the plasmid construct was used as mock. (C) HeLa S3 cell lines were transfected with equal amounts (1 µg) of the individual FLAG tagged plasmid constructs. For the confirmation of protein expression, the transfected truncated form, RAB32* was assessed separately in whole cell lysate (WCL), supernatant part or pellet part.

5.3 Conclusion

The results validated the expression of truncated proteins and suggested the translational buffering mechanism via mTORC1 pathway to avoid accumulation of truncated, toxic proteins upon splicing perturbation (Figure 5.4). Our results demonstrate that beyond the many RNA quality control pathways, cells contain a negative feedback mechanism to respond to the production of truncated proteins, possibly to prevent further damage and to survive till the source of stress has subsided.

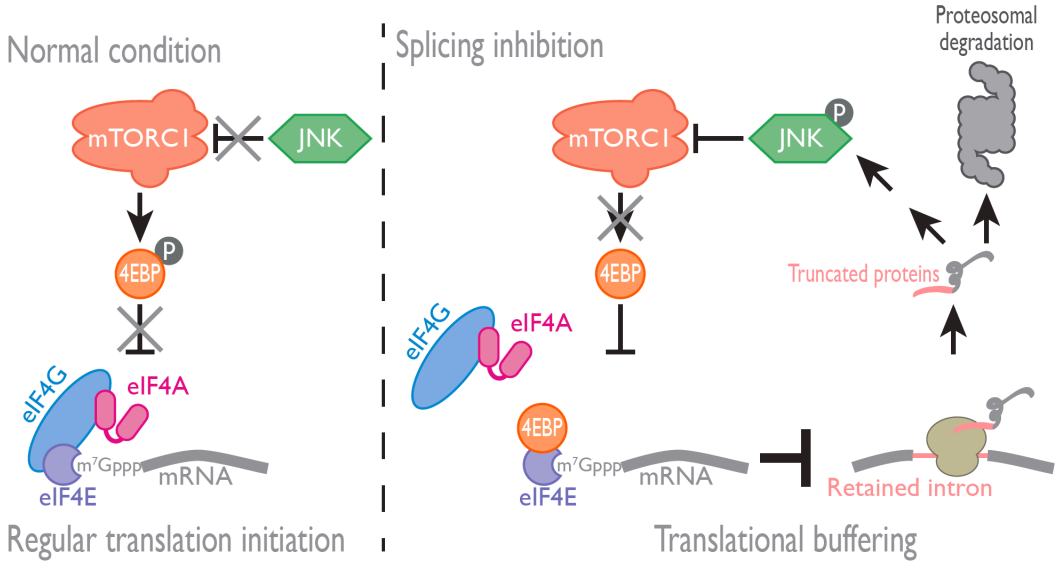

Figure 5.4 Schematic representation of summary model for the study.

5.4 Materials and methods

5.4.1 Compounds and cell culture

Compounds SSA, acetylated SSA and pladienolide B were solubilized in methanol. HeLa S3 cells were maintained in DMEM supplemented with 10% heat inactivated Fetal Bovine Serum in a humidified incubator at 5% CO2 and 37˚C.

5.4.2 Western blotting

Western immunoblotting was performed as explained in methods (4.4.2, Chapter 4). Some other antibodies used were monoclonal ANTI-FLAG M2 antibody produced in mouse (SIGMA, F1804), anti-phospho-JNK (Thr183/Tyr185) (CST, 4668, 1:500), anti-JNK1(2C6) (CST, 3708S, 1:1000), anti-JNK2 (56G8) (CST, 9258, 1:1000), anti-SAPK/JNK (CST, 9252, 1:1000), anti-β-actin (MBL, M177-3), anti-β-actin (LI-COR,926-42212).

5.4.3 RNA interference and transfection

ON-TARGETplus Non-targeting siRNA #1 (D-001810-01-05), ON-TARGETplus Human MAPK8 (5599) siRNA-SMARTpool against human JNK1 (L-003514-00-0005), and ON-TARGETplus Human MAPK9 (5601) siRNA-SMARTpool against human JNK2 (L-003505-00-0005) were obtained from Dharmacon. For the knockdown experiment, 2×10^5 HeLa S3 cells per well were seeded in six-well plates. On the next day, 30 pmol of siRNA was transfected into cells using Lipofectamine RNAiMAX Transfection Reagent (Thermo Fisher Scientific, 13778150) according to the manufacturer's manual. After 42 hr post-transfection, cells were treated with the compounds and lysed as mentioned above for the western immunoblotting.

5.4.4 Luciferase reporter assay

HeLa S3 Cells (75,000) were seeded onto each well of the 24 well plates. Experiment was performed in triplicates. RNAi of JNK1/2 was performed for 48 hr and equal concentration (0.02 μg) of *in vitro* transcribed capped and poly(A) tailed mRNAs were transfected in 24-well dishes using a TransIT-mRNA transfection Kit (Mirus, MIR 2250) according to the manufacturer`s instruction. Two hr after 100 ng/mL SSA treatment, mRNAs were transfected, and 4 hr post-transfection cells were washed with PBS and lysed with 1x passive lysis buffer (Promega). The luciferase assay was performed using Luciferase reporter assay system (Promega, E1910) according to the manufacturer`s instructions. *Renilla* luciferase (RLuc) was detected by *Renilla*-GLO. Luminescence was detected with a GLOMAX (Promega, 9100-102).

5.4.5 Plasmid constructs

pCDNA5 FRT TO-RAB32, pCDNA5 FRT TO-RAB32, pCDNA5 FRT TO-CDKN1B* and *pCDNA5 FRT TO-CDKN1B*:*

DNA fragment coding first coding exon and followed intron until the first in-frame stop codon from RAB32 and CDKN1B gene (RAB32* and CDKN1B*), the translated phenotypes under SSA treatment in ribosome profiling experiment, were PCR amplified from HEK cell genome. Simultaneously CDS region of RAB32 and CDKN1B were PCR amplified from HEK cell cDNA, respectively. The N-terminal 1x FLAG tag was inserted in-frame upstream to them during the PCR amplification. These PCR products were inserted into expression plasmid *pcDNA5/FRT/TO* (Invitrogen, V6520-20) via HindIII and BamHI site by Gibson assembly (NEB, E5520). The sequences of the final constructs were verified by plasmid sequencing. Primers used for the cloning are listed as following:

FLAG_F_pcdna	TCTAGCGTTTAAACTTAGCCACCATGGACTACAAGGACGACGATGACAAG
RAB32-F	ACAAGGACGACGATGACAAGATGGCGGGCGGAGGAGCCGGGGAC
RAB32*-R	ACCACACTGGACTAGTGTCAAACTTCTGGAAAAGGCCCCCT
RAB32-R	ACCACACTGGACTAGTGTCAGCAACACTGGGATTTGTTCTC
CDKN1B-F	ACAAGGACGACGATGACAAGATGTCAAACGTGCGAGTGTCTAAC
CDKN1B*-R	ACCACACTGGACTAGTGTTAACACCCTCCAGCAGGCAAAGC
CDKN1B-R	CCACACTGGACTAGTGTTACGTTTGACGTCTTCTGAGGCCA

5.4.6 DNA transfection

Transfection of 1 μg of each individual DNA were performed in six-well plates using transfection reagent, FuGENE HD (Promega, E2311) for the Hela S3 cells according to the manufacturer's instructions. Cell lysis was performed 48 hr post-transfection.

Chapter 6 General Discussions

Cell possess different layers of quality control mechanisms to monitor proper gene expression and maintain proteostasis. While the splicing process allows synthesis of a diverse selection of protein products from a single gene, the complicated process is subjected to multiple levels of quality controls to maintain robust gene expression (Brogna *et al.*, 2016) (Wolff *et al.*, 2014). Here, I present evidence demonstrating a layer of surveillance for splicing defects, which we would like to call a translational buffering mechanism to avoid accumulation of protein products from aberrantly spliced mRNAs (Figure 5.4).

Splicing of pre-mRNA to remove introns is an essential mechanism for the normal cellular function. Functional genes such as SF3B1 are essential genes, thus mutation or knockout of this gene would result in non-viable cells. To study the aspects of splicing and gene regulation, many target specific small molecule modulators of splicing are hence used as an advantage including SSA (Figure 1.7) (Kaida *et al.*, 2007) (Kotake *et al.*, 2007) (Mizui *et al.*, 2004) (Sakai *et al.*, 2002a, 2002b) (Albert *et al.*, 2007, 2009; Gao *et al.*, 2013) (Effenberger *et al.*, 2017). Comprehensive functional gene regulation studies upon splicing inhibition are still lacking. In this project, simultaneously using global profiling techniques, namely RNA sequencing and ribosome profiling, we could delineate the observed changes either in reference to the transcriptome or the translatome upon inhibition of splicing. We found that several unspliced transcripts were translated under SSA (Figure 2.4) which provided a global view of transcripts managing to avoid mRNA quality control (Appendix 8). It supports the previous reports indicating pre-mRNAs could not be held inside the nucleus but get transported out to the cytoplasm mediated by export adaptor ALYREF following the SSA treatment to the cells. Hence, inevitably a large number of truncated protein products are produced (Kaida *et al.*, 2007) (Mayas *et al.*, 2010) (Yoshimoto *et al.*, 2017) (Carvalho *et al.*, 2017).

Translation from retained introns is suppressed in different steps. Firstly, since transcription is coupled to splicing, splicing inhibition has been reported to cause pol II mediated transcription elongation arrest to reduce the abnormal transcripts (Koga *et al.*, 2014). Additionally, a considerable fraction of intron retained pre-mRNAs remains inside the nucleus, especially in nuclear speckles (Kaida *et al.*, 2007) (Boutz

et al., 2015). Also, the nuclear exosome having exo- and endonuclease activity including a 5'-3' exonuclease Rat1P/Xrn2 degrade the unspliced transcripts (Moore *et al.*, 2006). In the cytoplasm, the leaked transcripts with retained introns are surveyed by translation dependent NMD system due to the presence of in-frame premature termination codons directing them for degradation, although the specificity of NMD to the transcripts is poorly understood (Ge and Porse, 2014) (Carvalho *et al.*, 2017). Nevertheless, several layers of quality control exist prior to the translation of aberrant transcripts, the accumulation of truncated proteins translated from intron retained mRNAs induces proteotoxicity (Figure 5.2A and 5.3) and hence cell blocks translation via mTORC1 inhibition as a feedback mechanism further suppressing the accumulation of translated aberrant proteins (Figure 4.2). mTORC1 mediated translation initiation control provides the novel surveillance mechanism to sustain proteostasis during splicing inhibition and following translation of truncated proteins.

The truncated peptides upon SSA treatment could not be validated by western blotting for except P27* due to the lack of N-terminal antibodies whereas the FLAG tagged exogenous expression of representative transcripts were observed (Figure 5.3C and Appendix 7). Another concern could be unlike P27*, SSA-induced truncated proteins may be either stable but not detectable in western blotting or unstable, degraded by proteasome-mediated pathway. Furthermore, truncated proteins could be either soluble (like p27*, Appendix 7) or aggregated (RAB32*, Figure 5.3C). Intron databases were prepared for the group of transcripts showing the translation under splicing inhibition. Although mass spectrometry did not show the good correlation with the ribosome profiling data, at least fraction of truncated peptides was observed both in the suspension and pellet of cell lysate upon SSA treatment in LC/MS-MS analysis substantiating the translation of truncated peptides and aggregation of some of those proteins (data not shown). The low correlation might be due to the high background in LC/MS-MS, affected by the stability of peptides whereas ribosome profiling provides inference of the active translation only. Importantly, overexpression of truncated aggregated protein, such as RAB32* seems to be more likely showing proteotoxicity and subsequent mTORC1 inhibition (Figure 5.3B, C) whereas the effect was not observed for soluble truncated

protein such as for p27* (Appendix 7). Yet, the overexpression of SSA-induced single truncated protein may not exactly mimics as combined effect that was observed with the treatment of SSA. Nonetheless, the SSA-induced translated introns are actually the NMD targets (Appendix 8) since the distance from PTC to the consecutive exon-exon junction is higher than 55 nucleotides, but these transcripts seem to evade EJC mediated NMD, where the mechanism of evasion is still a mystery.

Besides, although SF3b inhibitors have been reported to kill tumor cells specifically and hold promised in the therapeutic venues (Nakajima *et al.*, 1996b) (Nakajima *et al.*, 1996a) (Kotake *et al.*, 2007) (Eskens *et al.*, 2013), however, the exact mechanism is still unclear. In previous study, truncated cyclin dependent kinase 2 (CDK2) inhibitor protein, p27* was reported to be stable and biologically active like the full-length protein, p27, which gets elevated upon SSA and stated as one of the reasons at least playing a role partly to inhibit the cancer cell growth (Kaida *et al.*, 2007) (Figure 2.4D).

From this study, transcription as well as translation of pathways related to cancer genes and cell cycle genes were observed globally sensitive (Appendix 1, 5, and 6). Indeed, microarray based transcriptome wide analysis has also reported global interference of gene expression including *VEGF* could be potential reason of anti-tumor activity of SSA (Furumai *et al.*, 2010). Nonetheless, translation efficiency of many of the oncogenes such as *CYR61, CDK9, SGK1, KIF23, PABC4, RAE1* and others were reduced (Appendix 1A, 1B and Table: Appendix2), downregulation of these genes at translation level could be one of the basis for the anti-tumor activity by SF3b inhibitors. Also, genes from cell cycle functional pathways showing decreased translation under SSA also support the inhibition of tumor cell growth (Figure 3.3 B). Cumulative decrease in translation efficiency for cell proliferation genes validates the result from functional pathway analysis (Appendix 1C). Furthermore, genes functioning in negative regulation of apoptosis also showed cumulative decrease in translation efficiency (Appendix 1D) as revealed before for the RNA expression by microarray analysis (Furumai *et al.*, 2010) along with *Mcl-1* dependent SSA-induced apoptosis (Larrayoz *et al.*, 2016).

Moreover, since the hallmark of most of the human cancers is hyperactive mTORC1 and consequently higher translation rates (Laplante and Sabatini, 2012) (Saxton and Sabatini, 2017), SF3b inhibition may simply counteract the activated mTORC1 pathway. Hence, it appears likely that SSA's antitumor activity stems from its action on several biological systems and pathways rather than one particular oncogenic target.

Although SSA affects the exon-skipping as well, we primarily investigated the SSA-induced intron retention and the subsequent gene regulation. Many of the ribosomal proteins were observed independent of splicing, but it could not be reasoned well as assessment of 5' splice site strength and intron length were not significant to resist the SSA`s intron retention activity (data no shown). We observed chemical splicing perturbation as well as genetic knockdown of SF3B1 showed mTORC1 inhibition, however, it is still an open question whether chemical splicing perturbation exactly mimics the genetic knockdown of SF3B1 in many of the gene regulation.

Future research should not only focus on cell cycle regulation by the SSA-induced translated introns but also take into account for possible immunogenic effects. It seems plausible that the production of aberrant proteins under splicing inhibition will also generate changed peptides to be presented by major histocompatibility complexes (MHCs) on the cell surface. Therefore, splicing inhibition might present an alternative venue into immunotherapy (Schumacher and Schreiber, 2015; Ott *et al.*, 2017). The truncated peptide candidates we observed in this study upon splicing inhibition may have similar potential of being specific neopeptides behaving as neoantigen that could be targeted by immune cells providing an exciting avenue of therapy. Also, we observed SSA induced enrichment of genes from antigen processing and presentation pathways, which would provide supporting evidence for this hypothesis (Figure 3.3 B). However, further studies will require turning towards the organismal level.

Summary and conclusion

In the current study, I report a novel surveillance mechanism to maintain protein homeostasis upon splicing inhibition. Essentially, the small molecule splicing modulation compound SSA has shown immense potential in the study of the gene expression regulation. This study demonstrates the potential of chemical biology in combination with the new technology of ribosome profiling to unveil a new negative feedback mechanism of quality control governing the protein output. Based on the results, I conclude as follows:

1. Chemical splicing inhibition by SSA leads to truncated peptides from intron translation.
2. Translation of such peptides in the cell causes proteotoxic stress and following downregulation of global translation via suppression of mTORC1 mediated translation initiation.
3. The cell buffers the production of aberrantly truncated proteins upon splicing inhibition by negative feedback mechanism to maintain proteostasis.

References

Aitken CE, Lorsch JR (2012) A mechanistic overview of translation initiation in eukaryotes. *Nat Struct Mol Biol*, **19:** 568–576

Albert BJ, McPherson PA, O'Brien K, Czaicki NL, Destefino V, Osman S, Li M, Day BW, Grabowski PJ, Moore MJ, Vogt A, Koide K (2009) Meayamycin inhibits pre-messenger RNA splicing and exhibits picomolar activity against multidrug-resistant cells. *Mol Cancer Ther*, **8:** 2308–2318

Albert BJ, Sivaramakrishnan A, Naka T, Czaicki NL, Koide K (2007) Total syntheses, fragmentation studies, and antitumor/antiproliferative activities of FR901464 and its low picomolar analogue. *J Am Chem Soc*, **129:** 2648–2659

Anders S, Huber W (2010) Differential expression analysis for sequence count data. *Genome Biol*, **11:** R106

Boutz PL, Bhutkar A, Sharp PA (2015) Detained introns are a novel, widespread class of post-transcriptionally spliced introns. *Genes Dev*, **29:** 63–80

Brar GA, Weissman JS (2015) Ribosome profiling reveals the what, when, where and how of protein synthesis. *Nat Rev Mol Cell Biol*, **16:** 651–664

Brogna S, McLeod T, Petric M (2016) The Meaning of NMD: Translate or Perish. *Trends Genet*, **32:** 395–407

Bullard JH, Purdom E, Hansen KD, Dudoit S (2010) Evaluation of statistical methods for normalization and differential expression in mRNA-Seq experiments. *BMC Bioinformatics*, **11:** 94

Calviello L, Ohler U (2017) Beyond Read-Counts: Ribo-seq Data Analysis to Understand the Functions of the Transcriptome. *Trends Genet*, **33:** 728–744

Carvalho T, Martins S, Rino J, Marinho S, Carmo-Fonseca M (2017) Pharmacological inhibition of the spliceosome subunit SF3b triggers exon junction complex-independent nonsense-mediated decay. *J Cell Sci*, **130:** 1519–1531

Cheng J, Maquat LE (1993) Nonsense codons can reduce the abundance of nuclear mRNA without affecting the abundance of pre-mRNA or the half-life of cytoplasmic mRNA. *Mol Cell Biol*, **13:** 1892–1902

Corrionero A, Miñana B, Valcárcel J (2011) Reduced fidelity of branch point recognition and alternative splicing induced by the anti-tumor drug spliceostatin A. *Genes Dev*, **25:** 445–459

Cretu C, Agrawal AA, Cook A, Will CL, Fekkes P, Smith PG, Lührmann R, Larsen N, Buonamici S, Pena V (2018) Structural Basis of Splicing Modulation by Antitumor Macrolide Compounds. *Mol Cell*, **70:** 265–273.e8

Crick F (1970) Central dogma of molecular biology. *Nature*, **227:** 561–563

Crick F (1979) Split genes and RNA splicing. *Science*, **204:** 264–271

Darnell JE (2013) Reflections on the history of pre-mRNA processing and highlights of current knowledge: a unified picture. *RNA*, **19:** 443–460

de Sousa Abreu R, Penalva LO, Marcotte EM, Vogel C (2009) Global signatures of protein and mRNA expression levels. *Mol Biosyst*, **5:** 1512–1526

Doma MK, Parker R (2007) RNA quality control in eukaryotes. *Cell*, **131:** 660–668

Dziembowski A, Ventura AP, Rutz B, Caspary F, Faux C, Halgand F, Laprévote O, Séraphin B (2004) Proteomic analysis identifies a new complex required for nuclear pre-mRNA retention and splicing. *EMBO J*, **23:** 4847–4856

Effenberger KA, Urabe VK, Jurica MS (2017) Modulating splicing with small molecular inhibitors of the

spliceosome. *Wiley Interdiscip Rev RNA*, **8:**

Egecioglu DE, Chanfreau G (2011) Proofreading and spellchecking: a two-tier strategy for pre-mRNA splicing quality control. *RNA*, **17:** 383–389

Eskens FA, Ramos FJ, Burger H, O'Brien JP, Piera A, de Jonge MJ, Mizui Y, Wiemer EA, Carreras MJ, Baselga J, Tabernero J (2013) Phase I pharmacokinetic and pharmacodynamic study of the first-in-class spliceosome inhibitor E7107 in patients with advanced solid tumors. *Clin Cancer Res*, **19:** 6296–6304

Finci LI, Zhang X, Huang X, Zhou Q, Tsai J, Teng T, Agrawal A, Chan B, Irwin S, Karr C, Cook A, Zhu P, Reynolds D, Smith PG, Fekkes P, Buonamici S, Larsen NA (2018) The cryo-EM structure of the SF3b spliceosome complex bound to a splicing modulator reveals a pre-mRNA substrate competitive mechanism of action. *Genes Dev*, **32:** 309–320

Furumai R, Uchida K, Komi Y, Yoneyama M, Ishigami K, Watanabe H, Kojima S, Yoshida M (2010) Spliceostatin A blocks angiogenesis by inhibiting global gene expression including VEGF. *Cancer Sci*, **101:** 2483–2489

Galy V, Gadal O, Fromont-Racine M, Romano A, Jacquier A, Nehrbass U (2004) Nuclear retention of unspliced mRNAs in yeast is mediated by perinuclear Mlp1. *Cell*, **116:** 63–73

Gandin V, Masvidal L, Hulea L, Gravel SP, Cargnello M, McLaughlan S, Cai Y, Balanathan P, Morita M, Rajakumar A, Furic L, Pollak M, Porco JA, St-Pierre J, Pelletier J, Larsson O, Topisirovic I (2016) nanoCAGE reveals 5' UTR features that define specific modes of translation of functionally related MTOR-sensitive mRNAs. *Genome Res*, **26:** 636–648

Gao Y, Vogt A, Forsyth CJ, Koide K (2013) Comparison of splicing factor 3b inhibitors in human cells. *Chembiochem*, **14:** 49–52

Ge Y, Porse BT (2014) The functional consequences of intron retention: alternative splicing coupled to NMD as a regulator of gene expression. *Bioessays*, **36:** 236–243

Gingras AC, Raught B, Sonenberg N (1999) eIF4 initiation factors: effectors of mRNA recruitment to ribosomes and regulators of translation. *Annu Rev Biochem*, **68:** 913–963

Goodarzi H, Elemento O, Tavazoie S (2009) Revealing global regulatory perturbations across human cancers. *Mol Cell*, **36:** 900–911

Groppo R, Richter JD (2009) Translational control from head to tail. *Curr Opin Cell Biol*, **21:** 444–451

Hasegawa M, Miura T, Kuzuya K, Inoue A, Won Ki S, Horinouchi S, Yoshida T, Kunoh T, Koseki K, Mino K, Sasaki R, Yoshida M, Mizukami T (2011) Identification of SAP155 as the target of GEX1A (Herboxidiene), an antitumor natural product. *ACS Chem Biol*, **6:** 229–233

Hellen CU, Sarnow P (2001) Internal ribosome entry sites in eukaryotic mRNA molecules. *Genes Dev*, **15:** 1593–1612

Hershey JW, Sonenberg N, Mathews MB (2012) Principles of translational control: an overview. *Cold Spring Harb Perspect Biol*, **4:**

Hilleren PJ, Parker R (2003a) Cytoplasmic degradation of splice-defective pre-mRNAs and intermediates. *Mol Cell*, **12:** 1453–1465

Hilleren PJ, Parker R (2003b) Cytoplasmic degradation of splice-defective pre-mRNAs and intermediates. *Mol Cell*, **12:** 1453–1465

Hinnebusch AG, Lorsch JR (2012) The mechanism of eukaryotic translation initiation: new insights and challenges. *Cold Spring Harb Perspect Biol*, **4:**

Hrdlickova R, Toloue M, Tian B (2017) RNA-Seq methods for transcriptome analysis. *Wiley Interdiscip*

Rev RNA, **8:**

Hsieh AC, Liu Y, Edlind MP, Ingolia NT, Janes MR, Sher A, Shi EY, Stumpf CR, Christensen C, Bonham MJ, Wang S, Ren P, Martin M, Jessen K, Feldman ME, Weissman JS, Shokat KM, Rommel C, Ruggero D (2012) The translational landscape of mTOR signalling steers cancer initiation and metastasis. *Nature*, **485:** 55–61

Ingolia NT (2016) Ribosome Footprint Profiling of Translation throughout the Genome. *Cell*, **165:** 22–33

Ingolia NT, Brar GA, Rouskin S, McGeachy AM, Weissman JS (2013) Genome-wide annotation and quantitation of translation by ribosome profiling. *Curr Protoc Mol Biol*, **Chapter 4:** Unit 4.18

Ingolia NT, Brar GA, Stern-Ginossar N, Harris MS, Talhouarne GJ, Jackson SE, Wills MR, Weissman JS (2014) Ribosome profiling reveals pervasive translation outside of annotated protein-coding genes. *Cell Rep*, **8:** 1365–1379

Ingolia NT, Ghaemmaghami S, Newman JR, Weissman JS (2009) Genome-wide analysis in vivo of translation with nucleotide resolution using ribosome profiling. *Science*, **324:** 218–223

Isken O, Maquat LE (2008) The multiple lives of NMD factors: balancing roles in gene and genome regulation. *Nat Rev Genet*, **9:** 699–712

Iwasaki S (2018) Ribosome Profiling Wet Protocol in Iwasaki Lab, ver

1.0.2, Laboratory protocol (Unpublished).

Iwasaki S, Floor SN, Ingolia NT (2016) Rocaglates convert DEAD-box protein eIF4A into a sequence-selective translational repressor. *Nature*, **534:** 558–561

Iwasaki S, Ingolia NT (2017) The Growing Toolbox for Protein Synthesis Studies. *Trends Biochem Sci*, **42:** 612–624

Jefferies HB, Reinhard C, Kozma SC, Thomas G (1994) Rapamycin selectively represses translation of the "polypyrimidine tract" mRNA family. *Proc Natl Acad Sci U S A*, **91:** 4441–4445

Johnson AW (1997) Rat1p and Xrn1p are functionally interchangeable exoribonucleases that are restricted to and required in the nucleus and cytoplasm, respectively. *Mol Cell Biol*, **17:** 6122–6130

Johnson GL, Nakamura K (2007) The c-jun kinase/stress-activated pathway: regulation, function and role in human disease. *Biochim Biophys Acta*, **1773:** 1341–1348

Kaida D, Motoyoshi H, Tashiro E, Nojima T, Hagiwara M, Ishigami K, Watanabe H, Kitahara T, Yoshida T, Nakajima H, Tani T, Horinouchi S, Yoshida M (2007) Spliceostatin A targets SF3b and inhibits both splicing and nuclear retention of pre-mRNA. *Nat Chem Biol*, **3:** 576–583

Kaida D, Schneider-Poetsch T, Yoshida M (2012) Splicing in oncogenesis and tumor suppression. *Cancer Sci*, **103:** 1611–1616

Katz Y, Wang ET, Airoldi EM, Burge CB (2010) Analysis and design of RNA sequencing experiments for identifying isoform regulation. *Nat Methods*, **7:** 1009–1015

Kervestin S, Jacobson A (2012) NMD: a multifaceted response to premature translational termination. *Nat Rev Mol Cell Biol*, **13:** 700–712

Khan K (2014) Chemical biology of splicing inhibitors. *Graduate School of Science and Engineering*, **PhD:** 60–61

Koga M, Satoh T, Takasaki I, Kawamura Y, Yoshida M, Kaida D (2014) U2 snRNP is required for expression of the 3' end of genes. *PLoS One*, **9:** e98015

Koodathingal P, Novak T, Piccirilli JA, Staley JP (2010) The DEAH box ATPases Prp16 and Prp43 cooperate to proofread 5' splice site cleavage during pre-mRNA splicing. *Mol Cell*, **39:** 385–395

Kornblihtt AR, Schor IE, Alló M, Dujardin G, Petrillo E, Muñoz MJ (2013) Alternative splicing: a pivotal step between eukaryotic transcription and translation. *Nat Rev Mol Cell Biol*, **14:** 153–165

Kotake Y, Sagane K, Owa T, Mimori-Kiyosue Y, Shimizu H, Uesugi M, Ishihama Y, Iwata M, Mizui Y (2007) Splicing factor SF3b as a target of the antitumor natural product pladienolide. *Nat Chem Biol*, **3:** 570–575

Langmead B, Salzberg SL (2012) Fast gapped-read alignment with Bowtie 2. *Nat Methods*, **9:** 357–359

Laplante M, Sabatini DM (2012) mTOR signaling in growth control and disease. *Cell*, **149:** 274–293

Larrayoz M, Blakemore SJ, Dobson RC, Blunt MD, Rose-Zerilli MJ, Walewska R, Duncombe A, Oscier D, Koide K, Forconi F, Packham G, Yoshida M, Cragg MS, Strefford JC, Steele AJ (2016) The SF3B1 inhibitor spliceostatin A (SSA) elicits apoptosis in chronic lymphocytic leukaemia cells through downregulation of Mcl-1. *Leukemia*, **30:** 351–360

Lejeune F, Li X, Maquat LE (2003) Nonsense-mediated mRNA decay in mammalian cells involves decapping, deadenylating, and exonucleolytic activities. *Mol Cell*, **12:** 675–687

Li J, Kim SG, Blenis J (2014) Rapamycin: one drug, many effects. *Cell Metab*, **19:** 373–379

Lindquist S (1981) Regulation of protein synthesis during heat shock. *Nature*, **293:** 311–314

Liu J, Xu Y, Stoleru D, Salic A (2012) Imaging protein synthesis in cells and tissues with an alkyne analog of puromycin. *Proc Natl Acad Sci U S A*, **109:** 413–418

Liu TY, Huang HH, Wheeler D, Xu Y, Wells JA, Song YS, Wiita AP (2017) Time-Resolved Proteomics Extends Ribosome Profiling-Based Measurements of Protein Synthesis Dynamics. *Cell Syst*, **4:** 636–644.e9

Lovén J, Orlando DA, Sigova AA, Lin CY, Rahl PB, Burge CB, Levens DL, Lee TI, Young RA (2012) Revisiting global gene expression analysis. *Cell*, **151:** 476–482

Vigevani L (2016) Molecular mechanisms of alternative splicing regulation by antitumor drugs targeting U2 snRNP. *Gene Regulation, Stem Cells and Cancer Program,* Center for Genomic Regulation (CRG), **PhD:** 8

Ma XM, Blenis J (2009) Molecular mechanisms of mTOR-mediated translational control. *Nat Rev Mol Cell Biol*, **10:** 307–318

Maier T, Güell M, Serrano L (2009) Correlation of mRNA and protein in complex biological samples. *FEBS Lett*, **583:** 3966–3973

Mamane Y, Petroulakis E, LeBacquer O, Sonenberg N (2006) mTOR, translation initiation and cancer. *Oncogene*, **25:** 6416–6422

Mayas RM, Maita H, Semlow DR, Staley JP (2010) Spliceosome discards intermediates via the DEAH box ATPase Prp43p. *Proc Natl Acad Sci U S A*, **107:** 10020–10025

McCarthy DJ, Chen Y, Smyth GK (2012) Differential expression analysis of multifactor RNA-Seq experiments with respect to biological variation. *Nucleic Acids Res*, **40:** 4288–4297

McGlincy NJ, Ingolia NT (2017) Transcriptome-wide measurement of translation by ribosome profiling. *Methods*, **126:** 112–129

Mizui Y, Sakai T, Iwata M, Uenaka T, Okamoto K, Shimizu H, Yamori T, Yoshimatsu K, Asada M (2004) Pladienolides, new substances from culture of Streptomyces platensis Mer-11107. III. In vitro and in vivo antitumor activities. *J Antibiot (Tokyo)*, **57:** 188–196

Moore MJ, Schwartzfarb EM, Silver PA, Yu MC (2006) Differential recruitment of the splicing machinery during transcription predicts genome-wide patterns of mRNA splicing. *Mol Cell*, **24:** 903–915

Nakajima H, Hori Y, Terano H, Okuhara M, Manda T, Matsumoto S, Shimomura K (1996a) New antitumor substances, FR901463, FR901464 and FR901465. II. Activities against experimental tumors in mice and mechanism of action. *J Antibiot (Tokyo)*, **49:** 1204–1211

Nakajima H, Sato B, Fujita T, Takase S, Terano H, Okuhara M (1996b) New antitumor substances, FR901463, FR901464 and FR901465. I. Taxonomy, fermentation, isolation, physico-chemical properties and biological activities. *J Antibiot (Tokyo)*, **49:** 1196–1203

Nürenberg E, Tampé R (2013) Tying up loose ends: ribosome recycling in eukaryotes and archaea. *Trends Biochem Sci*, **38:** 64–74

Ott PA, Hu Z, Keskin DB, Shukla SA, Sun J, Bozym DJ, Zhang W, Luoma A, Giobbie-Hurder A, Peter L, Chen C, Olive O, Carter TA, Li S, Lieb DJ, Eisenhaure T, Gjini E, Stevens J, Lane WJ, Javeri I, Nellaiappan K, Salazar AM, Daley H, Seaman M, Buchbinder EI, Yoon CH, Harden M, Lennon N, Gabriel S, Rodig SJ, Barouch DH, Aster JC, Getz G, Wucherpfennig K, Neuberg D, Ritz J, Lander ES, Fritsch EF, Hacohen N, Wu CJ (2017) An immunogenic personal neoantigen vaccine for patients with melanoma. *Nature*, **547:** 217–221

Popp MW, Maquat LE (2013) Organizing principles of mammalian nonsense-mediated mRNA decay. *Annu Rev Genet*, **47:** 139–165

Proud CG (2018) Phosphorylation and Signal Transduction Pathways in Translational Control. *Cold Spring Harb Perspect Biol*,

Raj A, van Oudenaarden A (2008) Nature, nurture, or chance: stochastic gene expression and its consequences. *Cell*, **135:** 216–226

Reed R (2003) Coupling transcription, splicing and mRNA export. *Curr Opin Cell Biol*, **15:** 326–331

Sakai Y, Tsujita T, Akiyama T, Yoshida T, Mizukami T, Akinaga S, Horinouchi S, Yoshida M, Yoshida T (2002a) GEX1 compounds, novel antitumor antibiotics related to herboxidiene, produced by Streptomyces sp. II. The effects on cell cycle progression and gene expression. *J Antibiot (Tokyo)*, **55:** 863–872

Sakai Y, Yoshida T, Ochiai K, Uosaki Y, Saitoh Y, Tanaka F, Akiyama T, Akinaga S, Mizukami T (2002b) GEX1 compounds, novel antitumor antibiotics related to herboxidiene, produced by Streptomyces sp. I. Taxonomy, production, isolation, physicochemical properties and biological activities. *J Antibiot (Tokyo)*, **55:** 855–862

Salimullah M, Sakai M, Mizuho S, Plessy C, Carninci P (2011) NanoCAGE: a high-resolution technique to discover and interrogate cell transcriptomes. *Cold Spring Harb Protoc*, **2011:** pdb.prot5559

Satoh T, Kaida D (2016) Upregulation of p27 cyclin-dependent kinase inhibitor and a C-terminus truncated form of p27 contributes to G1 phase arrest. *Sci Rep*, **6:** 27829

Saxton RA, Sabatini DM (2017) mTOR Signaling in Growth, Metabolism, and Disease. *Cell*, **169:** 361–371

Schneider-Poetsch T, Usui T, Kaida D, Yoshida M (2010) Garbled messages and corrupted translations. *Nat Chem Biol*, **6(3):** 189–198

Schumacher TN, Schreiber RD (2015) Neoantigens in cancer immunotherapy. *Science*, **348:** 69–74

Schwanhäusser B, Busse D, Li N, Dittmar G, Schuchhardt J, Wolf J, Chen W, Selbach M (2011) Global quantification of mammalian gene expression control. *Nature*, **473:** 337–342

Shoemaker CJ, Green R (2012) Translation drives mRNA quality control. *Nat Struct Mol Biol*, **19:** 594–601

Smith CW, Patton JG, Nadal-Ginard B (1989) Alternative splicing in the control of gene expression. *Annu Rev Genet*, **23:** 527–577

Smith DJ, Query CC, Konarska MM (2008) Nought may endure but mutability": spliceosome dynamics and the regulation of splicing. *Mol Cell*, **30:** 657–666

Sonenberg N, Hinnebusch AG (2009) Regulation of translation initiation in eukaryotes: mechanisms and biological targets. *Cell*, **136:** 731–745

Su KH, Cao J, Tang Z, Dai S, He Y, Sampson SB, Benjamin IJ, Dai C (2016) HSF1 critically attunes proteotoxic stress sensing by mTORC1 to combat stress and promote growth. *Nat Cell Biol*, **18:** 527–539

Su KH, Dai C (2017) mTORC1 senses stresses: Coupling stress to proteostasis. *Bioessays*, **39:**

Thoreen CC, Chantranupong L, Keys HR, Wang T, Gray NS, Sabatini DM (2012) A unifying model for mTORC1-mediated regulation of mRNA translation. *Nature*, **485:** 109–113

Trapnell C, Pachter L, Salzberg SL (2009) TopHat: discovering splice junctions with RNA-Seq. *Bioinformatics*, **25:** 1105–1111

Trcek T, Sato H, Singer RH, Maquat LE (2013) Temporal and spatial characterization of nonsense-mediated mRNA decay. *Genes Dev*, **27:** 541–551

Tseng CK, Wang HF, Burns AM, Schroeder MR, Gaspari M, Baumann P (2015) Human Telomerase RNA Processing and Quality Control. *Cell Rep*, **13:** 2232–2243

Vigevani L, Gohr A, Webb T, Irimia M, Valcárcel J (2017) Molecular basis of differential 3' splice site sensitivity to anti-tumor drugs targeting U2 snRNP. *Nat Commun*, **8:** 2100

Vilchez D, Saez I, Dillin A (2014) The role of protein clearance mechanisms in organismal ageing and age-related diseases. *Nat Commun*, **5:** 5659

Villa N. FC. (2014) *Mechanism of Translation in Eukaryotes.In: Parsyan A. (eds) Translation and Its Regulation in Cancer Biology and Medicine.* Springer, Dordrecht,

Wahl MC, Will CL, Lührmann R (2009) The spliceosome: design principles of a dynamic RNP machine. *Cell*, **136:** 701–718

Wang ET, Sandberg R, Luo S, Khrebtukova I, Zhang L, Mayr C, Kingsmore SF, Schroth GP, Burge CB (2008) Alternative isoform regulation in human tissue transcriptomes. *Nature*, **456:** 470–476

Wang Z, Gerstein M, Snyder M (2009) RNA-Seq: a revolutionary tool for transcriptomics. *Nat Rev Genet*, **10:** 57–63

Weinberg DE, Shah P, Eichhorn SW, Hussmann JA, Plotkin JB, Bartel DP (2016) Improved Ribosome-Footprint and mRNA Measurements Provide Insights into Dynamics and Regulation of Yeast Translation. *Cell Rep*, **14:** 1787–1799

Will CL, Lührmann R (2001) Spliceosomal UsnRNP biogenesis, structure and function. *Curr Opin Cell Biol*, **13:** 290–301

Will CL, Lührmann R (2011) Spliceosome structure and function. *Cold Spring Harb Perspect Biol*, **3:**

Wolff S, Weissman JS, Dillin A (2014) Differential scales of protein quality control. *Cell*, **157:** 52–64

Wu G, Fan L, Edmondson MN, Shaw T, Boggs K, Easton J, Rusch MC, Webb TR, Zhang J, Potter PM (2018) Inhibition of SF3B1 by molecules targeting the spliceosome results in massive aberrant exon skipping. *RNA*,

Yoshimoto R, Kaida D, Furuno M, Burroughs AM, Noma S, Suzuki H, Kawamura Y, Hayashizaki Y, Mayeda A, Yoshida M (2017) Global analysis of pre-mRNA subcellular localization following splicing inhibition by spliceostatin A. *RNA*, **23:** 47–57

You KT, Li LS, Kim NG, Kang HJ, Koh KH, Chwae YJ, Kim KM, Kim YK, Park SM, Jang SK, Kim H (2007) Selective translational repression of truncated proteins from frameshift mutation-derived mRNAs in tumors. *PLoS Biol*, **5:** e109

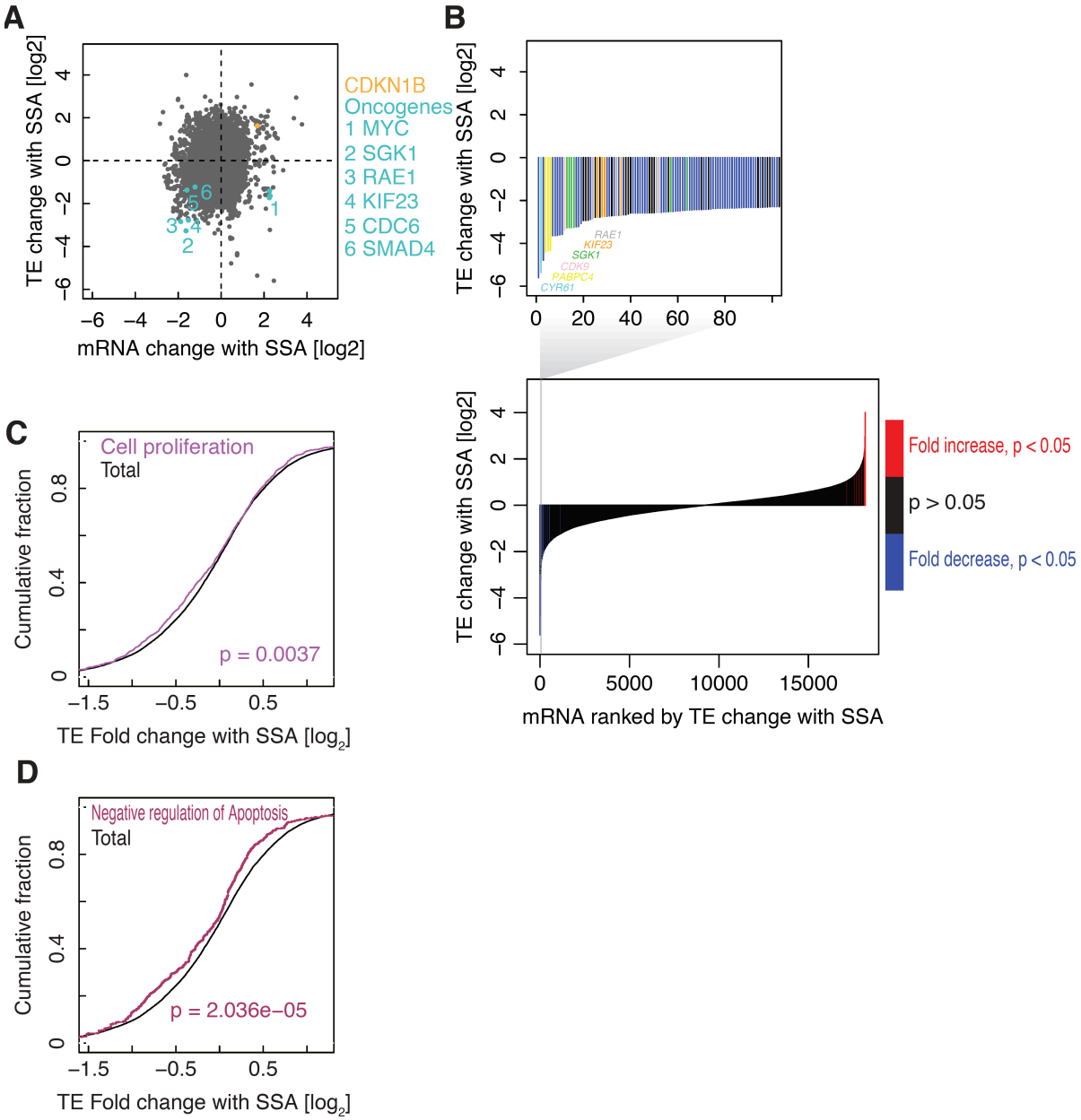

Appendix 1 SSA treatment leads to decreased translation efficiency in a number of oncogenes.

(A) MA (log ratio) plot showing TE fold change for each of the mRNAs with emphasis on *CDKN1B* (tumor suppressor) and several oncogenes. (B) TE fold change rank plot from the highest fold decrease to the highest translation fold increase (lower panel). Some of the oncogenes that are most sensitive to SSA in TE change have been highlighted (upper panel, zoomed). Cumulative distribution of TE fold change by SSA corresponding to cell proliferation (C) and negative regulation of apoptosis genes (D). Significance is calculated by Mann-whitney U test.

Appendix 2 SSA sensitive Transcription and Translation efficiency change of the genes and transcripts

		Fold change by SSA				Fold change by SSA	
Gene	**Transcript ID**	**Transcription**	**Translation Efficiency**	**Gene**	**Transcript ID**	**Transcription**	**Translation Efficiency**
AL832891	uc021opf.1	2.46	-5.60	RABEPK	uc004bpk.3	0.35	-1.95
CYR61	uc001dle.3	1.68	-5.36	TPT1	uc010tfp.1	1.12	-1.95
PABPC3	uc001upy.3	0.47	-4.79	NIPBL	uc003jkl.4	-0.44	-1.93
PABPC4	uc001cdl.2	0.74	-4.41	GPS2	uc002gfx.1	0.53	-1.92
PABPC4	uc001cdm.2	0.75	-4.35	GPS2	uc002gfz.1	0.53	-1.92
PABPC4	uc010oiv.1	0.75	-4.32	RFC3	uc001uva.3	-0.55	-1.91
PABPC1	uc011lhc.1	0.44	-3.64	RFC3	uc010ted.1	-0.55	-1.91
PABPC1	uc003yjt.1	0.43	-3.64	UMPS	uc011bkb.2	-1.20	-1.88
GLTSCR2	uc002phm.2	0.52	-3.63	XPOT	uc009zqm.2	0.10	-1.88
PABPC1	uc003yjs.1	0.43	-3.60	POLR2B	uc003hcm.1	0.03	-1.87
PABPC1	uc011lhd.1	0.43	-3.58	IREB2	uc002bdr.2	-1.45	-1.87
CDK9	uc004bse.2	-0.30	-3.38	POLR2F	uc010gxi.3	0.84	-1.86
SGK1	uc011ect.2	-1.63	-3.27	APH1A	uc001ety.2	0.05	-1.86
SGK1	uc011ecw.2	-1.64	-3.27	BTBD3	uc002wny.3	-1.12	-1.85
SGK1	uc003qeo.4	-1.64	-3.26	BTBD3	uc002woa.3	-1.12	-1.85
SGK1	uc011ecv.2	-1.64	-3.26	ANAPC16	uc001jsw.3	0.46	-1.85
KLF4	uc004bdh.3	2.27	-3.23	ANAPC16	uc001jsv.3	0.46	-1.85
CHERP	uc010xpg.1	-0.14	-3.22	ANAPC16	uc021psp.1	0.46	-1.85
CHERP	uc002nei.1	0.38	-3.07	LSM14A	uc002nva.4	-0.46	-1.85
DKK1	uc001jjr.3	-1.08	-2.88	LSM14A	uc002nvb.4	-0.46	-1.85
KIF23	uc010ukc.2	-1.53	-2.78	NIP7	uc002exa.3	-1.45	-1.84
KIF23	uc002asb.3	-1.52	-2.75	TEAD1	uc021qdx.1	-0.43	-1.84
KIF23	uc010bii.3	-1.51	-2.75	LSM14A	uc010xru.2	-0.42	-1.82
SIK1	uc002zdf.2	-1.19	-2.74	RNPS1	uc002cpt.3	-0.64	-1.81
AMOTL2	uc003eqf.2	-0.82	-2.72	RNPS1	uc002cpu.3	-0.64	-1.81
C1orf43	uc009wos.1	0.39	-2.70	RNPS1	uc002cpw.3	-0.64	-1.81
MGA	uc001zog.1	0.31	-2.70	RFC3	uc001uuz.3	-0.59	-1.81
KIF23	uc002asc.3	-1.54	-2.69	HSPA8	uc001pyp.3	-1.19	-1.79
AMOTL2	uc003eqg.1	-0.87	-2.67	RBM39	uc002xed.3	-0.88	-1.79
ZFAND5	uc010moy.1	-1.27	-2.58	HSPA8	uc009zbd.2	-1.19	-1.79
ZFAND5	uc031teb.1	-1.27	-2.58	UMPS	uc003ehl.4	-1.22	-1.78
ZFAND5	uc031tec.1	-1.27	-2.58	RNPS1	uc002cpx.3	-0.66	-1.76
ZFAND5	uc031ted.1	-1.27	-2.58	KIF20B	uc001kgr.1	-0.32	-1.76
ZFAND5	uc004aix.2	-1.27	-2.58	RFWD3	uc002fda.3	-1.44	-1.75
ZFAND5	uc004aiw.2	-1.27	-2.58	RFWD3	uc010cgq.3	-1.44	-1.75

ZFAND5	uc004aiy.2	-1.27	-2.58	HSPA8	uc001pyo.3	-1.18	-1.75
PUM1	uc010oga.1	-0.46	-2.55	SRI	uc011khg.2	0.44	-1.75
MPP6	uc003swx.3	0.63	-2.53	KIF20B	uc001kgs.1	-0.32	-1.75
MPP6	uc003swy.3	0.63	-2.53	DNTTIP2	uc001dqf.3	-0.63	-1.75
SGK1	uc003qen.4	-1.67	-2.52	MYC	uc003ysi.3	2.25	-1.73
BYSL	uc003orl.3	-0.98	-2.51	MRPL18	uc003qsw.4	-0.06	-1.72
SLC38A2	uc001rpg.3	-1.90	-2.50	HSPA8	uc009zbc.3	-1.17	-1.72
KIF2C	uc010olb.2	-1.88	-2.49	PPP2R4	uc011mbq.1	-0.47	-1.72
KIF2C	uc010olc.2	-1.87	-2.49	POLR2F	uc003aul.3	0.85	-1.72
CXCR4	uc002tuz.3	-0.76	-2.47	HSPA8	uc010rzu.2	-1.18	-1.70
CXCR4	uc002tuy.3	-0.75	-2.46	AHCTF1	uc001ibv.2	-1.23	-1.69
SGK1	uc011ecu.2	-1.60	-2.45	YTHDF2	uc021okf.1	-1.69	-1.68
RBM33	uc010lqk.1	0.83	-2.44	YTHDF2	uc001brc.3	-1.69	-1.68
KIF2C	uc001cmh.4	-1.87	-2.44	FEN1	uc021qkj.1	1.35	-1.67
CXCR4	uc010fnk.3	-0.76	-2.43	FEN1	uc001nsg.3	1.35	-1.67
CCNC	uc010kcs.3	0.47	-2.43	YTHDF2	uc010ofx.2	-1.67	-1.66
DCTN5	uc021tfi.1	-0.73	-2.42	YTHDF2	uc001bre.3	-1.67	-1.66
DNAJB1	uc002myz.1	-1.88	-2.42	CEBPZ	uc002rpz.3	-1.40	-1.66
AMOTL2	uc003eqh.1	-0.83	-2.42	GRWD1	uc002pjd.2	-1.22	-1.64
TMEM126A	uc001par.3	0.56	-2.39	WDR74	uc001nvm.2	-1.16	-1.64
PUM1	uc001bsj.1	-0.40	-2.37	WDR74	uc009yoi.2	-1.16	-1.64
KIF2C	uc001cmg.4	-1.88	-2.37	TRIM16L	uc002gug.1	-1.88	-1.63
SLC38A2	uc010sli.2	-2.24	-2.36	TRIM16L	uc002guh.1	-1.88	-1.63
DEPDC7	uc001mub.3	-0.64	-2.36	TRIM16L	uc002gui.1	-1.88	-1.63
WHSC1	uc003gdy.1	0.66	-2.35	TRIM16L	uc010vyg.1	-1.88	-1.63
WHSC1	uc003gea.1	0.66	-2.35	EIF5	uc001ymq.4	-2.02	-1.62
ARIH2	uc010hkl.3	0.04	-2.35	EIF5	uc001ymr.4	-2.02	-1.62
WHSC1	uc010icd.1	0.66	-2.35	EIF5	uc001ymt.4	-2.02	-1.62
WHSC1	uc010ice.1	0.66	-2.35	EIF5	uc001ymu.3	-2.02	-1.62
WHSC1	uc003geh.1	0.66	-2.35	NOP56	uc002wgh.3	-0.39	-1.62
TSC22D1	uc001uzn.4	-0.48	-2.35	GNL3	uc003dfd.3	-1.13	-1.61
SLC39A7	uc011dqv.2	0.59	-2.34	C17orf76-AS1	uc021tqt.1	0.75	-1.61
NFE2L2	uc002ulh.5	-2.04	-2.34	TRIM16	uc002gow.3	-1.81	-1.58
PUM1	uc010ogb.1	-0.42	-2.33	ZNF622	uc003jfq.3	-1.48	-1.57
NFE2L2	uc002ulg.5	-2.04	-2.33	PPP2R4	uc011mbo.2	-0.46	-1.55
NFE2L2	uc002uli.5	-2.04	-2.33	PHLDB2	uc003dyc.3	-0.76	-1.55
PUM1	uc001bsk.1	-0.37	-2.33	SLC39A1	uc001fdi.4	-0.57	-1.54
SLC39A1	uc010pee.3	-0.59	-2.33	SLC39A1	uc001fdj.4	-0.57	-1.54
DEPDC7	uc001muc.3	-0.66	-2.32	SLC39A1	uc031pph.1	-0.57	-1.54

C1orf43	uc001fek.3	0.35	-2.32	SLC39A1	uc001fdk.4	-0.57	-1.54
CCNC	uc003pqe.3	0.47	-2.31	SLC39A1	uc001fdl.4	-0.57	-1.54
PRPF38A	uc001ctv.4	-0.59	-2.29	SLC39A1	uc031ppi.1	-0.57	-1.54
PUM1	uc001bsi.1	-0.41	-2.29	PHLDB2	uc003dyd.3	-0.76	-1.54
PUM1	uc001bsh.1	-0.41	-2.29	PHLDB2	uc003dyh.3	-0.76	-1.54
USP10	uc002fii.3	-0.72	-2.28	GNL3	uc003dfe.3	-1.12	-1.54
USP10	uc010voe.2	-0.72	-2.28	GNL3	uc003dff.3	-1.12	-1.54
PIP5K1A	uc021oyo.1	-1.24	-2.24	SPECC1	uc002gwt.3	0.66	-1.53
DUSP1	uc003mbu.2	2.09	-2.24	C17orf76-AS1	uc021tqz.1	0.77	-1.53
PIP5K1A	uc001exi.3	-1.27	-2.22	ZWINT	uc031pvd.1	0.29	-1.53
PIP5K1A	uc001exj.3	-1.27	-2.22	SPECC1	uc002gwu.3	0.66	-1.53
ARIH2	uc003cvb.3	0.05	-2.21	PHLDB2	uc010hqa.3	-0.75	-1.53
ARIH2	uc003cvc.3	0.05	-2.21	PHLDB2	uc003dyg.3	-0.75	-1.53
DNTTIP2	uc009wdo.2	-0.49	-2.21	SZRD1	uc031plh.1	-0.09	-1.52
SLC38A2	uc001rph.3	-2.23	-2.20	SZRD1	uc001aym.5	-0.10	-1.52
HSPA8	uc010rzv.1	-1.21	-2.20	SAR1A	uc010qjh.2	-0.18	-1.48
C1orf43	uc001fei.2	0.30	-2.18	SAR1A	uc010qji.2	-0.18	-1.48
PRPF38B	uc001dvv.4	0.60	-2.13	MSH6	uc002rwc.2	-0.86	-1.45
USP1	uc001daj.2	-1.53	-2.13	CPSF6	uc001suu.4	0.25	-1.44
USP1	uc001dak.2	-1.53	-2.13	CPSF6	uc001sut.4	0.25	-1.43
USP1	uc001dal.2	-1.53	-2.13	EIF4B	uc010snu.2	0.47	-1.42
WHSC1	uc003gdz.4	0.50	-2.13	CD97	uc002myn.3	-0.81	-1.42
WHSC1	uc003geb.4	0.50	-2.13	SAR1A	uc010qjj.2	-0.17	-1.42
WHSC1	uc003gec.4	0.50	-2.13	DAB2	uc003jlw.3	-1.02	-1.41
WHSC1	uc003ged.4	0.50	-2.13	DAB2	uc003jlx.3	-1.01	-1.41
CSTF1	uc002xxl.1	-1.52	-2.12	EIF4B	uc001sbh.4	0.46	-1.41
CSTF1	uc002xxm.1	-1.52	-2.12	PPP1CC	uc021rdx.1	-0.21	-1.41
CSTF1	uc002xxn.1	-1.52	-2.12	TRIM16L	uc010vyf.1	-1.87	-1.40
IVNS1ABP	uc001grl.3	-0.42	-2.12	SPECC1	uc010cqx.3	0.66	-1.39
TTK	uc003pjc.3	-0.96	-2.11	SPECC1	uc002gwr.3	0.66	-1.39
TTK	uc003pjb.4	-0.96	-2.11	CD97	uc002mym.3	-0.82	-1.38
RLIM	uc004ebu.3	-1.21	-2.11	EIF4B	uc010snv.2	0.46	-1.37
RLIM	uc004ebw.3	-1.21	-2.11	TRIM16L	uc010cqg.1	-1.86	-1.37
RBM39	uc010gfn.3	-0.70	-2.11	NOL11	uc002jgd.1	-0.66	-1.36
RBM39	uc002xee.3	-0.70	-2.11	CITED2	uc021zga.2	2.08	-1.31
RBM39	uc010zvn.2	-0.70	-2.11	CITED2	uc003qip.2	2.08	-1.31
BRD4	uc002nau.4	0.29	-2.10	CITED2	uc021zgb.1	2.08	-1.31
RBM39	uc002xef.3	-0.71	-2.10	TIPARP	uc003fav.3	2.19	-1.31
DDX47	uc010shn.1	-0.05	-2.10	TIPARP	uc003faw.3	2.19	-1.31

NOP56	uc002wgi.3	-0.36	-2.10	TIPARP	uc021xgg.1	2.19	-1.31
USP22	uc002gyn.4	-1.92	-2.09	DNAJA2	uc002eeo.2	-0.97	-1.31
MLST8	uc002cpb.3	0.34	-2.06	CD97	uc002myl.3	-0.84	-1.30
C1orf43	uc001feh.2	0.29	-2.06	CITED2	uc021zfz.2	2.07	-1.30
MLST8	uc002coz.3	0.33	-2.05	TPT1	uc001uzy.1	0.90	-1.28
MLST8	uc002cpc.3	0.33	-2.05	RPS12	uc003qdx.3	0.91	-1.28
MLST8	uc002cpe.3	0.33	-2.05	LMO7	uc001vjv.3	-0.35	-1.27
MLST8	uc002cpf.3	0.33	-2.05	WDR43	uc002rmo.2	-1.28	-1.25
KIAA1967	uc003xcj.1	-0.98	-2.05	GPRC5A	uc001rba.3	-1.50	-1.25
USP22	uc002gyl.4	-1.97	-2.04	TPT1	uc001uzz.1	0.91	-1.24
SMAD2	uc002lcy.4	-0.02	-2.04	PPP6R3	uc001onw.3	-0.18	-1.23
SMAD2	uc002lcz.4	-0.02	-2.04	PPP6R3	uc001onx.3	-0.18	-1.22
BRIX1	uc003jja.3	-1.50	-2.04	SLC39A7	uc003odf.3	0.63	-1.20
SZRD1	uc010ocb.2	-0.10	-2.03	SLC39A7	uc003odg.3	0.63	-1.20
PNN	uc001wuw.4	-0.55	-2.02	PLK1	uc002dlz.1	-0.44	-1.17
PIP5K1A	uc001exk.3	-1.27	-2.02	RPL13A	uc002pnz.4	0.77	-1.16
RBM39	uc002xdz.3	-0.61	-2.02	RPL13A	uc031rlt.1	0.77	-1.16
MGA	uc010ucy.2	-0.20	-2.02	SEC11A	uc031qtj.1	0.34	-1.16
SZRD1	uc001ayk.5	-0.08	-2.02	HNRPDL	uc003hmt.3	0.05	-1.16
SMAD2	uc010xdc.3	-0.04	-2.02	RPL13A	uc002pny.4	0.76	-1.11
BRD4	uc002nat.3	0.15	-2.01	TMPO	uc001tfj.3	-0.19	-1.06
BRD4	uc002nas.3	0.15	-2.01	RPL37A	uc002vgf.3	0.96	-1.05
CHAF1A	uc002mal.3	-1.48	-2.00	RPS3A	uc011cie.2	1.06	-1.02
MGA	uc010ucz.2	-0.17	-2.00	RPS6	uc003znw.1	0.92	-1.01
SZRD1	uc001ayi.5	-0.08	-1.98	RPL37A	uc002vgg.3	0.93	-1.00
USP22	uc002gym.4	-1.91	-1.98	RPS6	uc003znv.1	0.95	-0.99
GPS2	uc002gfw.1	0.53	-1.97	RPS3A	uc003ilz.4	1.07	-0.95
PIP5K1A	uc010pcu.2	-1.25	-1.96	RPL18	uc010xzs.2	0.85	-0.90
NIPBL	uc003jkk.4	-0.42	-1.96	RPL35A	uc003fyr.3	0.91	-0.84
RABEPK	uc004bpi.3	0.35	-1.95	EEF1G	uc001ntm.1	0.98	-0.84
				EEF1G	uc010rlw.1	0.98	-0.83

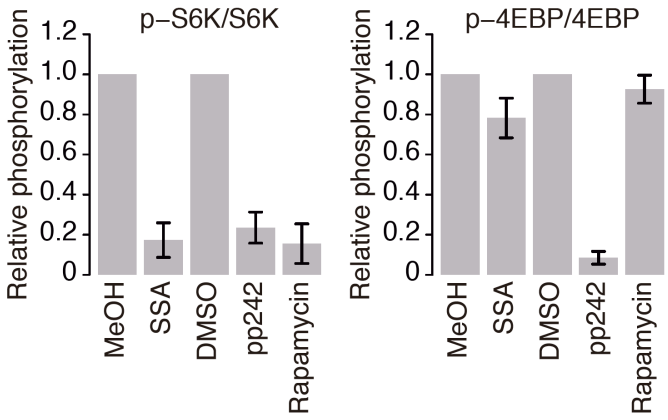

Appendix 3 SSA showed significant reduction in phosphorylation of mTORC1 substrates.

Quantification of western blot images for the total and phosphorylated form of S6K and 4EBP1 were performed by image studio ver 5.2 (LI-COR). Phosphorylated 4EBP1 assessed here was T47/46. Significance test is performed using Student`s T-test (n=3). (Supplementary to Figure 4A).

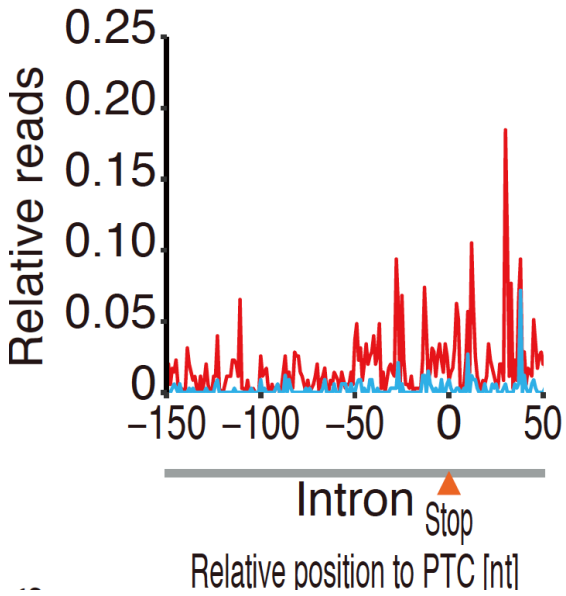

Appendix 4 Meta-gene analysis of RNA reads relative to the first in-frame pre-termination codon (PTC) of the translated introns. The reads are normalized relative to the sum of exonic reads for 100 nucleotides upstream to the splice site (supplementary to Figure 2.4B).

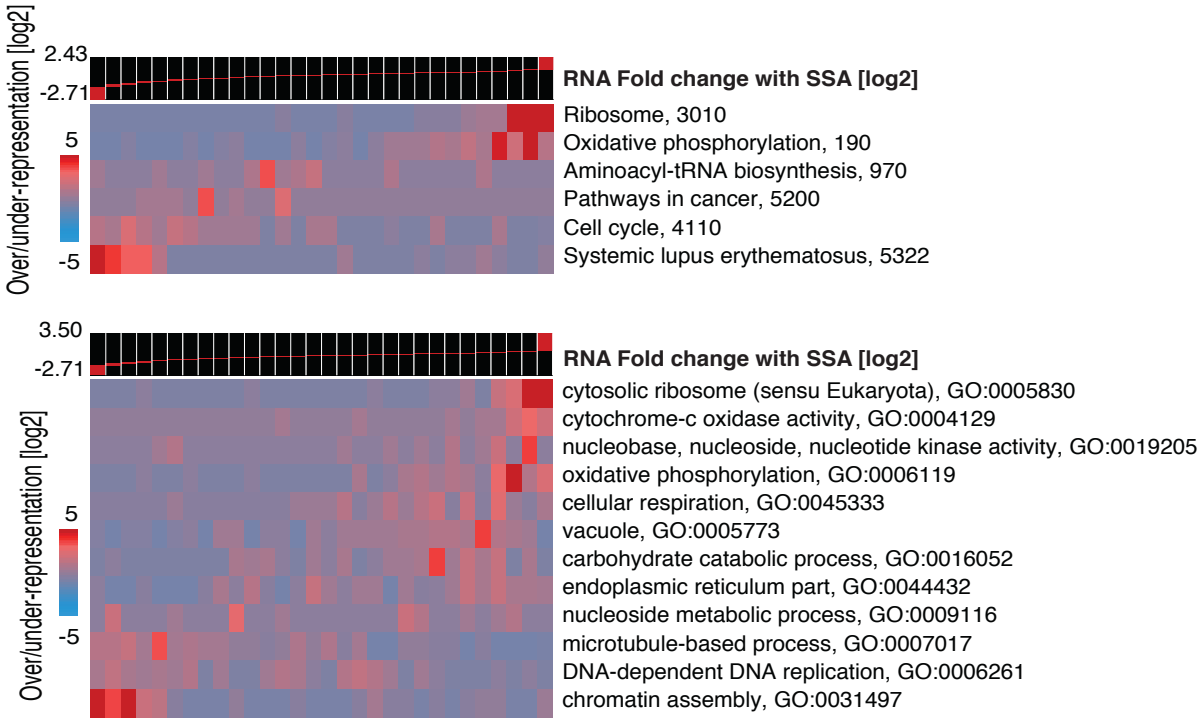

Appendix 5 KEGG pathway analysis along differential transcript fold change between SSA treated and untreated condition with iPAGE (upper panel) and GO pathway analysis (lower panel).

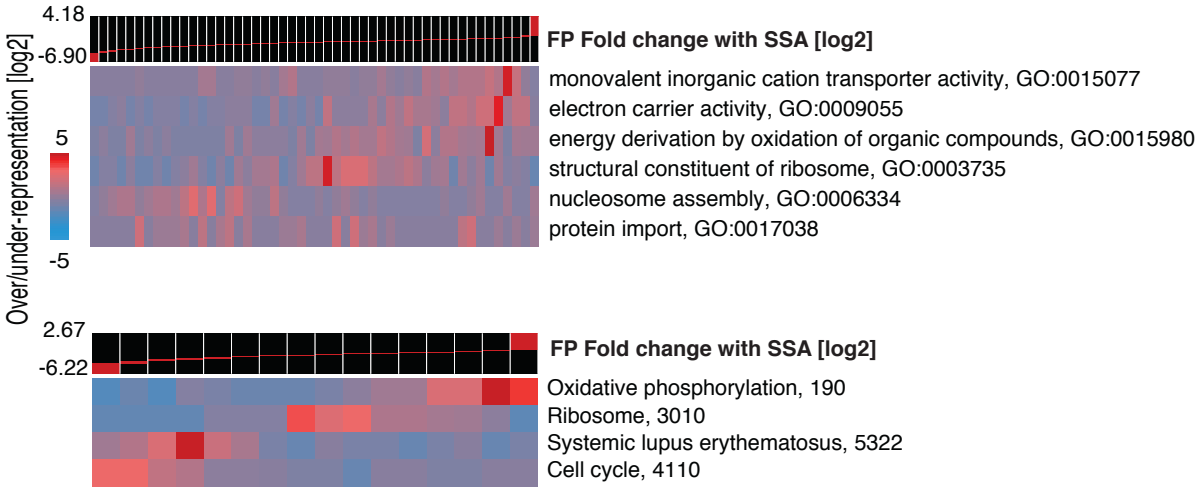

Appendix 6 GO pathway analysis along differential ribosome footprints fold change between SSA treated and untreated condition with iPAGE (upper panel) and KEGG pathway analysis (lower panel).

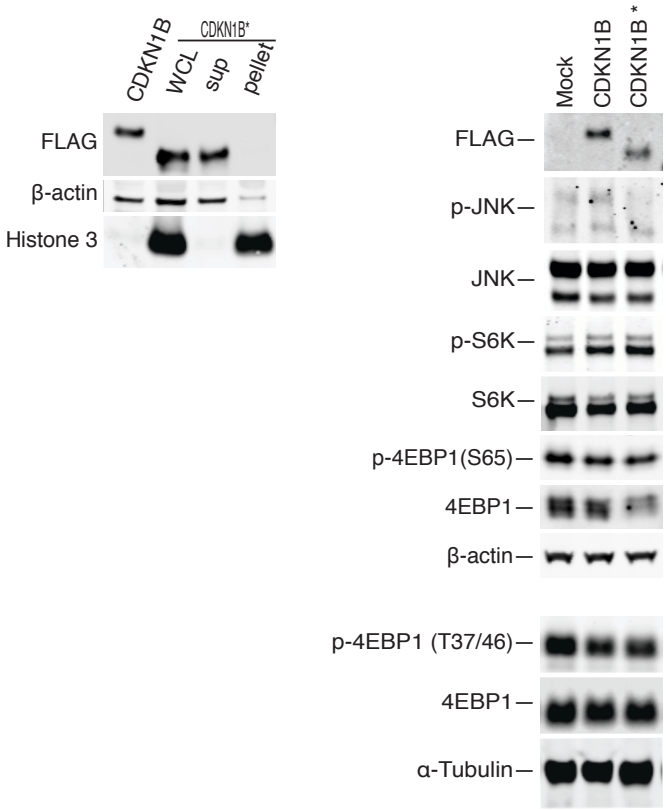

Appendix 7 p27* protein is soluble and did not affect mTORC1 activity (supplementary to Figure 5.3).

(Left Panel) HeLa S3 cell lines were transfected with equal amounts (1 µg) of the individual FLAG tagged plasmid constructs (Figure 5.3A). For the transfected truncated form, CDKN1B*, separately whole cell lysate (WCL), supernatant part or pellet part have been assessed for the presence of expressed protein. HeLa S3 cell lines were transfected with equal amounts (1 µg) of the individual FLAG tagged plasmid constructs using FuGENE HD (promega) as the DNA transfection reagent. Cells were harvested 48 hr post transfection. (Right panel) Total and phosphorylated stress activated protein kinase JNK and key mTORC1 substrates S6K and 4EBP1 have been analyzed by western blotting using the indicated antibodies. Transfection reagent without the plasmid construct was used as mock.

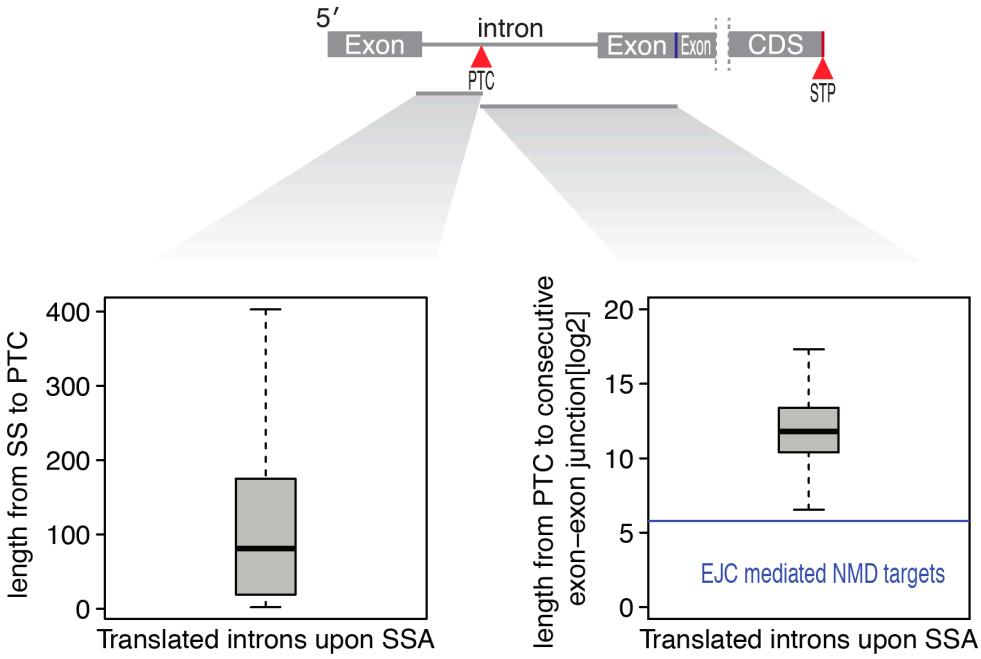

Appendix 8 Translated introns upon SSA were assessed for length of PTC from 5` SS (left panel) and length from PTC to consecutive exon-exon junction (right panel).

All of the translated introns have higher length than 55 nt, threshold for EJC mediated NMD targets.

Journal paper

- Chhipi Shrestha JK, Schneider-Poetsch T, Iwasaki S, Yoshida M (2019) Translational buffering upon splicing inhibition. *Manuscript in preparation for submission.*

Poster presentations

- Chhipi Shrestha JK, Schneider-Poetsch T, Iwasaki S, Yoshida M (July 19-21, 2017) *Analysis of splicing inhibition in gene regulation*. 19th Annual meeting of RNA Society of Japan, Toyama International conference center, University of Toyama.

- Chhipi Shrestha JK, Schneider-Poetsch T, Iwasaki S, Yoshida M (May 29- June 3, 2018) *Translational buffering upon splicing inhibition*. 23rd Annual meeting of RNA international Society, University of California, Berkeley, United States.

- Chhipi Shrestha JK, Schneider-Poetsch T, Iwasaki S, Yoshida M (November 27, 2018) *Translational buffering upon splicing inhibition*. CSRS Interim Progress Report, Nihonbashi Life Science Hub, Tokyo, Japan.

Oral presentations

- October 26, 2018. *Translational buffering upon splicing inhibition*. RIKEN Bioscience Bldg Seminar, RIKEN, Wako, Saitama, Japan. (Presenter: Jagat Krishna Chhipi Shrestha)

- November 27, 2018. *Translational buffering in gene expression*. CSRS Interim Progress Report, Nihonbashi Life Science Hub, Tokyo, Japan. (Presenter: Dr. Tilman Schneider-poetsch)

- November 28-30, 2018. *Translational buffering upon splicing inhibition*. 41st Annual Meeting of the Molecular Biology Society of Japan (MBSJ), Pacifico Yokohama, Japan. (Presenter: Dr. Shintaro Iwasaki)

- March 24-28, 2019. *Translational buffering: consequent to splicing inhibition.* The 2019 Annual Meeting of The Japan Society for Bioscience, Biotechnology and Agrochemistry (JSBBA), Tokyo University of Agriculture, Japan. (Presenter: Jagat Krishna Chhipi Shrestha)